



Norges miljø- og  
biovitenskapelige  
universitet

Master's Thesis 2017 30 ECTS  
Faculty of Science and Technology  
Department of Mathematical Sciences and Technology (IMT)

# **Measurements and analysis of snow load reduction on flat roofs using a photovoltaic system in heating mode**

Iver Frimannslund  
Structural Engineering and Architecture



**Sublimere:** overføre fast stoff direkte til damp, opphøye, foredle; i psykologi: om dirigere (fortrengt) drift ved å la den få utløsning i åndsarbeid, kunstnerisk skaperdrift eller lignende. Av latin *sublimare* «løfte opp, opphøye», avledet av *sublimis* «høyt hevet», i overført betydning «hevet, stor» (derav låneordet **Sublim** «opphøyd, fullkommen»). Bruken av verbet *sublimere* i fysikken er kommet via alkymistene som eksperimenterte med overføringen av faste stoffer til væsker og gasser. *Sublimis* bygger på sub- «under, innunder» for å markere bevegelse oppover + adjektivet *limis, limus* «på skrå», uten sikker etymologi (Rey, de Vaan).

- Norsk Etymologisk Ordbok (Caprona 2013)

## Preface

First of all, I would like to express gratitude to my supervisor Thomas K. Thiis. Thanks for guidance and wisdom in this process of making this thesis, and for the initiative making it all possible. Few professors seem to have as much fun at the university as you.

Also a special thanks to Tommy Strömberg for being a progressive engineer with a yes-can-do attitude. Thanks for being so kind and letting me borrow the equipment needed to conduct the research presented in this thesis.

I would also like to express gratitude to the employees at the Spesialrådgivning department at Multiconsult for above average interesting conversations and cake.

## Abstract

Previous studies show that a large portion of the existing building stock in Norway is regarded as under-designed with respect to snow load. Unfortunately, few solutions are available for reducing heavy snow loads occurring on roofs to this date and building owners often rely on shoveling snow off the roof in a heavy snowfall scenario. The PV-heating system intends to be a modern solution for snow load reduction. The system functions by sending current back into the PV-modules, inducing a heat flow at the module surface, allowing for snow load reduction.

This thesis combines measurements and theoretical analysis to investigate the PV-heating system. The objective is to uncover how feasible a PV-heating system is for reducing snow loads in a sub-arctic climate. The measurements and analysis were performed with the specific intent to document the load reducing capabilities of a PV-heating system operating under varying climatic conditions. Different strategies for the snow load reduction are investigated. Melting the snow is the obvious way of reducing the load. *Sublimation*, the instant transition from solid to vapor, serves as an alternative to melting, conducive under different climatic conditions. Several experiments were performed, including the test of a full scale PV-heating system and a case study with single modules. Through additional research questions, the thesis also explores the system's relation to current laws and design regulation, and if melting snow on the module surface can result in higher solar gains.

The results indicate that the potential of reducing snow loads with a PV-heating system is existent. Melting snow on the module surface is unproblematic, but the transportation of water from the roof surface can be challenging. The snow's capability for water-saturation and the freezing of water at the roof can result in insufficient load reduction. A drainage system with heated gutters is recommended to ensure proper load reduction for the roof. Tests of sublimating the snow also showed potential. A sublimation amount of  $0.86 \text{ kg/m}^2$  per day was achieved during a case study in Nordmarka, Oslo. To truly uncover the potential of load reduction by sublimation, further research is recommended. An automation of the system, implementing live data measured on site and weather forecast, is considered advantageous to optimize ablation and save energy.

Melting snow on the module surface allows for enhancing solar gains during the winter season. This thesis weighs the energy used to melt the snow against the potential of producing energy during winter. The results of analysis and theoretical calculation are indicative of an existing potential of enhanced solar gains and a possible new application of the system.

The relation to the law and design regulations is also investigated to consider how the system can be implemented in existing and new buildings. The thesis concludes that further documentation of the system's load reduction capabilities is needed to integrate the system into the design regulations and to establish of a legal precedent for the system.

## Sammendrag

Tidligere studier viser at en større del av den norske bygningsmassen er underdimensjonert i forhold til snølast. Det finnes få løsninger for eiere av byggverk til å redusere snølasten. De fleste er avhengig av å måke snølasten fra taket når slike tunge laster inntreffer. Et solcellesystem i varmemodus sikter på å redusere snølasten for underdimensjonerte tak. Systemet fungerer ved å sende strøm tilbake til solcellepanelene, som derav utvikler varme. På denne måten sikter systemet på å kunne redusere snølasten på taket.

Oppgaven tar sikte på å dokumentere hvorvidt det er mulig å redusere tung snølast med et solcellesystem i varmemodus. Feltmålinger, beregninger og bakgrunnsteori er presentert i denne oppgaven med hensikt om å avdekke hvorvidt en slik snølastreduksjon lar seg gjøre. Feltmålingene er utført med hensikt om å smelte og sublimere snø fra solcellepanelene. Sublimasjon er når et fast stoff går direkte til gass uten å noen gang være i flytende fase. Ved å sublimere snø kan man slippe avrenningsproblematikken på taket. Feltmålingene inkluderer en snølastreduksjonstest av et ferdig installert solcellesystem som i varmemodus, samt et case-study med enkeltpaneler. I tillegg til å utforske hvordan snølasten reduseres optimalt forsøker oppgaven å gi svar på hvordan systemet passer inn med gjeldende lover og forskrifter om dimensjonering av tak. Oppgaven sikter også på å avdekke hvorvidt det er mulig å øke inntaket av solenergi ved å smelte snø på solcelleoverflaten.

Resultatet indikerer at det finnes et potensial i å redusere snølasten ved å bruke et solcellesystem i varmemodus. Å smelte selve snøen på solcellepanelet er uproblematisk, men å transportere smeltevannet vekk fra takoverflaten kan være en utfordring. Snøens evne til å suge opp vann, samt faren for at smeltevannet fryser, kan være en reel hindring for lastreduksjonen. Det anbefales å bruke et avrenningssystem med varmekabler som forhindrer at vannet forblir på taket. Resultatene viser og at å sublimere snø har potensial for å redusere snølasten. Gjennom målinger utført i denne oppgaven ble det dokumentert en sublimasjonsrate på  $0.86 \text{ kg/m}^2$  per dag. For å virkelig avdekke potensialet for å sublimere snø med solcellepaneler i varmemodus burde videre forskning utføres. Det kan også være hensiktsmessig å automatisere systemet ved å implementere live data fra målinger på taket samt værmelding. På den måten kan man optimalisere snølastreduksjonen og spare energi.

Det viser seg og at det er mulig å kunne hente inn mer energi enn man bruker ved å smelte snø på solcellepanelene. Hvis det er et snødekke på panelene, og det er betraktelig mye solinnstråling, kan det lønne seg å smelte vekk denne snøen for så å kunne hente inn solenergien igjen. Teoretiske beregninger indikerer at det er der er mulig å hente inn mer strøm enn man bruker ved å anvende et solcellesystem på denne måten.

For at systemet skal passe inn i forskrifter for dimensjoner av tak, må systemet dokumenteres i større grad. Lovverket krever en søknad om bruksendring til kommunen hvis man skal installere et slikt system. Det kan etableres presedens for saken hvis det viser seg at systemet er trygt og effektivt.

## Content

Preface .....	3
Abstract.....	4
Sammendrag.....	5
1 Introduction .....	10
1.1 Background .....	10
1.2 Problem .....	11
1.3 Limitations .....	11
1.4 Structure of the thesis.....	12
Chapter 2 – Theory .....	12
Chapter 3 – Method .....	12
Chapter 4 – Results.....	12
Chapter 5 – Discussion .....	12
Chapter 6 – Conclusion .....	12
2 Theory .....	13
2.1 The snow load standard .....	13
2.1.1 Determination of the snow load.....	13
2.1.2 Thermal coefficient Ct.....	15
2.1.3 Snow loads on roofs with snow control .....	18
2.2 Development of the snow load.....	19
2.2.1 Historic perspective on the snow load .....	19
2.2.2 Future climate predictions .....	20
2.2.3 Vulnerability of the existing building stock .....	22
2.3 The law regarding measures on under-designed structures .....	24
2.3.1 Project classes .....	24
2.3.2 The Planning and Building Act .....	24
2.3.3 Building Application Regulations .....	25
2.4 Phase changes and energy balance of snow .....	26
2.4.1 The phase diagram .....	26
2.4.2 Molecular theory.....	26
2.4.3 Enthalpy.....	28

2.5 Sublimation of snow .....	30
2.5.1 Principles .....	30
2.5.2 Conditions conducive for sublimation .....	32
2.5.3 Documented sublimation rates .....	33
2.5.4 Metamorphism in snow .....	34
2.5.5 Estimating sublimation with the Bulk Aerodynamic Flux Method .....	36
2.6 PV systems .....	38
2.6.1 Function and configuration .....	38
2.6.2 PV-heating systems .....	41
2.6.3 PV-systems and snow .....	43
2.6.4 Thermography of PV modules .....	44
3. Method .....	50
3.1 The ASKO Roof .....	50
3.2 Aerial Thermography of a PV-system .....	53
3.2.1 The drone .....	53
3.2.2 The process of mapping the roof .....	54
3.2.3 Processing the results .....	55
3.2.4 Estimating the atmospheric transmission coefficient .....	60
3.3 Snow load reduction test of a full scale PV-heating system .....	62
3.3.1 Climatic conditions .....	62
3.3.2 Cases .....	63
3.4 Case study in Nordmarka .....	64
3.4.1 Setup .....	66
3.4.2 Data collected .....	67
3.4.3 Cases .....	69
3.5 Estimating sublimation using the Bulk Aerodynamic Flux method .....	72
4 Results .....	75
4.1 Aerial thermography of a PV system .....	75
4.1.1 Overview map .....	76
4.1.2 Module detail map .....	77
4.1.3 Single infrared photos .....	78
4.1.4 Calculation of radiated effect from PV-modules .....	80



4.1.5 Calculation of thermal coefficient $C_t$ , using heat flow from PV-modules .....	81
4.2 Test of a full scale PV-heating system.....	83
4.2.1 Case 1.....	84
4.2.2 Case 2.....	87
4.2.3 Case 3.....	90
4.3 Case study in Nordmarka .....	91
4.3.1 Case 1 – ASKO Setup .....	91
4.3.2 Case 2 – Sublimation .....	94
4.3.3 Case 3 – Maximum effect.....	101
4.4 Analysis .....	105
4.4.1 Equivalent heat emission through a roof .....	105
4.4.2 Energy and time required for melting snow into water .....	106
4.4.3 Equivalent solar gain – for which snow depth is melting expedient? .....	107
4.4.4 Roof surface temperatures under a snowpack .....	109
4.4.5 Estimated sublimation rates .....	110
4.4.6 Activity diagram for the automation of a PV-heating system.....	111
5 Discussion .....	114
5.1 Optimal strategy for snow load reduction under varying climatic conditions .....	114
5.1.1 Melting .....	114
5.1.2 Sublimation.....	119
5.1.3 The Automation of the PV-heating system .....	123
5.1.4 Summary.....	127
5.2 The PV-heating system’s relation to law and regulations.....	128
5.2.1 The law regarding a PV-heating system on under-designed roofs .....	128
5.2.2 The relation to the design regulations.....	129
5.2.3 Summary.....	132
5.3 Melting snow on modules to enhance solar gains .....	133
5.3.1 Equivalent solar gain – for which snow depth is melting expedient? .....	133
5.3.2 Potential/applications.....	135
5.3.3 Summary.....	137
5.4 Further studies .....	138
6 Conclusion .....	139

References ..... 141  
Appendix A..... 145  
Appendix B..... 147

# 1 Introduction

## 1.1 Background

The origin of this thesis came out of a PV-system designer who wanted to measure the effect of and document their newly developed snow melting system. The system works by applying current to PV-modules to produce heat, enabling the ablation of snow on the module surface. The system designer thought this system could be applicable to existing under-designed flat roofs functioning as a load-reduction system. It could then serve as a compensation for the weight added by the PV-system, enabling even under-designed buildings to install PV-systems with this modification.

If the system is safe, effective and well documented, it could serve as a legitimate load reduction factor in the snow load standard, NS-EN-1991-1-3, making it possible to lower the load capacity for future roofs having this system.

The design snow load value, used as the base of the dimensioning of all roofs in Norway, has evolved significantly the past 40 years. A general trend of an increasing design snow loads have put many buildings in the under-designed category. New reports on the development of future climate predict even heavier snow loads to come. The current state of under-designed buildings and predictions of heavy snow loads to come provide the need and a market for systems able to reduce snow loads in a heavy snowfall scenario.

Since the PV-heating system is designed to clear snow off the module surface, the system can be applied to melt snow in winter with intent to enhance the solar gains. This secondary application could have a legitimate potential, and was to be further researched in this thesis.

When it was decided that it was room for a Master's thesis to document the sufficiency of the PV-heating system, it had not yet been installed. The system was untested at a large scale and there were was a wide range of unknown problems related to this new system; the optimal tactic for load reduction, the energy consequences of the snow load reduction, the impact of changing weather conditions, how the system is to be controlled and how to sufficiently drain the meltwater.

The investigation of the application of drones as a tool for documentation was progressing at NMBU at the time of this thesis. It was decided in an early stage that drones were to be used to make an infrared map of the modules running in heating mode. The potential of measuring snow load reduction combining 3D-models created from drone-based mapping software using photogrammetric techniques was also to be explored.

## 1.2 Problem

The objective of this thesis is to answer a main problem, supported by 3 research questions:

*How feasible is a PV-system in heating mode for reducing snow load on under-designed flat roofs in a sub-arctic climate?*

- *What is the optimal strategy for reducing snow load on PV-modules in heating mode under varying climatic conditions?*
- *How does the system relate to the law and regulations?*
- *Can melting snow on modules result in higher solar gains?*

## 1.3 Limitations

The thesis is limited to the civil engineering aspect of the snow load reduction.

PV-system theory is used for explaining the basic principles necessary to understand the function of the system, but does not investigate the importance of how different PV-products influence the result. This thesis primarily focuses on mono-crystalline PV-modules with a low angle tilt.

The thesis is based on findings applicable for Norway. The laws and regulations discussed are valid for Norway as a country and do not necessarily apply for other nations. The measurements performed and many of the calculations are based on a sub-arctic climate. A different climatic impact on the system is not investigated in this thesis, although the principles of the measurements and analysis should apply nonetheless.

The safety aspect of applying power to the modules is also not investigated.

## **1.4 Structure of the thesis**

The structure of the thesis is presented to gain a better understanding of how the chapters connect and relate to one another.

### **Chapter 2 – Theory**

The theory chapter will explain key concepts necessary to understand the rest of the thesis. The theory presented will be further used in numerous calculations and analysis presented in the results chapter.

### **Chapter 3 – Method**

The method chapter will explain how case studies, measurements and calculations have been performed. All the studies performed provide information relevant to the research questions posed. The chapter also provides information about the research objects that were performed measurements on, necessary to understand the scope and limitations of the results that are to be presented.

### **Chapter 4 – Results**

This chapter presents the results from the case studies and measurements collected in the thesis. Calculations based on findings from the results and research is presented in the analysis chapter.

### **Chapter 5 – Discussion**

The discussion aims to answer the problem and the research questions stated in the thesis. The discussion chapter is structured into 3 subchapters, each addressing its own research question.

### **Chapter 6 – Conclusion**

The conclusion chapter aims to summarize the findings of this thesis.

## 2 Theory

In order to understand the research presented in this thesis, knowledge of a few key concepts is necessary. This includes information of how buildings are designed to withstand the snow load, the energy balance and metamorphism of snow and how a PV-system functions. The theory presented gives basis to further understand the measurements and analysis performed in the thesis.

### 2.1 The snow load standard

The snow load standard NS-EN-1991-1-3 provides methods for designing structures meeting the requirements of Technical Regulations to the Planning and Building Act. Designing buildings in accordance with the snow load standard ensures that the design of the building is within the requirements of the law. NS-EN-1991-1-1-3 is a part of the Eurocode series used for building design for all countries in the European Union. A National Annex provides additional information of structural requirements specific for the nation in question.

The snow load standard focus on how to determine the snow load used for the design/dimensioning of roofs. This chapter will provide a basic understanding on the determination of the snow load, with emphasis on the *thermal coefficient* and the determination of snow loads on roofs with *snow control*.

#### 2.1.1 Determination of the snow load

A design snow load is set as the product of the characteristic snow load and three coefficients. The snow load standard states that snow loads on roofs shall be determined as follows for transient/persistent design situations(Standard Norge 2003):

$$S = \mu_i C_e C_t S_k \quad (1)$$

$S$  is the design snow load [ $kN/m^2$ ]

$\mu_i$  is the snow load shape coefficient

$C_e$  is the exposure coefficient

$C_t$  is the thermal coefficient

$S_k$  is the characteristic snow load on the ground [ $kN/m^2$ ]

The load shape coefficient ( $\mu_i$ ) is determined by how snow is distributed on the roof; drifted and undrifted snow is determinative for how the snow settles and affects the load arrangement on the roof. The load shape coefficient changes along with the shape and pitches of the roof, giving several different dimensioning snow loads over a single roof. The coefficient can be more or less than 1.

The exposure coefficient ( $C_e$ ) is determined by the topography of the site and whether the building is exposed or sheltered. The coefficient can be more or less than 1.

Topography	$C_e$
Windswept <sup>a</sup>	0,8
Normal <sup>b</sup>	1,0
Sheltered <sup>c</sup>	1,2

<sup>a</sup>*Windswept topography*: flat unobstructed area exposed on all sides without, or little shelter afforded by terrain, higher constructions works or trees.

<sup>b</sup>*Normal topography*: areas where there is no significant removal of snow by wind on construction work, because of terrain, other construction works or trees.

<sup>c</sup>*Sheltered topography*: areas in which the construction work being considered is considerably lower than the surrounding terrain or surrounded by high trees and/or surrounded by higher construction works.

Table 1. Recommended values for  $C_e$  for different topographies. The table is reproduced from NS-EN 1991-1-3.

The thermal coefficient ( $C_t$ ) allows for a reduction of the snow load on roofs with a heat flow larger than  $1 \text{ W/m}^2\text{K}$ . The value is further explained in the next chapter.

The characteristic snow load ( $S_k$ ) is the base value of the design snow load. The characteristic snow load is based on values of what snow load can occur on the ground for a specific location calculated with a recurrence interval of 50 years. The recurrence interval is a statistical evaluation of which snow loads that can be expected to occur within the specified time interval. For a 50 year recurrence interval, the load has a 2% chance of occurring every year. The recurrence interval is often referred to as the return period. The National Annex provides information of the characteristic snow values for Norway. The load is specified for all 434 municipalities in Norway, and is dependent on height above sea level for some specific locations. The load ranges between  $1,5\text{-}9,0 \text{ kN/m}^2$  throughout the country (Standard Norge 2008).

Height above sea level	$S_{k,0} [\text{kN/m}^2]$
0-150 m.o.h	3,5
151-250 m.o.h.	4,5
251-350 m.o.h.	5,5
>350 m.o.h.	6,5

Table 2. Characteristic snow load on the ground for the municipality of Oslo. The table is reproduced from the National Annex 4.1.

The combination of these factors gives the dimensioning snow load  $S$  [kN/m<sup>2</sup>]. It is this final number that the building must be designed in accordance with, providing the lowest limit of the snow load a building must be able to withstand.

### 2.1.2 Thermal coefficient $C_t$

The thermal coefficient is a factor for snow loads on glass-roofs. The factor was introduced in 1990 with the 3<sup>rd</sup> edition of NS3479, with intent to reduce the snow load for roofs experiencing significant heat transfer through the roof.

Although the coefficient is specifically for glass-roofs, the standard states in an undernote that  $C_t$  “*may also apply to other materials*” (ISO 2013b).

The framework presented is reproduced from the ISO 4355 standard. The formula assumes a characteristic snow load equal or higher than 1,5 kN/m<sup>2</sup>.

$$C_t = \left[ 1 - 0,054 \left( \frac{S_0}{3,5} \right)^{0,25} f(U_0, \theta) \right] \cos(2\beta) \quad 0^\circ \leq \beta \leq 45^\circ \quad (2)$$

Where:

$$f(U_0, \theta) = \begin{cases} 0 & U_0 < 1,0 \\ (\theta-5)[\sin(0,4U_0-0,1)]^{0,75} & 1,0 \leq U_0 \leq 4,5 \text{ and } 5 \leq \theta \leq 18 \\ \theta-5 & U_0 > 4,5 \text{ and } 5 \leq \theta \leq 18 \end{cases} \quad (3)$$

$U_0$  is the thermal transmittance assuming the external thermal surface resistance is equal to zero [W/(m<sup>2</sup>K)]. The value only represents the glass covered surface.

$\beta$  is the roof angle (°). If  $\beta < 0$  or  $U_0 < 0$ ,  $\beta = 0$  applies (i.e.  $C_t = 1,0$ );

$S_0$  is the characteristic snow load on the ground ( $S_0 \geq 1,5$  kN/m<sup>2</sup>);

$\theta$  is the lowest expected internal temperature during the winter (°C).

If  $\theta < 5$  °C,  $\vartheta = 5$  °C applies. If  $\theta > 18$  °C,  $\theta = 18$  °C applies in Formula (D.2).



The standard also states that: “If the thermal transmittance of the roof,  $U$ , is based on a different value of the external thermal surface resistance,  $R_e > 0$ ,  $U$  is transformed to  $U_0$  by Formula (D.3):

$$U_0 = \frac{U}{1 - UR_e} \quad (4)$$

*$U$  is the thermal transmittance of the roof [ $W/m^2K$ ]*

*$R_e$  is the external surface resistance for  $U$  [ $m^2K/W$ ]*

The standard also elaborates that: “A check that melting water can be drained from the roof surface without risk of icing shall always be carried out.”

A few basic heat transfer equations give basis for a further understanding the heat transfer taking place in a roof. Two methods are presented, estimating heat flow through the roof and the roof surface temperature between the roof and a snowpack. The methods are presented in accordance with Håndbok 53 from Sintef Byggforsk (Edvardsen & Ramstad 2010).

The heat emission through a roof can be calculated by multiplying the U-value of the roof with a temperature difference.

$$Q_{roof} = U_{roof}\Delta T \quad (5)$$

$Q_{roof}$  is the heat emitted [ $W/m^2$ ]

$U_{roof}$  is the U-value of the roof [ $W/m^2K$ ]

$\Delta T$  is the temperature difference between the inside and outside of the roof [ $K$ ]

The roof surface temperatures under between a snowpack and a roof can be determined by calculating the relative difference in thermal resistance between the snowpack and the roof. The boundary conditions are then set, allowing for calculating the temperature at the roof surface. Equation 6 calculates the temperature difference from the warm side boundary to the layer of interest. Equation 7 estimates the temperature occurring at the layer of interest itself.

$$\Delta\theta_{layer} = (\theta_1 - \theta_2) \frac{R_{layer}}{R_T} \quad (6)$$

$\Delta\theta_{layer}$  is the temperature difference between the boundary and the layer [ $^{\circ}C$ ]

$\theta_1, \theta_2$  is the boundary temperature at the warm and cold side [ $^{\circ}C$ ]

$R_{layer}$  is the temperature resistance from the boundary till the layer of interest [ $m^2K/W$ ]

$R_T$  is the total resistance between the boundaries [ $m^2K/W$ ]

$$\theta_{layer} = \theta_1 - \Delta\theta_{layer} \quad (7)$$

$\theta_{layer}$  is the temperature at the layer

### 2.1.3 Snow loads on roofs with snow control

Annex F in the ISO 4355 standard provides a framework for snow load reduction based on a control device or method able to guaranty snow load removal during a heavy snowfall. The framework is presented in accordance with ISO 4355 (2013a).

The design snow load for a roof with snow control can be calculated with the following equation:

$$S = \mu_b S_n - S_c \quad (8)$$

$\mu_b$  is the basic load coefficient, defining the reduction of the snow load on the roof due to a slope of the roof and the material coefficient  $C_m$

$S_n$  is the snow load on the ground with accumulation over  $n$  days [ $\text{kN/m}^2$ ]

$S_c$  is the controlled snow load [ $\text{kN/m}^2$ ]

Where:

$$S_n = C_t d_n \rho_n g \quad (9)$$

$C_e$  is the exposure coefficient explained in 2.1.1.

$d_n$  is defined as the annual maximum value of snow accumulation [ $\text{m}$ ] for  $n$  days with a return period of 100 years, estimated from meteorological data of the ground snow depth observed for a certain period.  $n$  is typically corresponding with the duration of single event of snow duration of each building site.

$\rho_n$  is the equivalent density for ground snow with roof control

$g$  is acceleration due to gravity

The controlled snow load,  $S_c$ , is particularly interesting. According to the standard,  $S_c$  is determined after “field research and experiments investigating the capacity of sliding or melting devices”. The load is determined by documenting the difference in snow load before and after removal in a heavy snowfall scenario. The load reduction has to be guaranteed during a heavy snowfall. The standard explains that for a melting device, the length of the evaluation period  $n$  [day] is decided with the performance and reliability of the roof snow control system.

To summarize; Annex F presents the framework which allows for a reduction of the design snow load with an undefined system, provided that the device or method guaranties the removal of snow load.

## 2.2 Development of the snow load

The snow load used for designing roofs has shown a general trend of increasing since first established by the National Office of Building Technology and Administration in 1949 in Norway. The increase in snow load results in existing buildings, designed for the snow load at the time, now being regarded as under-designed in the current standards. Such under-designed buildings can take less load than what is expected to occur in a buildings lifetime, and is to some degree in danger of collapsing if experiencing a heavy snow load. This chapter explores the historic development of the snow load, reports of future climate predictions and the vulnerability of the existing building stock.

### 2.2.1 Historic perspective on the snow load

The snow load has evolved with increasing knowledge and statistics on heavy snowfalls. The growing knowledge and information of snow loads has resulted in the snow load developing from a general load with little variations, to a load varying with local topography and local climate (Meløysund et al. 2008). An adaption of the snow load for the individual municipalities has been introduced over the years. The use of coefficients adjusting the load for the individual location and design are also introduced as the snow standard developed. A table is made, showing the development of the design snow load since first established in 1949.

<b>Standard</b>	-	NS 3052	NS 3479	NS 3479 3 <sup>rd</sup>	NS 3490	NS 3491-3
<b>Year</b>	1949	1970	1979	1990	1999	2001
<b>General load /Characteristic load</b>	1,5	1,5	1,5-3,5	1,5-3,5	-	1,5-9,0
<b>Changes</b>	-	Snow maps introduced	$S_k$ with 5 year RP	$C_t$ introduced	$S_k$ with 50 year RP	$C_e$ introduced, $S_k$ altered

*Table 3. Table of the development of the snow load. RP stands for return period. The table is produced from a presentation of the development of the snow load in Vivian Meløysund's Phd (Meløysund 2010).  $S_k$  is the characteristic snow load, while RP stands for return period.*

The table shows how coefficients are introduced with new standards, and how the span of the general load/characteristic snow load increases. The return period used for calculating the load is introduced in 1979 and significantly increased from 5 years to 50 in 1999. The local adaption to climate and individual design of buildings indicate how older buildings are less adapted to their circumstances.

In Oslo, the change of the snow load standard in 2001 resulted in an increase from 2.5 to 3.5 kN/m<sup>2</sup> for areas below 150 above sea level, and from 2.5 to 4.5 kN/m<sup>2</sup> for areas between 150-250 m above sea level. This is accordingly equivalent to an increase of 40% and 80%. For some municipalities such as Namskogan, the snow load increased with 114 % in the change of the snow load standard (Standard

Norge 2008). Consequently, the severe increase of the characteristic/general snow load value has placed many older, existing buildings in the under-designed category compared to the existing design regulations.

### 2.2.2 Future climate predictions

A report from Sintef Byggforsk on request by the Directory of Building Quality, aims to predict the development of climate and vulnerability of buildings in Norway in the period of 2071-2100. Two versions of the report are issued and referred to in this thesis. Although the annual mean temperature is likely to increase for the whole of Norway, heavier snow loads are expected (Flyen et al. 2010). The report states that the warmer and wetter climate is likely to increase the occurrence of *wet winter-precipitation (våt vintervedbør)*. The term means heavy and wet precipitation occurring during winter, contributing to heavy snow loads on roofs (Kvande et al. 2011).

The figure below illustrates how change in distribution and amount of wet-winter precipitation is likely to change towards 2100.

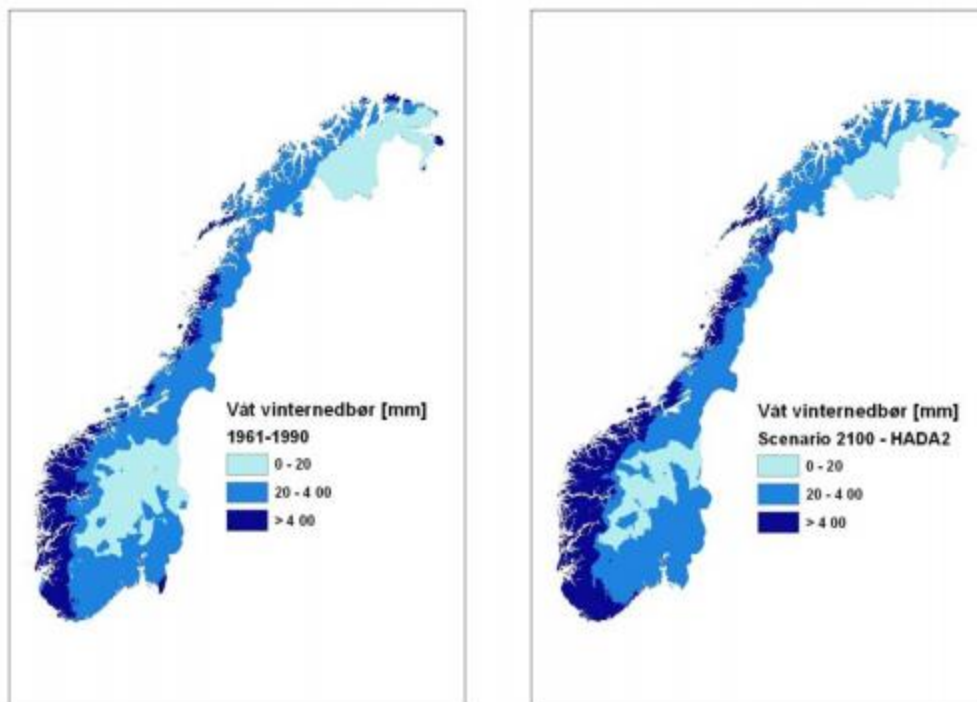


Figure 1. Wet winter-precipitation for the period 1961-1990, and a possible future scenario for year 2100. (Flyen et al. 2010)

The dispersion of wet-winter precipitation will result in a large amount of the current building stock to experience an increase in snow loads. The report provides a table indicating how many existing buildings that is likely to experience a heavy increase of wet-winter precipitation towards 2100 (see figure 2).

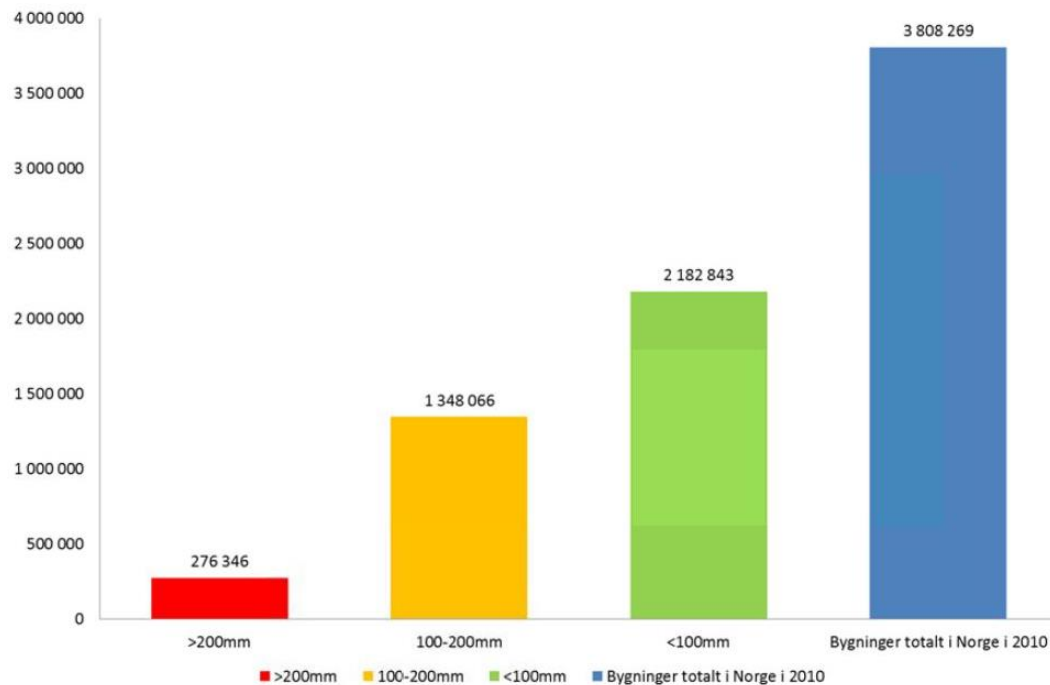


Figure 2. Total number of existing buildings in mainland-Norway affected by a change in winter precipitation towards 2100. The colors signify an increase in wet-winter precipitation arranged by amounts in mm. (Kvande et al. 2011)

The report states that around 600 000 buildings in Norway lies in an area in danger of a heavy increase in wet winter-precipitation (Flyen et al. 2010). The authors further recommend an adaptation of the snow load standard in regards to dimensioning roofs (Flyen et al. 2010):

*“The snow load standard used for the dimensioning of roofs should pay attention to future climate change. A review of this is recommended. An annex with snow loads for climate scenarios may be appropriate. It is quite clear that there must be strict requirements on the performance and design of buildings in the future. Robust constructions able to withstand heavy impacts of ice, water and snow should be chosen. The solutions must be based both on the current climate and on the future climate of the areas in question. This requires further development of instructions and empirical documentation.»*

### 2.2.3 Vulnerability of the existing building stock

As previously mentioned, the general trend of increased design snow loads have resulted in many buildings now being regarded as under-designed compared to the current design regulations. Many buildings are vulnerable to heavy snow loads, and rely on shoveling snow of the roof in a heavy snowfall scenario. This chapter investigated the reliability of the existing building stock in Norway and sheds light on previous incidents of collapse due to heavy snowfall.

In a doctoral thesis by Vivian Meløysund, the reliability of the Norwegian building stock is investigated. The thesis includes a study investigating the reliability level of 20 existing buildings in regards to snow and wind load actions (Meløysund 2010). The buildings are chosen from five high-snowfall and five high-wind municipalities in Norway. All the buildings investigated are larger buildings typically used in public, commercial or storage context. The results show that 18 out of 20 buildings have a utilization ratio higher than 1, and that 11 out of 20 have a higher utilization ratio than the load increase should imply. This means that the increases in design loads do not alone account for the under-design of 11 out of 20 buildings researched in the study. The study concludes that *“4,5% of the total bulk of buildings in Norway may have to low capacity according to current regulations.”* (Meløysund 2010).

The thesis presents a table of large buildings that have been significantly damaged or collapsed where snow has triggered or caused the damage.

Building	Type of building	County	Built (year)	Time of collapse/ damage
Hatlestrand skule	Swimming bath	Hordaland	1974	2010
Rimi, Larvik	Shop	Vestfold		2009
Gameleveien, Lørenskog	Industrial facility	Akershus		2008
Gimlemoen, Kristiansand	Sports hall	Vest-Agder		2007
Europris, Kristiansand	Shop	Vest-Agder		2007
Rudshøgda, Ringsaker	Storehouse	Hedmark		2006
Lier	Sports hall	Buskerud		2006
Skien	Barn	Telemark		2006
Ringerike ridesenter	Sports hall	Buskerud		2006
Rønholt, Porsgrunn	Barn	Telemark		2006
Øvre Mosby, Kristiansand	Barn	Vest-Agder		2006
Larvik	Industrial facility	Vestfold		2006
Stongelandet skole	Swimming pool	Troms	1971	2000
Bardufoss Samfunnshus	Community hall	Troms	1965	2000
Lenangen Skole	School	Troms	1970	2000
Målselv	Community hall	Troms		2000
Storvoll Skole	School	Nordland	1990*	2000
Tromsø Tennishall	Sports hall	Troms		2000
Løkenås-hallen	Sports hall	Akershus	1978/ 1996*	1999
Lofothallen	Sports hall	Nordland		1999
Aukra	Industrial facility	Romsdal		1996
Asker Tennishall	Sports hall	Akershus		1994
Drammen	School	Buskerud		1994
Harstad	Industrial facility	Troms		1988
Birkenes-hallen	Sports hall	Aust Agder		1987
Svelvik Karosseri	Industrial facility	Vestfold		1987
Epokehallen	Drill hall (military facility)	Troms	1982	1983
Tromsø	Industrial facility	Troms		1975

\* Year of rebuilding or reconstruction.

*Table 4. Cases of collapse as a result of major snow load (Meløysund 2010).*

The existing buildings vulnerable to heavy snow loads often have large spans and light structural materials which often have crowds of people present (Meløysund 2010). The current option for keeping such buildings safe under a heavy snow load consists of clearing snow off the roof or performing an upgrade of the structural elements of the building. It is often difficult for building owners to know when the snow load is too heavy for the buildings capacity although a guideline from the building authority has been issued. Vivian Meløysund's study highlights the severity regarding existing under-designed buildings in Norway. Few solutions for reducing heavy snow loads are available to this date.



## 2.3 The law regarding measures on under-designed structures

All building owners in Norway have to follow the rules and regulations of the Planning and Building Act(PBL). The measures performed on existing buildings have to be done in accordance with PBL. The Building Application Regulations (SAK10) serve as a supplement to PBL, elaborating how to go forth in an application process. This chapter focuses on how a measure not designed for in the original plan can be performed, and how it relates to the law.

### 2.3.1 Project classes

In Norway, buildings are put into categories depending the project complexity, difficulty and risk towards health, safety and environment called project classes (tiltaksklasser). The project classes are determinative for which measures that requires an application to be approved. This thesis will focus on buildings with a project class of 2. Project class 2 covers projects or tasks that are(Planning Application Regulations):

*a) not very complicated or have a low degree of difficulty, but in which deficiencies or errors will have moderate consequences for health, safety and the environment.*

*b) moderately complicated or have a moderate degree of difficulty, but in which deficiencies or errors will have minor to moderate consequences for health, safety and the environment.*

Smaller residential buildings are normally project class 1, while buildings such as schools, larger storage facilities, apartment blocks and work buildings are normally project class 2(Planning Application Regulations).

### 2.3.2 The Planning and Building Act

PBL explains how the building owner is responsible for the building's condition Paragraph 31-3 states that (Plan og bygningsloven):

*“The owner or the person responsible is obliged to keep structures and installations covered by this law in such a condition that there is no risk of damage to, or significant inconvenience to persons, property or the environment, and so they do not appear to spoil themselves or the relation to the environment.”*

In the case of an under-designed roof, the owner is obliged to take the necessary measures to avoid risk of damage and inconvenience to person, properties and environment. Paragraph 31-2, measures on existing buildings, describes how measures on buildings that has to be done in accordance with the law(Plan og bygningsloven 2008).

*“Measures on existing buildings must be designed and constructed in accordance with the provisions laid down in or pursuant to law. In buildings that are, or used, contrary to later adopted plan, the renovation,*

*additions, extensions, under construction, change of use or major extension or modification of previously operating is only permitted when it is in accordance with the plan.”*

However, it is written in the paragraph that the municipality may grant permission for a change of use not in compliance with the technical requirements(Plan og bygningsloven 2008):

*The municipality may grant permission for change of use and the necessary reconstruction and rehabilitation of existing buildings even when it is not possible to adapt the structure to the technical requirements without disproportionate costs, if the user changes or rebuilding is prudent and necessary to ensure appropriate use. The municipality may impose conditions in the permit. The Ministry may issue regulations to regulate the municipal right to grant permission under this paragraph.*

To get permission for a deviance from the technical regulations an application in accordance with the Building Application Regulations must be sent to the municipality.

### **2.3.3 Building Application Regulations**

The Building Application Regulations (Byggesaksforeskriften), also called SAK10, complements the Planning and Building Act, regarding building permits, quality assurance and control, supervision, and the approval of undertakings of responsibility where the rules are not followed(Planning Application Regulations 2010b).

According to Section 2-1 in SAK10, buildings in project class 2 are required to apply for a change of use if(Planning Application Regulations 2010a):

*a) structures or parts of structures are used or adapted for purposes other than those pursuant to the permission or legally established use*

*b)...*

Point b) and c) exist but is not as relevant.

Applying for a change of use is a complicated process. Section 5-4 – *Information that shall be disclosed in applications for permission for projects*, elaborates which information is relevant for an application(Planning Application Regulations 2010a). The applications shall include information of: *description of the nature of the project, the project's magnitude and degree of utilization, drawings and site plans with dimensions* and so on.

The municipality processing involves a preliminary conference with intent to clarify the project's assumptions and framework for further processing (Section 6-1). The municipality further needs to coordinate with other possible authorities (Section 6-2). The application is a bureaucratic process often time consuming for both parties involved.

## 2.4 Phase changes and energy balance of snow

Understanding the energy balance of snow and the transition between the phases of solid, liquid and vapor is essential when researching any kind of snow melt system. This chapter will explore the behavior of snow when applied heat.

### 2.4.1 The phase diagram

A phase diagram describes in which phase a material is in equilibrium, depending on temperature and pressure. If a material is in equilibrium, no phase change in the material will occur. The diagram assumes a constant volume. The curves separating the different areas represent the process of a phase change.

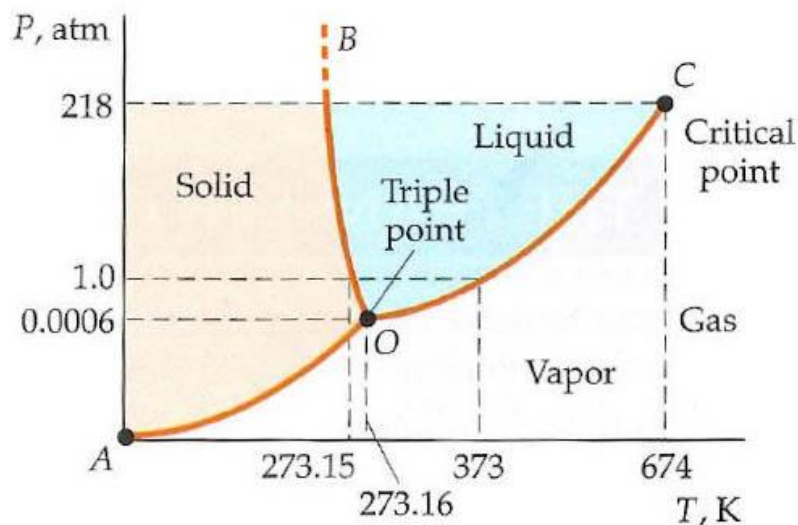


Figure 3. Phase diagram for water. Curve OB is the melting curve. Curve OA is the sublimation curve. (Tipler & Mosca 2008)

Studying the phase changes occurring at the pressure of 1 atmosphere is most relevant when investigating naturally occurring phenomena in snow. Sublimation is the process of a material transitioning directly from solid to vapor without ever existing in liquid form. The phase diagram for water shows that sublimation does not occur at temperatures below 100°C under normal atmospheric pressure. However, melting occurs at normal atmospheric pressure and temperatures.

### 2.4.2 Molecular theory

Describing the phase changes of a material through molecular theory is a useful tool for better understanding the intricate mechanics of enthalpy.

The energy used to increase the temperature of a material is energy used to increase the movement of the molecules in the material. Temperature itself is defined as the average translational kinetic energy of

molecules(Tipler & Mosca 2008). Increasing the temperature of a material is due to increased movement of molecules in the material.

However, every material has a maximum temperature for which phase they can exist in equilibrium (except the plasma phase), as described in the phase diagram. Further heating the material will not cause an increase in temperature, but the energy will be used for breaking up the intermolecular attraction. The potential energy of the material is increased, while the kinetic energy stays the same. This is the reason additional heat is needed for inducing a phase change in a material.

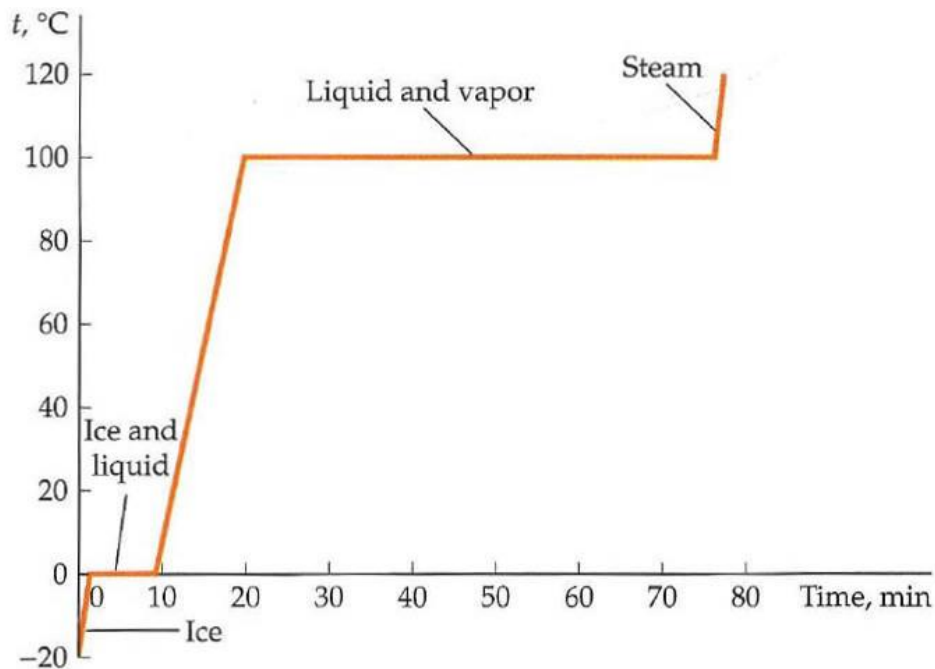


Figure 4. The diagram shows the time required for a material to go from ice at  $-20^{\circ}\text{C}$  to steam at  $120^{\circ}\text{C}$  when applying constant heat to a closed system. The temperature of the material does not increase in periods of phase transition although significant amounts of energy are applied. This energy is used to break up the molecular bonds of the water. (Tipler & Mosca 2008)

### 2.4.3 Enthalpy

Enthalpy is a measurement of energy in a thermodynamic system(Wikipedia). When applying heat to a system, the energy will either go to increasing the temperature of the system, or changing to changing the phase of the material to some extent. This subchapter presents a framework for understanding and calculating how applied heat affects the energy balance and composition of phases in a closed system.

*Specific heat capacity* is a constant describing the increase in temperature of a specific material with given mass when applying energy to the material in a closed system. The specific heat capacity constant is measured in kJ/kg\*K or J/mol. Sensible heat is a similar term, used for describing the amount of heat needed to change the temperature of a substance. Each material has a certain specific heat capacity constant, depending on how the material behaves on a molecular level. Using this constant, one can calculate the energy required for a material to heat up or cool down.

$$Q_{sensible\ heat} = mc\Delta T \quad (10)$$

$Q_{sensible\ heat}$  is the energy used [kJ]

$m$  is the mass of the material [kg]

$C$  is the specific heat capacity for the material [kJ/kg\*K]

$\Delta T$  is the difference in temperature between before and after heating[K]

Material	Specific heat capacity [kJ/kgK]
Water	4,18
Snow	2,05

Table 5. Specific heat for water and snow. The values are from (Tipler & Mosca 2008)

*Latent heat* is the heat required for inducing a phase change in the material. Instead of increasing the material temperature, the heat is used to break up the intermolecular bonds, changing the phase of the material. The unit for latent heat is [kJ/kg], and describes how many joules per kilo are required to change the materials phase. The change from one phase to another is gradual and occurs over time when heat is applied. *Latent heat of fusion* ( $L_f$ ) is the energy required for a material to transition from

solid to liquid. *Latent heat of vaporization* ( $L_v$ ) is the energy required for a material to transition from liquid to vapor. The latent heat of sublimation is the energy required for a material to transition from solid to vapor and is equal to the sum of the latent heat of fusion and vaporization. For water, it is equal to 2830 kJ at 0° (Oke 1987).

One can calculate the energy required for a phase change by multiplying the latent heat constant with the mass of the material.

$$Q_{\text{Latent heat}} = mL_{\text{phase}} \quad (11)$$

$Q_{\text{Latent heat}}$  is the energy required to induce the phase change [kJ]

$m$  is the mass of the material [kg]

$L_{\text{phase}}$  is the latent heat constant for the specific material and phase change [kJ/kg]

Phase change	Latent Heat constant [kJ/kg]
Fusion (0 °C)	333,5
Vaporization (100 °C)	2257
Sublimation (0 °C)	2830

Table 6. Latent heat constants for different phase changes in water. (Oke 1987; Tipler & Mosca 2008)

Sublimation requires the most energy of all phase changes in water. It takes 8,5 times as much energy to sublimate water as to melt it at 0°C. Another way to put it is that you will have 8,5 times less ablation when sublimating compared to melting for the same energy input.

Figure 4 presented in 2.4.2 have plateaus of constant temperature during the phase changes. The energy amounts needed to induce the phase change is determined by the latent heat constant of the material. The composition of the material changes with time applied heat. The more heat applied, the higher the concentration of the coming phase. The theory coheres with that of the phase diagram,- a material will only exist in equilibrium between the temperatures and pressures of the phase change marked by the curves.

## 2.5 Sublimation of snow

Sublimation of snow is a natural occurring phenomenon, taking place almost invisibly. Sublimation occurs to some extent at all snow covered areas, but is documented to the largest extent for topographies such as forest canopies, alpine sites and glaciers. No previous research on purposely inducing sublimation in snow was found during the period of this thesis.

### 2.5.1 Principles

Sublimation in snow occurs when there is a difference in the *partial pressure* [Pa] of water vapor between the snow and the air. Partial pressure is defined as the pressure a gas would exert alone, without the presence of other gases, in a closed system (Tipler & Mosca 2008). If the partial pressure of vapor is higher in the pores of the snow than in the air, a moisture flux occurs, transferring humidity from snow to air. This is sublimation. If the partial pressure is higher in the air than in the snow, humidity will transfer from the air to snow, depositing water at the snow surface. This phenomenon is called *condensation*.

The difference in partial pressure is always the driving force for humidity transport. The partial pressure of water vapor in air has a linear relationship with *specific humidity* [kg water/kg air], which is the standard unit used for calculating and presenting sublimation amounts. Specific humidity can be calculated by looking at the psychrometric chart.

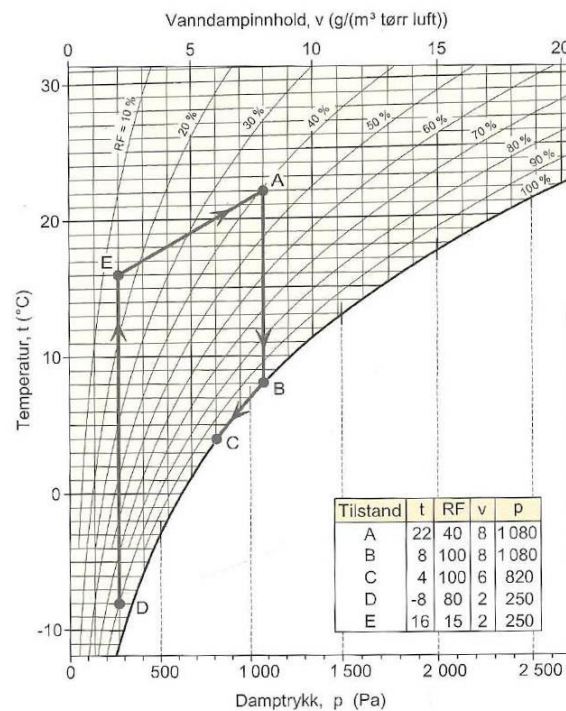


Figure 5. The psychrometric chart shows the relation between partial pressure, specific humidity, relative humidity and temperature. (Edvardsen & Ramstad 2010)

Humidity and temperature gradients is a useful way for describing when sublimation typically occurs in a snowpack. The gradients describe the change of humidity or temperature through the snowpack. A gradient is based on the boundary conditions on both sides of the snowpack, and how the conditions change through a cross section of the snowpack. In general, the slope of a gradient (assumed linear) is calculated by dividing the difference in boundary conditions with the thickness of the snowpack.

$$\text{TempGradient} = \frac{dT}{dx} = \frac{T_2 - T_1}{dx} \quad \text{HumidityGradient} = \frac{dS}{dx} = \frac{S_2 - S_1}{dx} \quad (12)/(13)$$

$T_2, T_1$  is the temperature boundary conditions [ $^{\circ}\text{C}$ ]

$S_2, S_1$  is the humidity boundary conditions [ $\text{g}/\text{kg}$ ]

$dx$  is the thickness of the snowpack [ $\text{m}$ ]

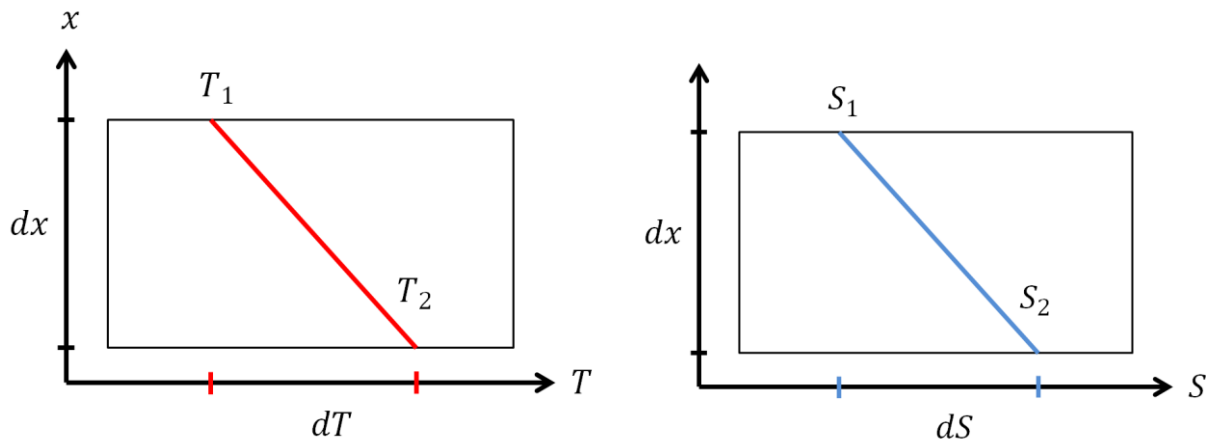


Figure 6. Illustration of a temperature gradient (left) and a humidity gradient (right).

According to the phase diagram for water, sublimation does not occur under normal atmospheric pressure. However, differences in temperature across the small thickness of a snow grain can cause snow to sublime instantly. *Temperature gradient metamorphism* describes the metamorphism of snow under a constant temperature gradient (Male 1980), typically caused by heat flux through the ground. Male (1980) puts it eloquently:

*“If it is assumed that grains in a layer near the ground have a higher temperature, then water will sublime from the top of these grains, move across an air space, and condense on the grains immediately above. This process repeats itself between adjacent layers of grains as long as the temperature gradient exists.”*

For this reason, sublimation can take place in snow at temperatures below zero.



### 2.5.2 Conditions conducive for sublimation

For sublimation to occur, a humidity gradient between the snowpack and the atmospheric boundary layer must be present. Everything that is able to affect the humidity levels of the snow or air is considered a factor influencing the occurrence of sublimation.

Previous studies (Hood et al. 1999; Meiman et al.) have documented a diurnal periodicity of sublimation. The snow is warmed during the day by increased air temperatures or solar radiation. The specific humidity of the pore spaces in the snow rises, enhancing sublimation rates. However, the specific humidity of the air is usually lower at nighttime compared to daytime, creating a larger potential of high sublimation rates if able to induce a temperature gradient in the snow.

Wind speed seems to work as an accelerator for the sublimation process. Hood et al.(1999)reported that a strong turbulent mixing is necessary for sublimation to occur. One can think of wind as a contributor for mixing the humid air layer at the snow surface with the less humid atmospheric air. Wind transport the humid air away from the snow, preventing the air from getting saturated with moisture, working as a sort of accelerator for the process of sublimation. In the study at Niwot Ridge, the sublimation rates measured was most correlated with high wind speed, out of several factors such as air temperature, air humidity and solar radiation(Hood et al. 1999).

The microstructure and density of the snow strongly influences to potential of sublimation and is further discussed in 2.5.4.

### 2.5.3 Documented sublimation rates

There is a wide range of studies documenting the sublimation rates [mm/day] and net sublimation amounts [% of total SWE] occurring at various types of topographies. The amounts are given in mm SWE (snow-water-equivalent), describing the water equivalent of the snow sublimated. If 1 mm SWE is sublimated, this will equal 1 kg/m<sup>2</sup> of snow transported into the atmosphere.

Previous studies documenting sublimation use different methods and the results also differ a lot in the documented amounts. Some methods applicable for estimating sublimation are presented in the next subchapter.

A table by Jackson & Prowse (Jackson et al. 2009) show the different vapor losses from a wide range of studies. The different studies use different methods. The results differ from negligible amounts to impressive numbers up to 45-60% of the seasonal snow precipitation.

Table VI. Selected studies and methods investigating vapour losses from snow

Study	Methods	Site type	Sublimation/Evaporation
Bernier and Swanson, 1993	B.A., Gr	Forest and Open	0.25–1.07 mm d <sup>-1</sup>
Doty and Johnston, 1969	Gr	Open	0.15 (January) –1.56 (April) mm d <sup>-1</sup>
Fassnacht, 2004	B.A.	Various sites in USA	0.23–0.67 mm d <sup>-1</sup>
Fox <i>et al.</i> , 2008	SNTHERM	Glacier	Negligible
Golding, 1978	B.A.	Sub-alpine forest	1.2 mm d <sup>-1</sup> (1975), 2.0 mm d <sup>-1</sup> (1976)
Gustafsson <i>et al.</i> , 2001	SNTHERM	Open fields	8% of total SWE losses
Hood <i>et al.</i> , 1999	A.P.	Alpine	0.9–1.8 mm d <sup>-1</sup>
Kaitera and Teräsvirta, 1972	B.A.	Boreal forest	0.35 (sub-canopy) –0.45 (open) mm d <sup>-1</sup>
Kaser, 1981	Gr	Alpine	Mean 0.25 mm d <sup>-1</sup> , maximum 2.0 mm d <sup>-1</sup>
Koivusalo and Heikinheimo, 1999	SNTHERM, UEB	Boreal forest	Negligible
Liston and Sturm, 2004	Review	Tundra/arctic	35–50% of annual arctic precipitation
Lundberg and Koivusalo, 2003	SC	Boreal forest	11–30% intercepted snow
Marks and Dozier, 1992	B.A.	Alpine	Mean 2 mm d <sup>-1</sup>
Martinelli, 1960	Gr	Alpine	+/-0.67 mm d <sup>-1</sup>
Meiman and Grant, 1974		Alpine, forest, open	45–60% snow season precipitation
Molotch <i>et al.</i> , 2007	E.C.	Sub-alpine forest	0.41–0.71 mm d <sup>-1</sup>
Nakai <i>et al.</i> , 1999a	E.C.	Boreal forest canopy	1.2 mm d <sup>-1</sup> (snow covered)
Nakai <i>et al.</i> , 1999b	E.C.	Boreal forest canopy	0.6 mm d <sup>-1</sup> (n = 60)
Parviainen and Pomeroy, 2000	B.A., E.C.	Boreal forest	0.16–0.72 mm d <sup>-1</sup>
Pomeroy <i>et al.</i> , 1997	SC, model	Forest/tundra	37 mm/winter (28% total SWE)
Pomeroy <i>et al.</i> , 1998	B.A.	Boreal forest	0.41–1.88 mm d <sup>-1</sup>
Pomeroy and Essery, 1999	E.C.	Prairie	1.8 mm d <sup>-1</sup>
Rylov, 1969	Gr	Open (semi-desert)	0.08 (January) –0.6 (April) mm d <sup>-1</sup>
Schmidt <i>et al.</i> , 1998	B.A., Gr	Sub-alpine forest	0.61 (south), 0.43 (north) mm d <sup>-1</sup>
Storck <i>et al.</i> , 2002	Gr, SC	Sub-alpine forest	100 mm/winter, <1 mm d <sup>-1</sup>
Suzuki <i>et al.</i> , 1999	B.A., Gr	Larch forest	0.55–0.96 mm d <sup>-1</sup>
Suzuki <i>et al.</i> , 2006	B.A., SNTHERM	Taiga, larch forest	1.0 (forest), 2.0 (open) mm d <sup>-1</sup>
Zhang <i>et al.</i> , 2003	B.A., Gr	Taiga	0.2–1.0 mm d <sup>-1</sup>
Zhang <i>et al.</i> , 2004	B.A., Gr	Taiga, larch forest	0.22–0.32 mm d <sup>-1</sup>
Zhang <i>et al.</i> , 2008	A.P., E.C.	Flat plain, boreal forest	0–1.2 mm d <sup>-1</sup> (~20% total SWE) 4.8 (forest), 5.9 (open) mm d <sup>-1</sup>
		Aspen stand	0.12 (January)–1.05 (April) mm d <sup>-1</sup>
		Conifer stand	0.33 (February)–0.48 (April) mm d <sup>-1</sup>

Method of estimation abbreviations: A.P., aerodynamic profile; B.A., bulk aerodynamic; E.C., eddy covariance; Gr, gravimetric, lysimeter; SC, snow course.

Table 7. Table presenting sublimation amounts documented in previous studies (Jackson et al. 2009).

#### 2.5.4 Metamorphism in snow

Snow microstructure and density are highly determinative for the potential of sublimation. Investigating how the microstructure of natural deposited snow evolves over time provides insight into which conditions are conducive for sublimation. Metamorphism in dry snow is categorized into two main categories; *equitemperature metamorphism* and *temperature gradient metamorphism*. Equitemperature metamorphism is not discussed, due to temperature gradient metamorphism being most relevant for this thesis.

As previously explained, the temperature gradient metamorphism takes place when snow covers is subjected to a constant temperature gradient. Snow is a highly isolating material with thermal conductivities as low as 0.025 W/mK (Cote et al.(2012) cited by Nuijten et al. 2016 p.263). For comparison, mineral wool typically has a value of 0.037 W/mK (Edvardsen & Ramstad 2010). The isolating effect of snow combined with the heat emitted through the ground cause temperature gradients across the snow pack affecting the microstructure of the snow. According to Male (1980), a constant temperature gradient will eventually create crystal growth in the snow cover, depending on grain size, density and the magnitude of the gradient. Characteristic crystal with sharp edged, corners and flat surfaces called *Depth hoar* crystals are typically formed under the influence of a temperature gradient. Snow close to the ground is sublimated and deposited further up in the snowpack, creating the characteristic looking depth hoar crystal.

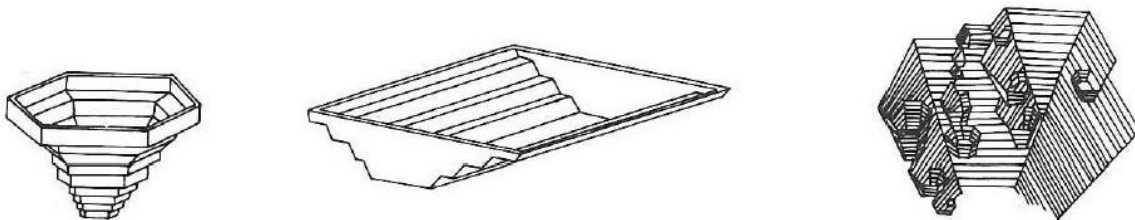


Figure 8. Illustration of depth hoar crystals.(Müller 1968)

A diagram from Schmidt 1972 explains the relation between sublimation rates, particle diameter and ambient temperature for a single ice particle. The diagram show how “high temperatures” of the ice is conducive for sublimation. The particle size is also strongly determinative for the possible sublimation amounts. The larger the diameter of the crystal, the higher the sublimation rate.

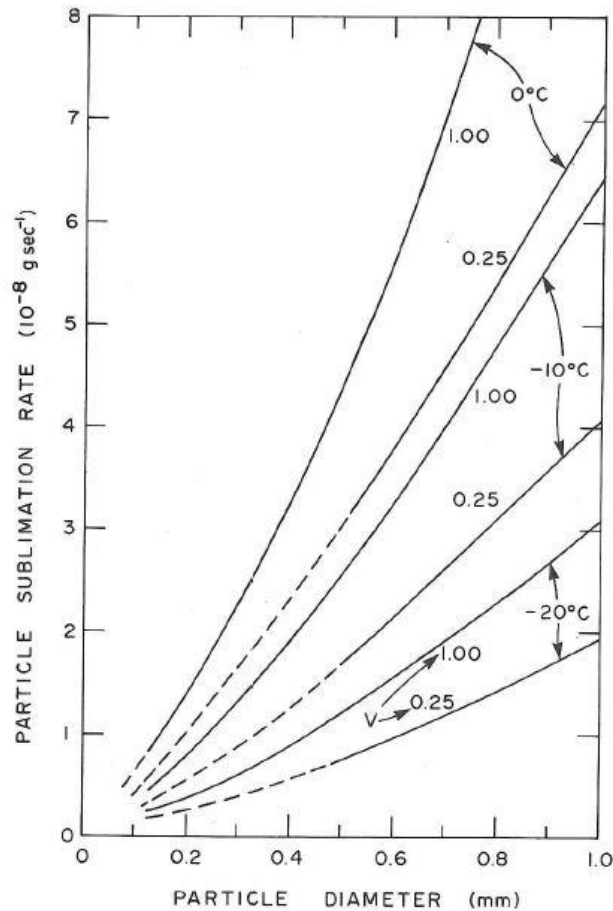


Figure 9. Sublimation rates as a function of particle diameter and temperature. (Schmidt 1972)

Metamorphism of snow strongly influences the snow grain size and the composition of the snowpack. The potential of sublimation is dependent on the snow microstructure as shown in the figure. It is sure that metamorphism of snow affects the potential of sublimation, but the subject is complex. The investigation of how snow metamorphism affects sublimation is limited in this thesis.

### 2.5.5 Estimating sublimation with the Bulk Aerodynamic Flux Method

There are several methods for quantifying surface sublimation for snow covers. Such methods are the aerodynamic profile method(AP), the eddy covariance method(EC) and the bulk aerodynamic flux method(BF). A scientific paper was published by Sextstone et al.(2016) comparing the different method's abilities to quantify sublimation. The paper concluded that EC and BF methods are "superior for estimating surface sublimation in snow covered forested openings"(Sextstone et al. 2016).

The bulk aerodynamic flux method is meant for and works best for large, uniform, flat surfaces, but has in later years proven to be applicable in complex terrain with non-ideal field situations(Moore 1983). However, the method assumes uniform heat fluxes, and must therefore be viewed with a high degree of uncertainty when applied to areas with a heterogeneous/non-uniform heat flux. This thesis will further investigate the BF-method's applicability for estimating sublimation on a small, local area.

The BF method calculates latent heat flux using input data from snow surface temperature, air temperature, relative humidity, wind speed and barometric pressure. The formula for latent heat flux is stated below (Sextstone et al. 2016).

$$Q_{BF} = \rho L_s C_E u_r (q_s - q_r) \quad (14)$$

$Q_{BF}$  is the latent heat flux [ $W/m^2$ ]

$\rho$  is the density of the air [ $kg/m^3$ ]

$L_s$  is the latent heat of sublimation [ $J/kg$ ]

$C_E$  is the transfer coefficient for latent heat

$u_r$  is the wind speed [ $m/s$ ]

$q_s$  is the specific humidity of the snow [ $kg/kg$ ]

$q_r$  is the specific humidity of the air [ $kg/kg$ ]

The transfer coefficient for latent heat ( $C_E$ ) is estimated with a complicated calculation, using elements of Monin-Obukhov Similarity Theory.  $C_e$  is calculated based on roughness lengths for wind speed ( $Z_0$ ), humidity ( $Z_q$ ) and the atmospheric stability parameter ( $\delta$ ). According to Andreas (1987), the factor is "almost always between  $1,0 \cdot 10^{-3}$  and  $1,5 \cdot 10^{-3}$ ".  $C_E$  is regarded as the greatest uncertainty in the BF method (Sextstone et al. 2016).

For calculating the sublimation rates from the latent heat fluxes, the formula below is used (Oke 1987).

$$S_R = (Q_{BF}/L_S) * 3600 \quad (15)$$

$Q_{BF}$  is the latent heat flux [ $W/m^2$ ]

$L_S$  is the latent heat of sublimation [ $J/kg$ ]

$S_R$  is the sublimation rate [ $kg/m^2h$ ]

## 2.6 PV systems

### 2.6.1 Function and configuration

A Photovoltaic cell, often referred to as a solar cell, is a device for turning the energy radiated from the sun into electricity. Photons from the sun hit the cell, exciting electrons in the cell. The charge is separated, creating a negative charge at the front of the cell and positive charge at the back of the cell. This occurs in the layer of doped silicon, designed to separate charge when subjected to solar radiation. The front layer is of the n-type silicon while the back is of the of p-type silicon. Between the layers is a junction, designed for keeping the charge separated. Strips of metal at the front layer are used lead the current in the cell. The separated charge creates an electric potential between the front and the back of the module, and will induce a current in the metal strips of the cell. A complete module constitutes of several PV-cells arranged in a certain electrical configuration with additional components: a front glass layer, an encapsulant front/back layer, a protective layer at the back, an aluminum frame and a junction box. The *junction box* is where the module is connected, and where the *bypass diodes* are installed.

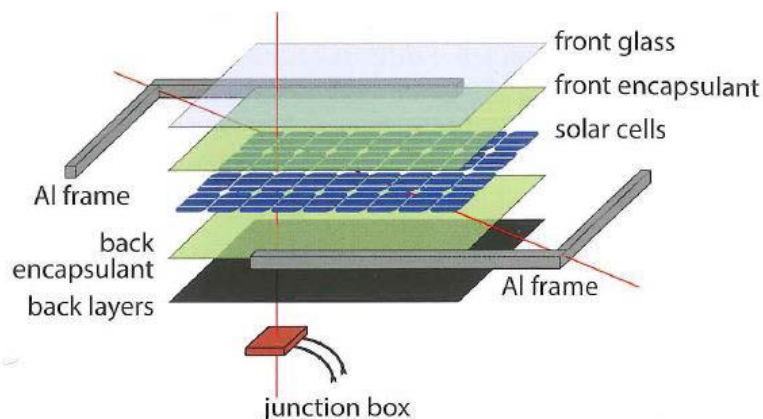


Figure 10. The composition of a module. (Smets et al. 2016)

It is important to differentiate between a PV module, a solar panel and a PV array. A PV module constitutes of several cells electrically connected together in a series and/or parallel configuration. The typical size of a module is 1.6 m x 1.0 m. Several modules electrically connected together on one supporting structure make up a solar panel. A PV array consists of several solar panels connected together (Smets et al. 2016).

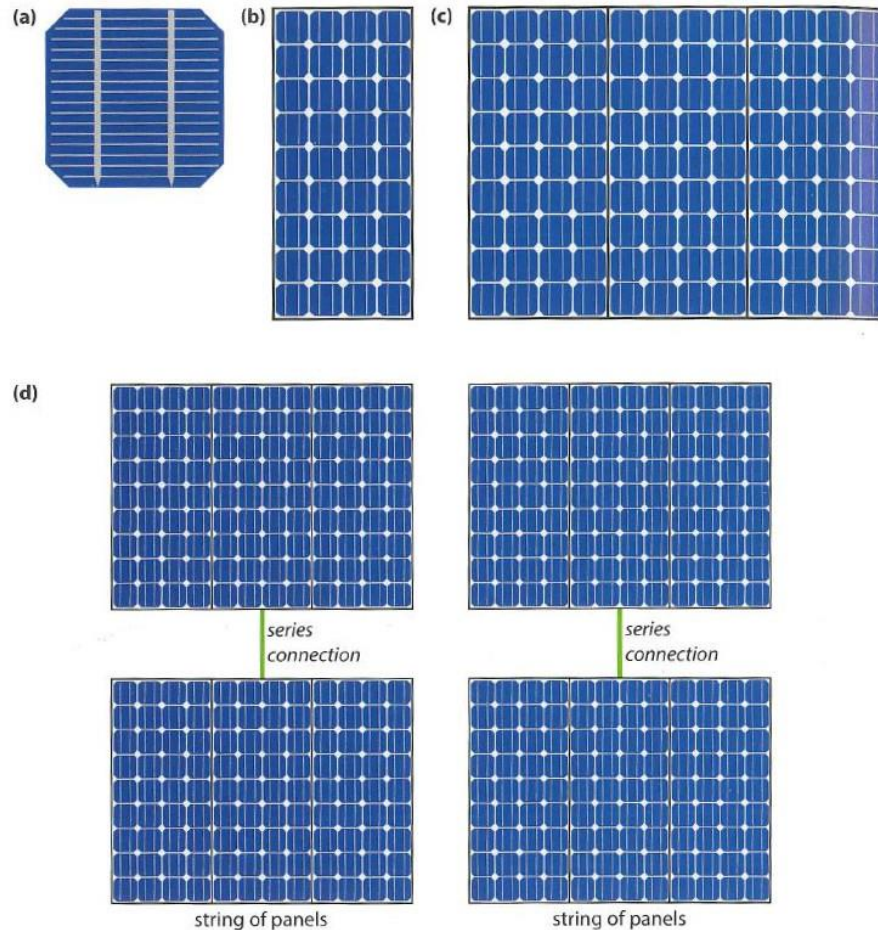


Figure 11. The composition of a PV-system. A) is a solar cell, b) is a PV-module, c) is a solar panel and d) is a PV-array. (Smets et al. 2016)

There are several ways of connecting the cells together in a module. Typically, strings of series-connected cells are connected in parallel. The number of cells connected in a string varies, but 10-30 cells per string, with 2-6 strings is a quite normal configuration. The electrical configuration is determinative for the modules behavior, and significantly influences how the module reacts to shading problems, soon to be explained.

In a series configuration, the current generated is limited by the cell with the lowest current (Smets et al. 2016). This poses a problem when a single cell is dysfunctional or shaded, limiting the generated power for the whole string. A non-functioning cell not only limits the power output, but it might induce reverse current internally in the string. The electric potential is higher for the cells working optimally, while the non-functioning cell has a lower or a non-existent electric potential. The voltage varies throughout the string, causing the current to respond thereafter. Reverse current dissipates energy instead of producing, and heats up the area subjected to the reverse current. This is called *reverse bias* and is the cause for *hot spots*; abnormal high cell temperatures causing problems such as material cracks, increased degradation



and junction breakdowns(Smets et al. 2016). Hot spots is one thing, but the general temperature of a module is also strongly determinative for the efficiency. Acciani et al.(2010) stated that: *“Efficiency depends strongly on the temperature of the PV Modules and an overheating causes decrease of the produced energy”*.

*Bypass diodes* only allow current to pass through in one direction. Bypass diodes are necessary in PV-modules due to its ability to prevent the current from running in reverse. Bypass diodes are usually connected for each string of cells in a module. The diode prevents the reverse current, but in addition stops the power production for the whole string. This means that if one cell in a string of 20, is shaded to a degree where reverse-bias would have occurred, the power production is stopped for the whole string due to the bypass diode. For a module with the typical configuration of series connected cells, a simple soil stain on one cell can stop the power production for the 20 cells connected in the same string.

## 2.6.2 PV-heating systems

PV-modules are installed to generate electricity from solar radiation. However, sending current back into the PV-modules will produce heat at the module surface. This phenomenon allows for new applications of a PV-system. Companies as Innos and KEI Solar (Innos 2017; KEI Solar 2017) deliver complete systems for clearing snow off roofs by sending current back into the PV-modules. Tesla's Elon Musk recently announced on twitter that their solar tiles can incorporate heating elements to "*clear snow of roofs and keep generating energy*" (Elon Musk 2016), although it is still somewhat unclear if this means sending current back into the solar tiles or incorporating heating cables in the roof.

The idea is relatively new and the solutions for the cause differ. KEI Solar and their "HAIN system" rely on the panels being tilted at an angle of 15° or higher, causing an "avalanche effect", sliding the snow off the modules. This clears the modules of snow, allowing for power production in times of seasonal snow covers. However, it does not reduce the snow load in a significant matter unless the system covers the complete area of a sloped roof, sliding the snow onto the ground. Otherwise, the snow will be slid onto the roof, leaving the load approximately the same.



Figure 12. The HAIN system covering the complete area of a sloped roof.

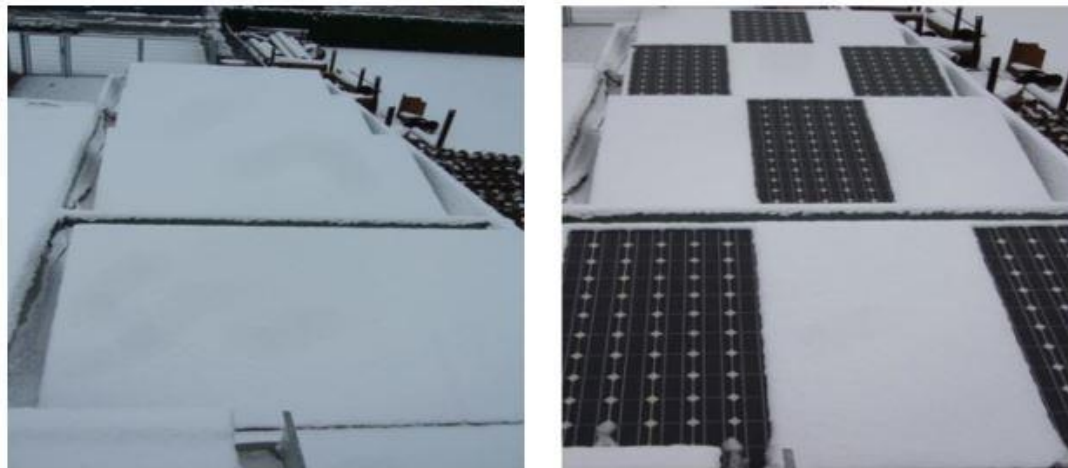


Figure 13. The HAIN system installed at a flat roof. The heat applied at the module surface slide the snow towards the lower end of the module, clearing the surface, although not necessarily reducing the load.

The Innos “*Weight Watcher*” (Innos 2017) system relies on modules assembled on a flat roof with a low angle tilt. It is this system that is tested and analyzed in this thesis. For the Weight Watcher system, the intent is not slide the snow off, but to gradually melt or sublimate it. The system is designed to reduce the load, not to clear the module surface from snow. The Weight Watcher system relies on load sensors installed at the modules frame to measure the load on top of the modules. Several modules with load sensors across the roof register the experienced snow load. When the load reaches a certain limit, the system is activated, melting the snow until it reaches satisfying levels – thereof the name “Weight Watcher”. The company thought this system could be applicable for under-designed flat roofs unable to handle the snow load and/or the weight of a PV-system. The weight watcher system intends to compensate for the weight of the modules by reducing the snow load when required; enabling under-designed roofs to install PV-systems.



*Figure 14. The left picture shows how the Weight Watcher system is assembled. A large part of the roof surface is covered with modules. The modules have a low angle tilt preventing the snow from sliding off. The picture is a 3D model of the roof made from drone pictures produced in this thesis. The right picture shows the load sensor installed at the frame of the modules.*

PV-modules produce DC current. For the current to be applied to the grid, inverters are used, converting the DC to AC. For a PV-heating system, the current applied to the modules need to be DC. The HAIN system and the Weight Watcher functions by using rectifiers to convert AC to DC before applying power to the modules. New products made for optimizing energy storage combines inverters and rectifiers in one unit, allowing for converting the current both ways (Eltek ; Ferroamp). Such products can be implemented in a PV-system to accommodate the “heating mode”. Apart from the rectifiers and perhaps a customized drainage system, a PV-system capable of running in heating mode is essentially installed exactly the same as a normal PV-system.

### 2.6.3 PV-systems and snow

Snow poses a problem for PV-systems located in areas with colder climates. Snow reduces energy production during winter, non-uniform snow loads damage modules by bending frames and breaking glass (Mathiak et al. 2016) and generally increase the mean degradation rate (Köntges et al. 2016).

A homogeneous full-covering snow layer with substantial thickness will obviously prevent a PV-system from generating power due to the absorption and reflection of solar radiation. Low snow depths allows for some light to pass through, making power production possible. A partial snow cover is also problematic due to the configuration of series connected cell. For a string of cells to function properly, all of the cells need to have an equal exposure to sunlight as. If one cell is shaded by a partial snow cover, the electric potential will be unevenly distributed in the string as explained in 2.6.1. If severe enough, the bypass diode will block the current for the complete string, preventing reverse current and possible heat problems. The loss in power gains is therefore not proportional with the area of the snow surface covering the modules with the series-connected cell configuration.



*Figure 15. Partially snow covered modules. (Drews 2017)*

#### 2.6.4 Thermography of PV modules

According to Acciani et al. (2010), infrared analysis of PV-system is a sufficient way of documenting the systems state of health and further helps to evaluate if maintenance is needed. The International Electrotechnical Commission (IEC) provides a standard for an infrared inspection of modules. The standard states that (IEC 2009):

*“The purpose of an infrared (IR) camera inspection is to detect unusual temperature variations in operating PV modules in the field. Such temperature variations may indicate problem within the modules and/or arrays, such as reverse-bias cells, bypass diode failure, solder bond failure, poor connections and other conditions that lead to localized high temperature operation.”*

The standard further elaborates that it is anomalous temperature variations across a module or string that is of interest. Absolute temperature reveals little about a modules state of health, due to the variation in temperature at the module surface during the course of a day. The standard states that

*“array temperature is a function of irradiance, wind speed and ambient temperature, which vary significantly throughout the daylight hours”*

The temperature for a healthy module should be quite uniform. Hot spots are unwanted areas of high temperature, indicating dysfunctioning cells. It is normal for the PV-modules to have a temperature gradient towards the edges and supports. Bypass diodes and cable connections should also be checked for temperature anomalies (IEC 2009).

A practical guide to solar panel thermography issued by Testo (2014), illustrate how typical defects are visible with an infrared camera.

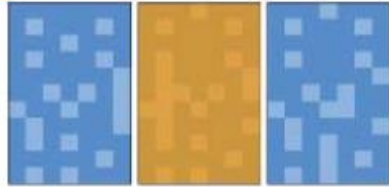
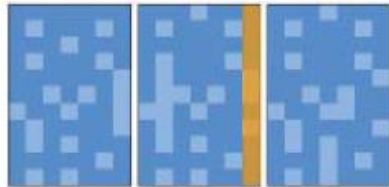
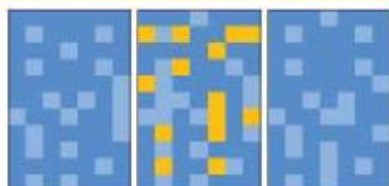

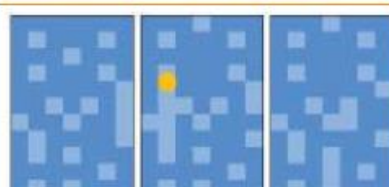
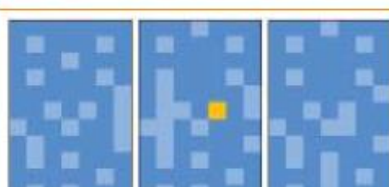
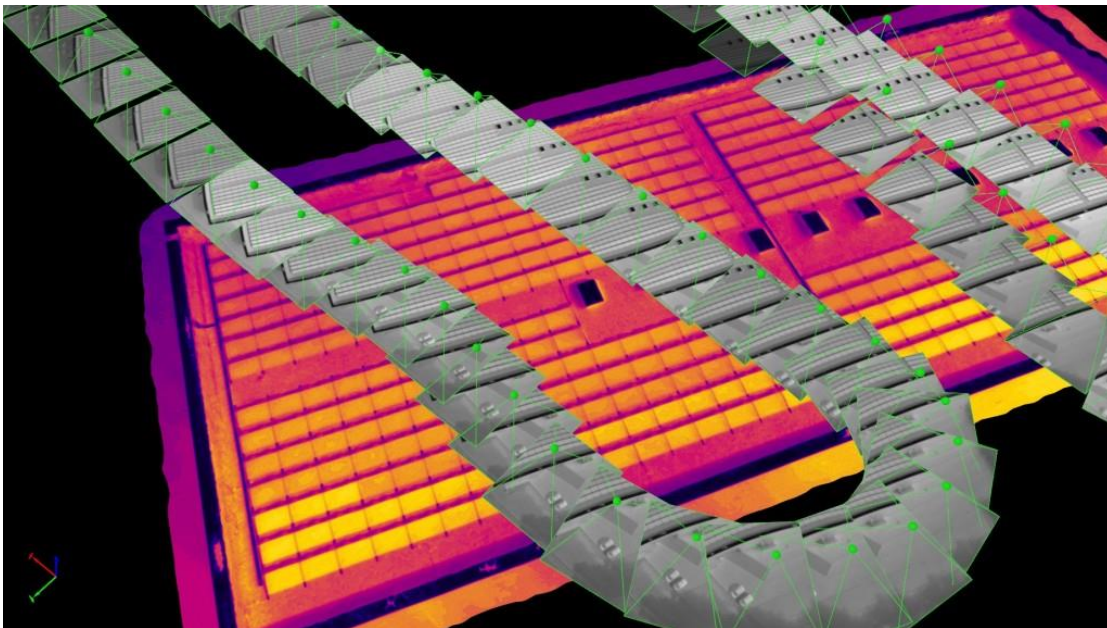
Solar panel representation	Description	Possible defects
	Panel overheating as compared with the other cells.	Panel is not working.
	Overheating pattern for a string of cells.	Short circuit in a cell string.
	"Patchwork pattern" where individual cells are randomly distributed and significantly hotter.	Panel is not working.
	Significant overheating of a part of a cell.	Cell rupture.
	Uneven heat pattern or overheated at specific points.	Cell crack or other impediment.
	Overheating of a single cell.	Undetermined.

Figure 16. Infrared illustration of various PV-module defects

This diagram can be used for detecting typical defects in infrared pictures. Comparing the defects illustrated at the diagram with actual infrared pictures of PV-modules can help indicate possible problems so further inspection can be performed.

An infrared analysis of a PV-system can be done with a handheld camera or using a camera mounted on a drone. New drones with infrared cameras pre-installed opens for a more accessible way of producing thermograms of PV-systems(DRONEexpert.nl). There are several advantages of inspecting a PV-system with a drone compared to with a handheld camera. Testo (2014) recommends an angle of 60-90° between when taking infrared pictures of PV-modules. The reflectance of the modules can pose problems for lower angles, viewing temperatures of the surroundings. Drones allow for a flexible adjustment of the angle between the module and camera, favorable for thermography. Producing *infrared maps* with photogrammetric software such as Pix4D(Pix4D 2017), allows for documenting large areas at a relatively short time interval. With an infrared map, it is easy to orientate and tell the modules apart. Handheld thermography of large PV-system demands for comprehensive orientation and logging of which module is where. Drone based inspection serves as a faster of inspecting and more user friendly way of presenting the results.



*Figure 17. Illustration of how an aerial inspection of a PV system can be performed. The drone flies over the PV-system in a predetermined flight pattern while taking infrared pictures. A map can be produced from the individual pictures using photogrammetric software (Pix4D & Maeder 2017).*

The measured radiation from an infrared camera does not only depend on the temperature of the object, but also from sources such as reflected radiation from surrounding objects and atmospheric transmission, see figure 13. The emissivity of the object of interest is also of great importance. Such factors influence the result and need to be compensated for by calibrating the camera or by using correction factors of the produced result.

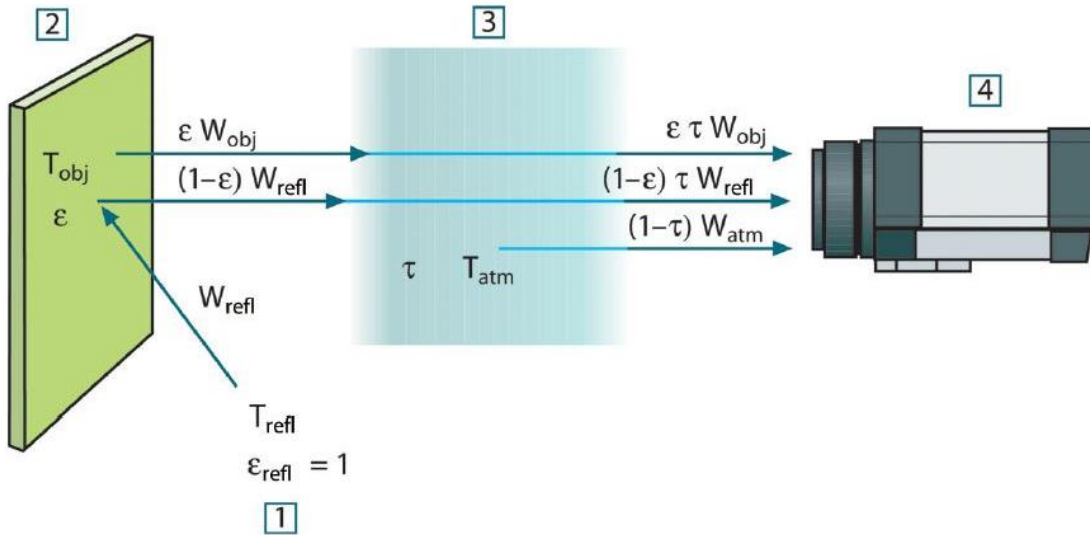


Figure 18. Illustration of all the radiation received by a camera. 1. Is radiation from the surroundings, 2. Is from the object, 3. Is from the atmosphere, and 4. Represents the camera itself. (FLIR 2011)

The figure shows how radiation from different sources other than the object of interest can influence the infrared wavelengths received by the camera. An equation of the radiation received by the camera allows for estimating the influence of disturbing radiative sources (FLIR 2011).

$$W_{tot} = \epsilon \tau W_{obj} + (1 - \epsilon) \tau W_{refl} + (1 - \tau) W_{atm} \quad (16)$$

$W_{tot}$  is the radiation received by the camera

$W_{obj}$  is the radiation from the object of interest

$W_{refl}$  is radiation from reflection at the object surface

$W_{atm}$  is radiation from the atmosphere

$(1 - \epsilon)$  is the reflectance of the object

$(1 - \tau)$  is the emittance of the atmosphere.



An infrared camera use theoretical principals from Stefan Boltzmann’s law. Stefan-Boltzmann’s law provides a framework for calculating the radiated effect based on the temperature of an object. The formula below is used for calculating energy exchange between objects in thermal equilibrium, radiating and absorbing energy at the same rate (Tipler & Mosca 2008).

$$W = e\sigma AT^4 \quad (17)$$

*W is the radiated/absorbed energy [W]*

*e is the emissivity of the object.*

*$\sigma$  is Stefan Boltzmann constant equal to  $5,6703 \cdot 10^{-8}$  [W/m<sup>2</sup>K<sup>4</sup>]*

*A is the area of the measured object with equal temperature [m<sup>2</sup>]*

*T is the temperature of the object [K]*

For objects not in thermal equilibrium, the radiated or absorbed energy can be calculated with the formula below (Tipler & Mosca 2008):

$$W = e\sigma A(T^4 - T_0^4) \quad (18)$$

Here *T* is the temperature of the object, while *T*<sub>0</sub> represents the temperature of the surroundings or another object. Knowing the temperature of the surroundings and the temperature of the object, the interchanging radiated effect can be calculated. If *T* > *T*<sub>0</sub>, heat is being radiated from the object to the surroundings. If *T* < *T*<sub>0</sub> heat is being absorbed by the object from the surroundings.

The emissivity of a radiating surface is a dimensionless quality depending of the composition of the surface object(Tipler & Mosca 2008). The emissivity describes to which degree an object absorbs and reflects radiation. If an object has an emissivity of 1, then the received radiation from the object is representable for the objects true temperature. This is called a blackbody and represents an ideal radiator(Tipler & Mosca 2008). If the object has an emissivity close to 0, then the received radiation is reflected to a large degree and is therefore little representable as the objects true temperature.

Emissivity of PV-modules differs from each single product. Fuentes et al.(1987) has estimated the emissivity value of 4 different modules to be between 0,83-0,87. A high emissivity value is favorable in PV-modules. An emissivity value close to one implies that more of the sunlight is absorbed, enhancing

the energy production of the module. A high emissivity value is also favorable when using an infrared camera, due to less reflected disturbing radiation from the surroundings. Local differences of emissivity do occur, but when observing a system with an IR-camera with angles above 40°, the local differences across the PV-plant are negligible (Buerhop-Lutz et al. 2011).

Atmospheric transmission in the infrared specter is a measure of the radiated heat of the atmosphere itself. Even though air exists in a gaseous state, it absorbs and emits radiation and is therefore considered as an influential factor in thermography. The influence of atmospheric transmission is determined by the air temperature, the relative humidity and the distance between the object and the camera (FLIR 2011). Compensating for the influence of atmospheric transmission can be done by adjusting the results in a software.

### 3. Method

The main problem stated in the thesis is best answered through empirical research and analysis of the results. Field measurements of PV-modules in heating mode under varying climatic conditions were the preferred method, which was strived for to accomplish. This chapter explains the measurements, modelling and analysis performed in this thesis.

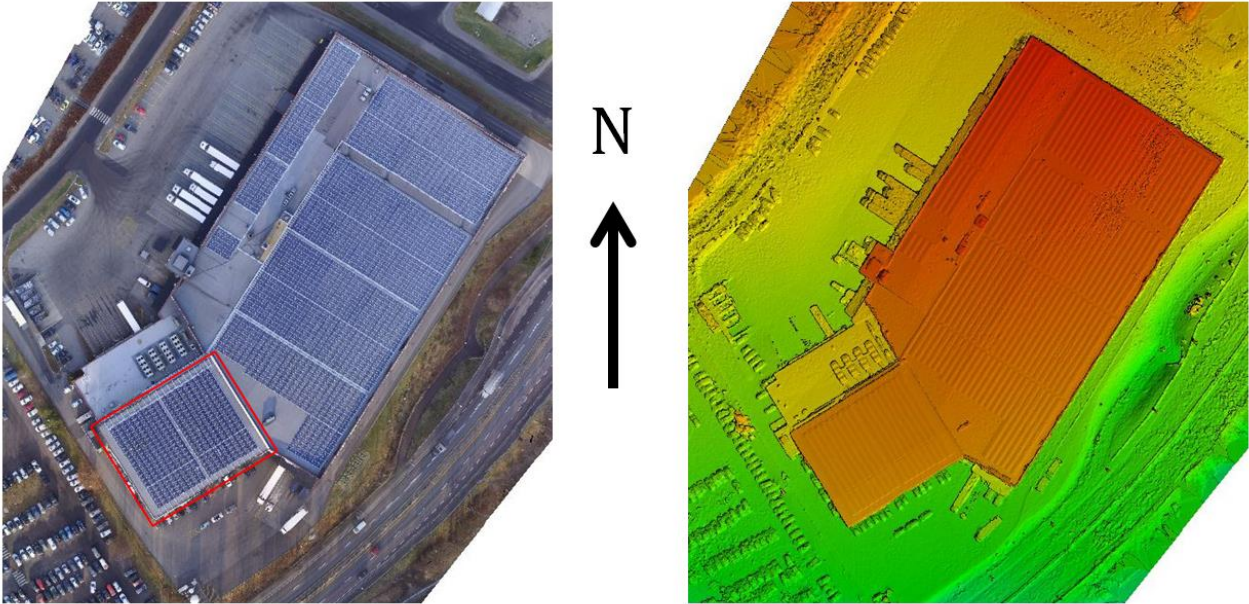
#### 3.1 The ASKO Roof

The main problem stated in the beginning of this thesis relies on testing a PV-heating system to be properly addressed. A PV-plant at ASKO was the only up-and-running system in Norway capable to power the heating-mode at the time of this thesis. The ASKO roof was the perfect choice for collecting data of the systems sufficiency, and it was available for testing during the time of my research.

This chapter will focus on the specifications of the ASKO roof for a better understanding of exactly how this system works and what its limitations are. The studies performed on the roof include an aerial thermography of the system running in heating mode and a snow load reduction test during winter. All the specifications presented are derived from public data or given from the system designer (Google ; Innos 2017).

ASKO is a part of NorgesGruppen,- a Norwegian grocery wholesaling group. ASKO has an environmental profile, aiming to be a climate neutral company, eliminating the emission of greenhouse gases in the company (ASKO Norge AS). The designer of the PV-heating system is a company called Innos. Innos is a company that produces their own solar modules and delivers complete PV-systems for sustainable business areas (Innos 2017).

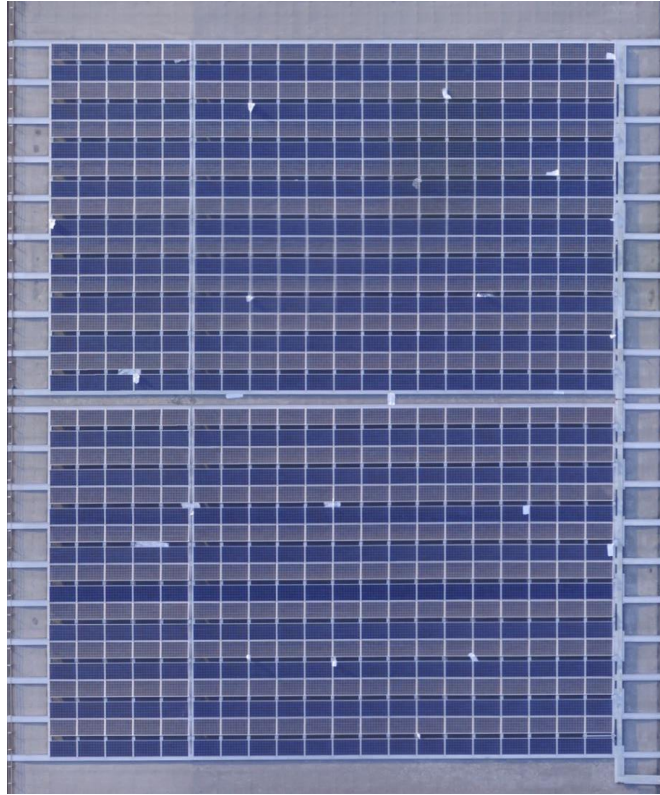
The ASKO facility in question is a warehouse/office space located at Kalbakken, Oslo. The facility is located approximately 125 meters above sea level, resulting in a characteristic snow load of 3,5 kN/m<sup>2</sup>. The whole facility consists of two main buildings. It is only a smaller part in one of these buildings where the PV-heating system is installed.



*Figure 19. Overview picture and a digital surface model of the ASKO facility indicating elevation on the roof. The pictures were produced using a drone and a photogrammetric software during this thesis. The red square marks the part of the roof with the PV-system capable of running in heating mode.*

The footprint of the building is approximately 40 x 48 meters making up 1920 m<sup>2</sup>. The building is a cold storage for food with additional office space. Most of the area adjacent to the roof is office and cantina. The roof is a unventilated *hot roof*, subjected to heat flow from the inside of the building.

720 modules making up an area of 1210,6 m<sup>2</sup> is installed on the roof. The modules cover 63,05% of the total roof area. The modules are of the type Innos Zero Blue 260. The modules lay in rows of 36, with 20 modules per row. The rows of PV-modules connected together in series are referred to as strings. The rows lie in a 66°/246° (East-North-East, West-South-West) direction, each row the opposite direction of the previous. The modules are tilted at an angle of 10°. Six inverters convert the DC-produced current to AC. Rectifiers are able to convert AC to DC from the main grid, powering the heating mode of the modules. Each string of modules can be controlled individually with a specific current and voltage. The system is theoretically capable of running a power of 50 Volts and 10 Amperes into each module. This results in an effect of 500 W per module without power losses. A performed effect of 252,1 W/m<sup>2</sup> is given by the manufacturer(Innos 2017).



*Figure 20. The 36 rows with modules of 20. The end of the heated gutters leading water away from the roof can be seen at the left and right side of the picture. The vertical line left of the center mark the roof kink. The silver dots are aluminum foil, further explained in 3.2.2.*

The system is installed with a *CAN bus device*, allowing for an automated control of the heating system depending on live data. The CAN bus can be programmed so that the power output to the modules is regulated by communicating with other devices providing information such as from weather forecast or live data measured on site. The only data triggering the power output to this day is information from load-sensors, measuring weight on top of 4 modules placed in each corner of the roof. The weight is recalculated to  $\text{kN/m}^2$  for each of the modules. The CAN bus device is programmed to feed maximum power to the modules whenever the measured load reaches a specific level. This is the reason for the system being coined the “*Weight-Watcher*” system(ASKO Norge AS ; Innos).

The roof pitch is designed to lead the water to the edges of the building. The roof is kinked, tilting two different ways. The kink is easily visible by looking at the line separating the modules as shown in figure 20. A customized drainage system is installed on the roof, designed for transporting water away from the roof underneath a thick snowpack. The drainage system is made of heated gutters aligned with the rows of modules. Each duct drains water from two rows. The gutters are heated by a standard heating cable system,- running electricity through wires with high resistance that produce heat. The water is transported to the West-North-West and the East-South-East edge of the roof.

## 3.2 Aerial Thermography of a PV-system

Thermography of the PV-heating system at the ASKO roof was performed using a drone. The intent was to document the quality of the system, locate possible hot spots and to estimate the efficiency of the system. Several individual infrared photos were taken and combined to infrared maps using a photogrammetric software for drone-based mapping called Pix4D. Two maps are produced, providing an overview look on the PV-heating system. In addition, several individual photographs are produced, highlighting the details of the system.

### 3.2.1 The drone

A customized DJI Phantom 3 Pro was used for the thermography. Gaitana et al. (2017) used this very same drone to perform an aerial survey of microclimate in urban environments published in a journal article at the International High-Performance Built Environment Conference.

The drone itself does not come with an infrared camera installed. A customization of the drone was necessary to develop a proper system capable of taking infrared pictures. The drone was mounted with an Optris PI 640 infrared camera, a mobile computer and an aluminum frame. The camera and the computer were connected to the power supply of the drone, increasing the power taken from the battery and thus shortening the air time. The equipment affected the weight of the drone, making it heavier and further reducing the air time. There was no gimbal installed for the infrared camera, demanding a steady flight to take clear pictures.



*Figure 21. Photograph of the drone used.*

The infrared camera used needs a computer configuration to get started before every session. This is necessary to set the picture interval, the format, where the photos are to be stored and so on. The necessity for the manual start up made it necessary to start the software and to configure the settings

before each flight. The computer mounted on the drone used does not come with a screen and disables the possibility to configure the camera through the computer directly. To make the configuration possible, the mobile computer was connected to a laptop via WIFI. The mobile computer's visual output was then duplicated to the laptop computer screen - the laptop now served as a mirror for the screen of the computer on the drone. The software could be entered using the laptop, enabling the configuration of the camera. This specific connection had to be set up before each flight of the drone.

### 3.2.2 The process of mapping the roof

For the infrared pictures, it is only pictures taken perpendicular to the ground that is of interest. The intent was to produce a 2D map from above, showing the temperatures of the modules. Perpendicular photos produce the best overview 2D maps in the software used. Such a flight was controlled with a drone app such as DroneDeploy or Lichi. These apps are made for mapping out areas at ground level. Here the flight pattern and speed were set before each run.

To create a map of several individual photos, overlap is crucial. The recommended overlap for drone-based mapping apps such as DroneDeploy is 70% sidelap and 60% frontlap(Dronedeploy).

A table was made based on the camera width and length angles and was used to determine the drone's speed, by setting the capturing rate, altitude of the drone and intentional overlap. Since the drones battery time was reduced by the increased weight of the drone, time was of essence. This meant flying as fast as possible while still ensuring sufficient overlap between the pictures.

Sekund/Bilde	Høyde[m]	Overlapp[%]	Fart[km/h]
1	30	40	28,5
1	30	60	19,0
1	30	70	14,3
1	30	75	11,9
1	30	80	9,5
1	30	85	7,1
1	50	40	47,5
1	50	60	31,7
1	50	70	23,8
1	50	75	19,8
1	50	80	15,8
1	50	85	11,9
1	70	40	66,5
1	70	60	44,4
1	70	70	33,3
1	70	75	27,7
1	70	80	22,2
1	70	85	16,6
1	90	40	85,5
1	90	60	57,0
1	90	70	42,8
1	90	75	35,6
1	90	80	28,5
1	90	85	21,4

Sekund/Bilde	Høyde[m]	Overlapp[%]	Fart[km/h]
2	30	40	14,3
2	30	60	9,5
2	30	70	7,1
2	30	75	5,9
2	30	80	4,8
2	30	85	3,6
2	50	40	23,8
2	50	60	15,8
2	50	70	11,9
2	50	75	9,9
2	50	80	7,9
2	50	85	5,9
2	70	40	33,3
2	70	60	22,2
2	70	70	16,6
2	70	75	13,9
2	70	80	11,1
2	70	85	8,3
2	90	40	42,8
2	90	60	28,5
2	90	70	21,4
2	90	75	17,8
2	90	80	14,3
2	90	85	10,7

Sekund/Bilde	Høyde[m]	Overlapp[%]	Fart[km/h]
3	30	40	9,5
3	30	60	6,3
3	30	70	4,8
3	30	75	4,0
3	30	80	3,2
3	30	85	2,4
3	50	40	15,8
3	50	60	10,6
3	50	70	7,9
3	50	75	6,6
3	50	80	5,3
3	50	85	4,0
3	70	40	22,2
3	70	60	14,8
3	70	70	11,1
3	70	75	9,2
3	70	80	7,4
3	70	85	5,5
3	90	40	28,5
3	90	60	19,0
3	90	70	14,3
3	90	75	11,9
3	90	80	9,5
3	90	85	7,1

Table 8. Overlap table made for determining the speed for the drone. The table is valid for the frontlap of the pictures.

A higher capturing rate enables the drone to fly at a faster speed which uses less battery and therefore makes it possible to map a larger area or fly faster, providing sufficient overlap. However, the computers

capacity to run the software and store the photos became a limitation. If the capturing rate was too low (2 sec/picture or less), the system would lag, resulting in an inconsistent capturing rate or even a total hang-up of the system. The rate was discussed and thoroughly tested. A capturing rate of 2 seconds per picture was sufficient for the system to function properly.

Altitude is strongly determinative for the quality of the photos. The lower the altitude, the better the quality. Low altitude results in low speed if not decreasing the overlap.

Three routes were planned at 30, 50 and 100 meters. The focus of the camera was set before each of the flights. High wind speeds resulted in some blurry pictures of the modules.

The software used for producing the map relies on recognizable points on the ground to combine individual photos to a larger map, further explained in the next chapter. Taking infrared pictures of a PV-heating system at low altitude poses a challenge due to the uniform structure of the system. The modules are neatly organized in rows and the heat emitted from the modules is quite uniform. The infrared pictures of the system look very much alike when flying at a low altitude. This poses a problem for the software, unable to separate one picture from the other and combining them to a map. It is as having a jigsaw puzzle where all the pieces look alike. For this reason, a contrast in the infrared specter was needed on the modules, to create some reference objects in the photos. The position of this object could help the software determine where the picture was taken and enhance the quality of the map. Different solutions were thought of for creating the infrared contrast on the roof surface. Candles could be placed on the roof showing a high temperature, or bags of ice could be spread out showing a low temperature, both solutions conducive for thermal referencing. The final solution was placing aluminum foil at the roof. Aluminum foil is a highly reflective material with a low emissivity. Taking a picture of aluminum foil with an infrared camera will not show the actual temperature of the aluminum foil, but rather the reflected temperature of the surroundings. For the case of the ASKO roof, the modules face the sky. Placing the aluminum foil on top of the modules will reflect the temperature of space (and lots of atmospheric transmission) when taking infrared pictures with a drone. Space is very cold, and will create temperatures way lower than what occurs at the roof surface. Different shapes of aluminum foil was made and spread out on the roof. This successfully created the contrast needed for the pictures to differ from one another.

### **3.2.3 Processing the results**

The raw files taken from the infrared camera were processed using different software in several steps. The pictures first needed to be adjusted in Matlab (Matlab 2017) before creating the infrared map in a software for drone-based mapping called Pix4D (Pix4D 2017). The maps were then applied a filter in Fiji, an open software for scientific image analysis (Fiji 2007).



Figure 22. Software used in chronological order.

Matlab was used to adjust the raw files before processing them in the photogrammetric software Pix4D. A csv-format was used to produce the infrared pictures. With a csv-format, each temperature in the infrared photo is given a specific number value. The number values range in a scale between 0 and 65535. The value is a number and is separated by a delimiter in the csv file. For converting the csv-file to a picture, a Matlab script was used. The script converts each number value into a pixel with a black, white or grey color corresponding to the number value. Setting the maximum and minimum value of the scale enables one to optimize the result for the specific purpose. If a value exceeds the upper or lower limit of the scale, it is given the same value as the maximum (white) or minimum (black) value of the scale. A very narrow scale will create a high contrast in the photo giving great detail within the range, but will convert values above or below the limit to within the given range. The risk is that upper and lower values might be excluded, producing a photo not representable for the real situation. A wide scale will produce lower contrast photos with a higher amount of grey pixels. Setting the scale in the software is a tool for producing highly detailed photos, adjusting the scale to the object of interest.

```
-1.5;-1.4;-1.5;-1.2;-1.2;-1.4;-1.5;-1.1;-1.2;-1.4;
-1.4;-1.1;-1.0;-1.1;-1.2;-1.3;-1.4;-1.5;-1.4;-1.3;
-1.4;-1.4;-1.2;-1.1;-1.3;-1.2;-1.2;-1.2;-1.2;-1.4;
-1.2;-1.2;-1.0;-1.0;-1.2;-1.4;-1.2;-1.2;-1.4;-1.2;
-1.1;-1.2;-1.0;-1.0;-1.1;-1.4;-1.2;-1.4;-1.4;-1.2;
-1.4;-1.2;-1.2;-1.3;-1.2;-1.2;-1.1;-1.2;-1.3;-1.3;
-1.2;-1.1;-1.2;-1.4;-1.5;-1.2;-1.3;-1.2;-1.2;-1.3;
-1.2;-1.2;-1.2;-1.2;-1.2;-1.2;-1.2;-1.4;-1.3;-1.4;
-1.0;-1.0;-1.2;-0.9;-1.2;-1.2;-1.2;-1.3;-1.2;-1.0;
-1.1;-1.1;-1.3;-1.4;-1.2;-1.2;-1.1;-1.1;-1.2;-1.1;
-1.4;-1.2;-1.2;-1.1;-1.0;-1.0;-1.1;-1.2;-1.2;-1.2;
-1.1;-1.2;-1.2;-1.1;-1.1;-1.2;-1.0;-1.1;-1.1;-1.2;
-1.0;-1.1;-1.1;-1.3;-1.3;-1.4;-1.1;-1.2;-1.0;-1.3;
-1.0;-1.2;-1.4;-1.3;-1.0;-1.1;-1.1;-1.1;-1.1;-1.2;
-1.0;-1.2;-1.2;-1.2;-1.2;-1.0;-1.0;-1.0;-1.1;-1.2;
```

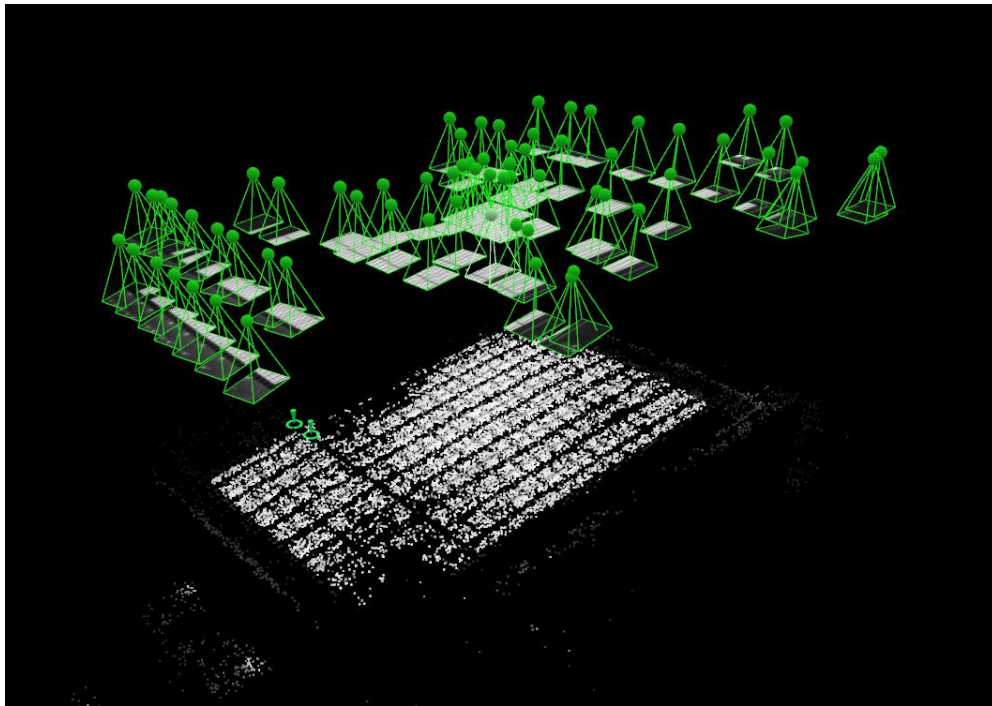
Figure 23. Example of an infrared picture in csv format. Each pixel is given a value separated by a delimiter. The matrix of numbers was converted into pixels by assigning each number a color value in Matlab.

The scale used to produce the infrared maps was set to the range of -5°C to 18°C in Matlab. This range included most temperatures registered in the infrared pictures, while still narrow enough to produce a detailed photo. The scale used to produce the single photos was set to a more narrow range. The high minimum temperature excludes the surroundings but produce great contrast for the objects within the set scale range. The single photographs presented were not processed in Pix4D. This is not the final scale for the infrared maps. The final scale is set in Pix4D.

After creating the pictures in Matlab, Pix4D was used to combine the photos to a map. Pix4D is an advanced photogrammetry software for drone-based mapping (Pix4D 2017). The software uses several individual photos to create a 3D model. The 3D model gives basis for producing numerous output results,

ranging from textured 3D- meshes, to terrain models and orthomosaic maps. Light specters such as RGB, NIR (near infrared) and IR (infrared) can be used to create a 3D model in Pix4d.

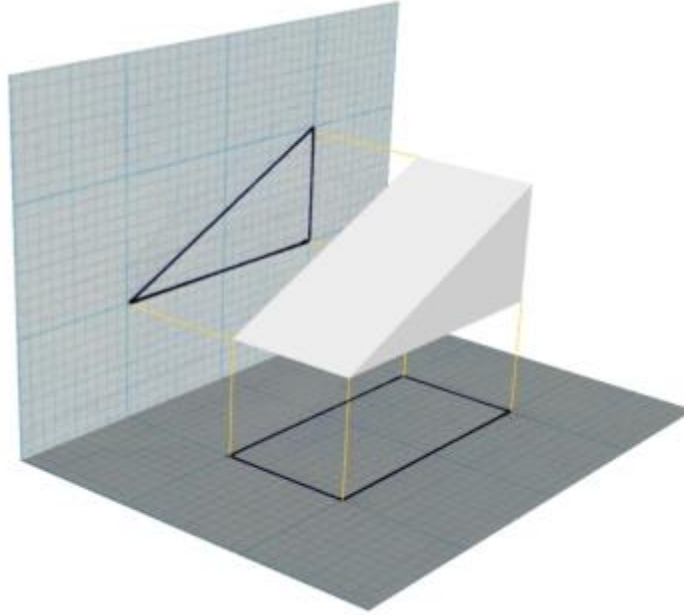
The software functions by recognizing common points on the ground and placing the aerial photos thereafter. The common points recognized across photos are called *tie points*. The more times the point is recognized in different pictures, the more weight the tie point is given when constructing the 3D model. A high overlap between photos results in a large number of recognized points and is conducive for an accurate 3D model. The tie points generated create a *point cloud*. The point cloud is a construction of the tie points in a 3D space. The point cloud gives the basis for merging a textured model, producing a coherent surface.



*Figure 24. The point cloud and the position of the cameras placed in 3D space. The green spheres represent where the picture is taken. Below are the tie points making up the point cloud.*

The geolocation of each photo can be extremely helpful when creating a 3D model. A geo-located photo is given a specific coordinate where the picture is taken, and uses the coordinate to determine the position of the drone at the time of the capture. The geolocation of a photo helps the software to place the pictures in 3D space, decreasing the dependency of tie points to determine the position of the photo. Geolocation increases the accuracy of the model. The infrared photos taken at ASKO were not geo-located, posing a challenge to combine the photos into a 3D model.

*Orthographic projection* is a technique used to represent a 3D-model in 2D. The software uses orthographic projection on the 3D model to create a 2D map.



*Figure 25. Illustration of orthographic projection.(Hughes 2013)*

The 2D map can then be processed in the software *index calculator*. The index calculator allows for the manipulation of pixel values. The pictures produced from Matlab have values ranging between 0 and 65535 and need to be scaled down to represent the temperature scale. It is also here the temperatures are corrected for the effect of emissivity and atmospheric transmission. The correction is done by creating a formula adjusting the value for every single pixel.

$$\alpha = T_{min} + \left(\frac{\beta}{65535}\right)T_{diff}e\tau \quad (19)$$

$\alpha$  is the corrected value of the pixel

$T_{min}$  is the lower boundry of the temperature set in Matlab

$\beta$  is the current pixel value

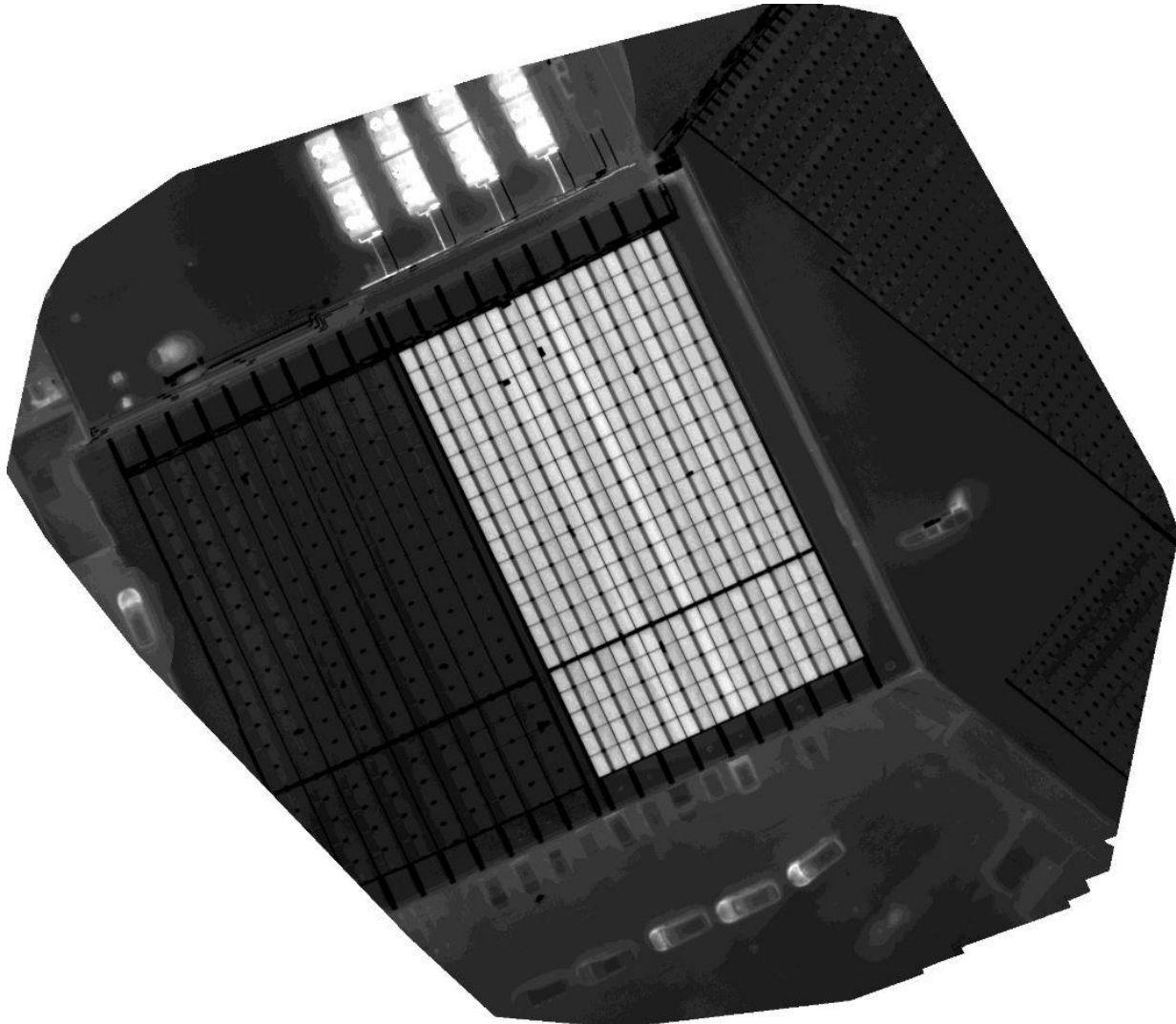
$T_{diff}$  is the difference between the boundary temperatures set in Matlab

$e$  is the emissivity of the modules

$\tau$  is the atmospheric transmission coefficient for the respective height

The emissivity of the modules was set to 0,87 based on typical theoretical emissivity values for PV-modules presented in 2.6.5. The atmospheric coefficient was determined to be 1,0123 for 30 meters and 1,0256 for 50 meters. The estimation of the coefficient is presented in the next chapter.

The final scale adjustments are then done using the *Color Maps* tool in Pix4D. Here, the final numbers representing the scale presented in the maps is set. This adjustment fine tunes the scale to fit the corrected pixel values. The spacing in the scale is also set, allowing for adjusting the numbers of color values representing the picture.



*Figure 26. Example of a raw file from Pix4d.*

The result exported from Pix4D was a black-white, uncropped, unrotated picture. The pictures were rotated and cropped in GIMP and a filter was then applied using Fiji. The filter was chosen to represent the typical visual impression of an infrared picture with orange and purple colors.

### 3.2.4 Estimating the atmospheric transmission coefficient

As explained in 2.6.4, the radiation measured by an infrared camera can come from other sources than the object of interest. Reflectance from surrounding objects and radiation from the atmosphere are the two main disturbing sources affecting the received wavelengths of the infrared camera. This chapter will explain how an atmospheric transmission coefficient can be calculated, which can be applied to the infrared pictures, compensating for the radiative effect of the atmosphere.

The disturbance of atmospheric transmission is caused by the *radiation emitted from the atmosphere*. If the atmosphere is not in thermal equilibrium with the surrounding objects, radiative exchange between the objects will occur as previously explained (equation 18). There are three main parameters determinative for the effect of atmospheric transmission: air temperature, humidity and distance. The larger the temperature difference between the atmosphere and the object of interest, the greater the disturbance will be. The larger the distance, the more air between the camera and the object, thus enhancing the disturbance.

The atmospheric transmission coefficient can be determined by comparing the temperature difference between raw pictures and pictures which are compensated for in regards to distance and air temperature. A study at NMBU was performed with intent to determine the atmospheric transmission coefficient. The coefficient was determined by taking infrared pictures of a brick wall, and comparing the results with and without compensating for air temperature and distance.

Firstly, the *reflected apparent temperature* was determined using a piece of aluminum foil. The reflected apparent temperature is a parameter used to compensate for the radiation reflected in the object (FLIR 2011). For the determination of this parameter, method 2 from the FLIR manual was used.

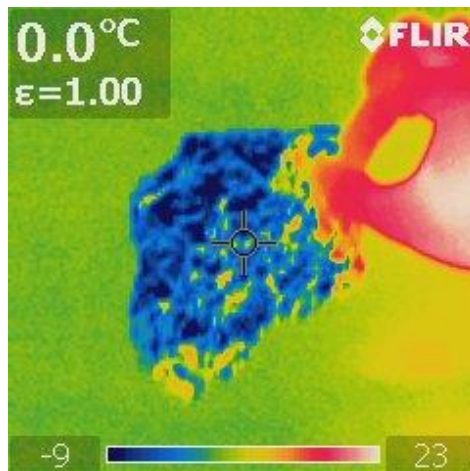


Figure 27. The reflective temperature is determined by looking at aluminum foil with an infrared camera over a short distance.

Then infrared pictures were taken from the brick wall at a distance of 30 and 50 meters, the same as the drone altitude at the aerial thermography performed at ASKO.

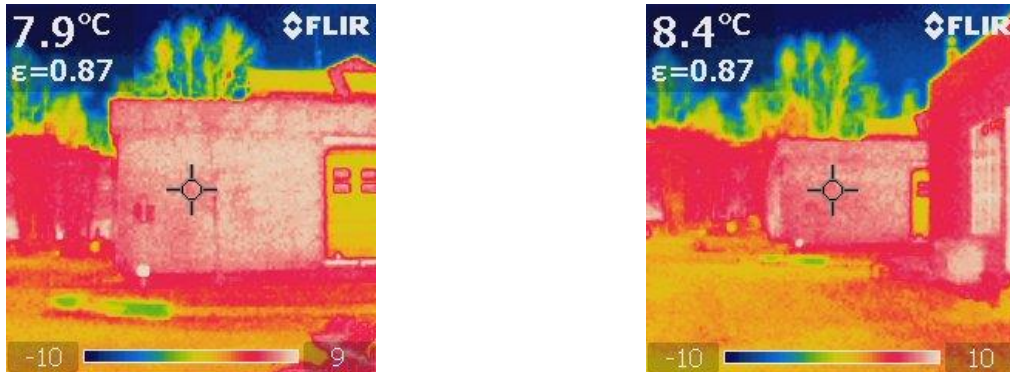


Figure 28. Infrared pictures at the brick wall at a distance of 30m (left) and 50m (right).

Then the pictures were processed in the FLIR tools software. A *reflective temperature* and *distance* parameter can be set, adjusting the registered temperature values. The effect of the adjustment was then evaluated.

Distance[m]	Unadjusted[°C]	Adjusted[°C]
30	7,8	7,9
50	7,8	8

Table 9. Table showing the effect of compensating for the atmospheric transmission.

The atmospheric transmission coefficient is then calculated by dividing the adjusted temperature with the unadjusted temperature. This is done for the distance of 30 and 50 meters, giving two separate atmospheric transmission coefficients.

$$\tau_d = \frac{T_1}{T_2} \quad (20)$$

$\tau_d$  is the atmospheric transmission coefficient for the respective distance

$T_1$  is the mean compensated temperature of the respective distance

$T_2$  is the mean uncompensated temperature of the respective distance

The atmospheric coefficient was determined to be  $\tau_{30} = 1,0123$  and  $\tau_{50} = 1,0256$ .

The air temperature this day was at NMBU was approximately 5°C.

### 3.3 Snow load reduction test of a full scale PV-heating system

Due to a recent snowfall, a test of the facility at ASKO was performed 08.02.2017. The goal was to test the heating-mode performance at a large scale and to collect data of the system's ability to reduce the snow load. Three strings of modules were applied power with different intensity for 2 hours. Three cases were made, investigating the snow load reduction under different conditions.

#### 3.3.1 Climatic conditions

The snow had fallen a couple of days prior to the testing. On average, there was a snow depth of 4,83 cm on the modules. However, the distribution was not uniform, see table 10. The snow depth was not large enough for creating a continuous snow layer over the modules. The modules are rigged on a frame rising above the roof level, and with a snow depth of 5 cm, the rim of the modules is exposed and wind is able to blow underneath.

Module	Sample 1	Sample 2	Sample 3
1	6	5	3
2	5	5	4
3	5,5	5,5	4,5
4	6	5	4
5	6	5	4
6	5,5	5,5	4
7	5,5	4	3
8	5,5	5	3,5
9	6	5,5	4
<b>Average depth [cm]</b>	<b>5,67</b>	<b>5,06</b>	<b>3,78</b>

Table 10. Measured snow depth before testing. Sample 1 is the lower part, 2 is the middle and 3 is the upper part of the module. The modules were randomly selected.

The "Weight watcher" system showed an average load of 4 kN/m<sup>2</sup> before testing. This was the mean load registered at 3 different modules equipped with load sensors.

The snow density samples were taken with a cylinder and weighed. The average density was 101.1kg/m<sup>3</sup>.

During the test, temperature and relative humidity of the air and snow were logged using the EI-Usb 2 by Lascar Electronics(Lascar Electronics). For the air, the average temperature was -6,8°C and the average relative humidity was 69,8%, both with small variations. Unfortunately, the logger was blown into the snow 45 minutes into the experiment, affecting the data logged. The conditions stayed approximately the same throughout the test.

No wind measurements were taken at the roof. According to Blinder Weather station, the average wind speed was 5,9 m/s between 10:00 and 14:00 the period when the test was performed(Yr). The wind

came from East-North-East, perpendicular to the rows of modules. Every other row was significantly exposed to the wind, while the other was sheltered.

### 3.3.2 Cases

As mentioned, the intent of the test was to evaluate the system's ability to reduce snow load at a large scale. The outcome of a maximum-power test was of interest, in addition to investigating the potential of sublimation. A total of 3 cases were performed simultaneously over 2 hours.

**Case 1:** Maximum effect, natural snow depth. The maximum effect of 50 volts and 10 A were applied to 2 strings, 20 modules each string. The two strings faced opposite directions. A logger was placed in the middle of the snowpack at one of the modules.

**Case 2:** Maximum effect, with additional snow shoveled on one module. Here, the intent was to document how the melting of snow would behave with a larger snow depth compared to the natural depth at the time. The average snow depth was 11 cm and the snow was more compact due to shoveling. The module used was on the same string as in case 1 and were applied the same effect. The string was facing the wind. One logger was placed at the top of the snowpack, while another was placed at the bottom.



*Figure 29. The module with additional snow before testing. The snowpack was not coherent across the modules, leaving the rim exposed.*

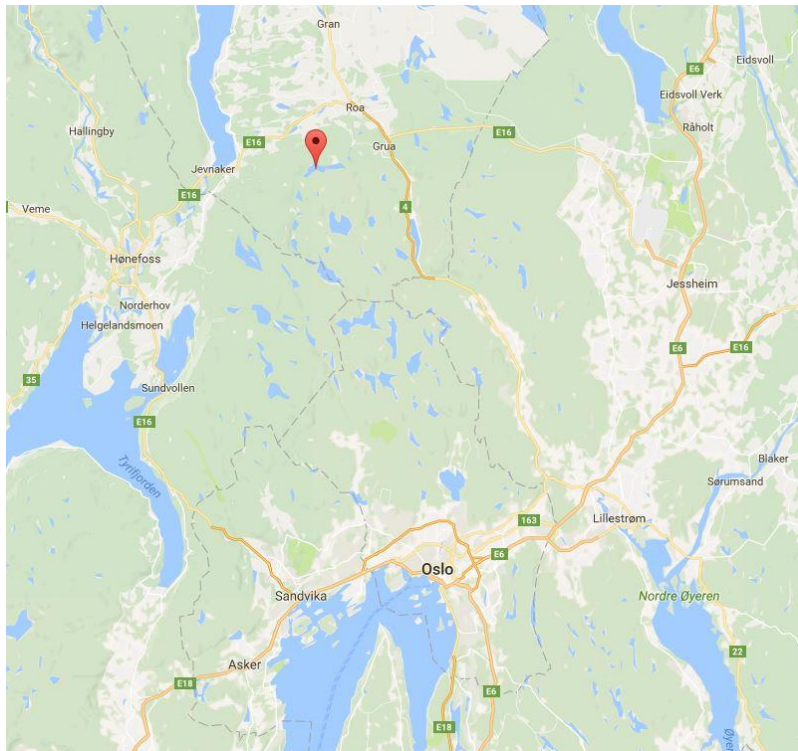
**Case 3:** Low effect, natural snowpack. Here the intent was to sublimate the snow. A current of 50 V and 5 A were applied to one string of modules. One logger was placed in the middle of the snowpack.



### 3.4 Case study in Nordmarka

In addition to the testing of the facility at ASKO, it was expedient to do a further case study of different possible snow load reduction scenarios. With 3 PV-modules, 2 rectifiers and the needed cables, a system was setup at Mylla, Nordmarka. The purpose was to further investigate the performance of the PV-modules in heating mode under varying climatic conditions. A total of three load reduction cases were performed, each with a specific intent to evaluate the performance under a specific climatic impact.

Mylla is located north in Nordmarka, just inside the county of Oppland. The location used is approximately 590 m above the sea level, and is subjected to sub-arctic climate conditions.



*Figure 30. Location of the test site is marked with the red dot. (Google)*

This study is different from the one performed at ASKO due to the climatic conditions, scale, the setup and the control of the power. Having an own PV-heating system allowed for comprehensive testing independent of having access to the ASKO roof. The testing was done during the course of a week, enabling for thorough measurements in different cases. The main reason for conducting the experiment at Nordmarka was due to better snow conditions. Nordmarka is colder and richer in snow than Oslo during winter, allowing for a more realistic snow load reduction scenario. The setup in Nordmarka is not similar to how a PV-system typically is installed on a roof, which must be taken into consideration when investigating the results.

The modules used for the experiment were of the type Innos Zero Blue 260 modules and the rectifiers were TTI QPX1200I, designed to produce up to 60 V and 50 A, resulting in a total power output of 3000 W per module. All three modules had been previously used in a load-capacity test, and were therefore bent to some extent. Infrared pictures were taken of the modules while subjected to power, to check the performance and the characteristic thermal footprint of each module. The thermography was done in forehand of the case study, at NMBU.



Figure 31. The test setup at NMBU.

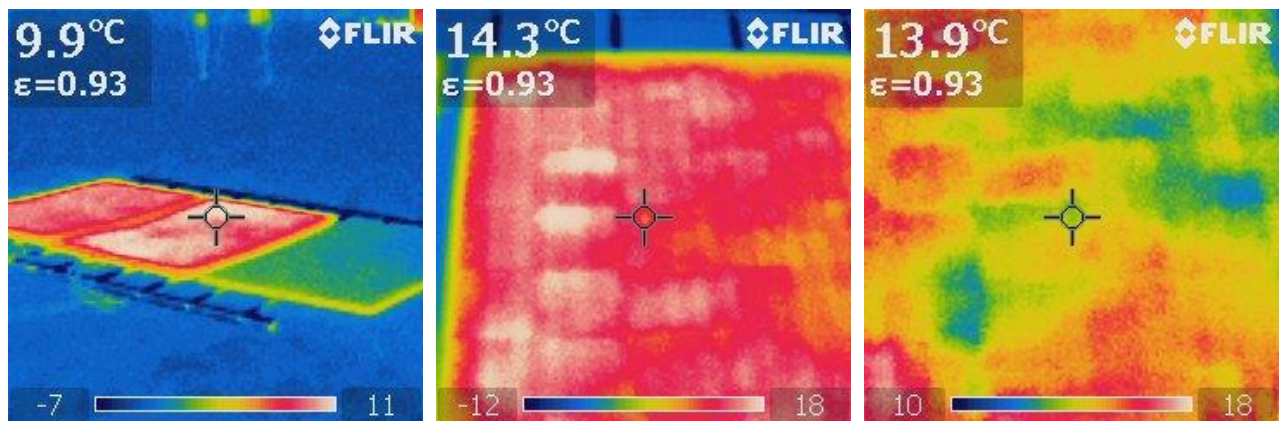


Figure 32. Infrared pictures of the setup reveal the thermal footprint of the modules. The temperature scale is not the same for the different pictures.

### 3.4.1 Setup

The modules were rigged at a flat parking space, at the front side of the cabin. The modules were placed in an open space, exposed to sun for most of the day. To avoid contact with the ground and conduction losses affecting the output performance of the modules, they were placed on top of ladders placed horizontally on the ground. This enabled the modules to lay only on their frames, leaving the back layer free of contact with the ground. Since the modules lay flat, sufficient drainage of water did not occur naturally.

The rectifiers were placed in an unheated room, protected from the weather.

Two of the modules were subjected to a current, while the third one served as a reference for comparison. The reference module will be referred to as module 1, while the modules subjected to the electric current will be referred to as module 2 and 3 as, as the sequence they form in the picture below (counting from left to right).



*Figure 33. The setup with the module numeration*

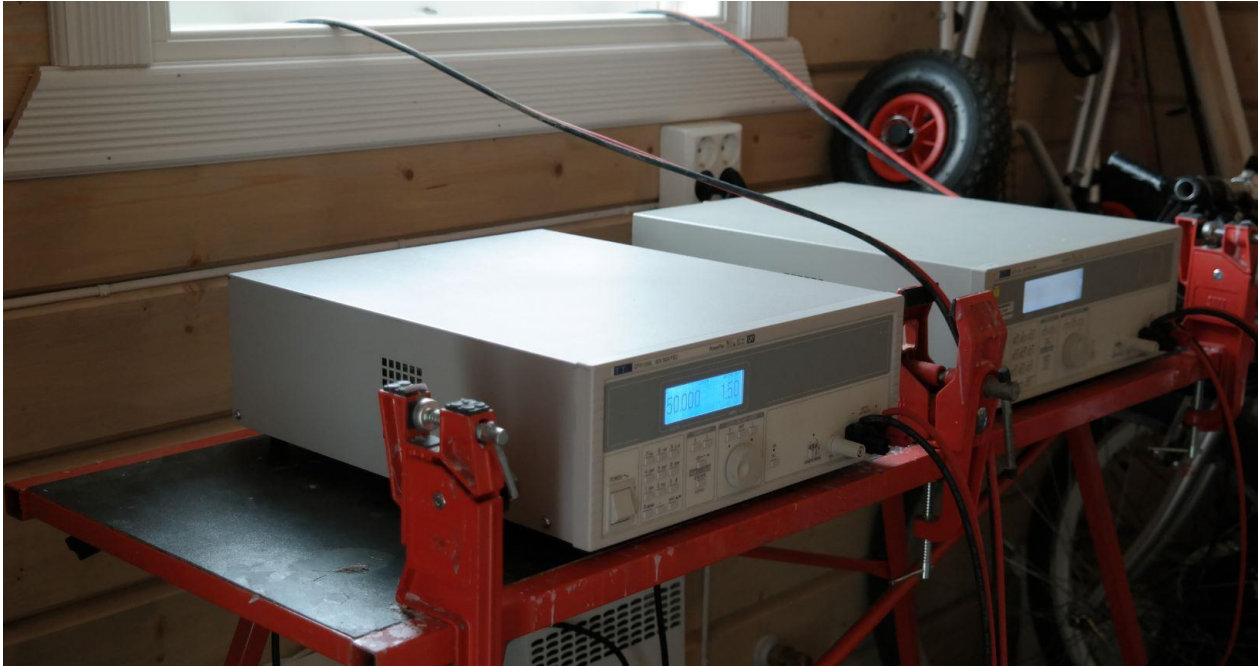


Figure 34. The rectifiers were located in a ski preparation booth next to the parking lot

3.4.2 Data collected

Lots of data were collected during the case study. The type of data and instruments used are listed below.

Data	Instrument	Model, brand
Temperature and RH	USB Logger	EI USB 2, Lascar Electronics
Snow density	Cylinder and a weight	-
Snow depth	Measure rod/ruler	-
*Wind	Online weather station	WH1080, Fine Offset
Heat emission/temperature	Infrared camera	FLIR
Visual observations	Camera	NX300, Samsung

Table 11. Data collected and instruments used at the Nordmarka case study.

\*Wind speed data were collected using a weather station located 2 km away from the test site. Wind, like many other weather phenomena, displays a behavior of microclimatic differentiation. The data is uncertain to some extent due to the distance between the weather station and the test-site. The public data is provided by the Cumulus Software used for retrieving, storing and displaying weather data from an automatic weather station(Cumulus Weather Station Software).

Measurements of the snow density were conducted by taking snow samples with a cylinder, and weighing the snow. The snow depth was always registered when taking a sample. A sample was made by sticking the cylinder down in a snowpack with even depth, then taking all of the snow from the sample into a plastic bag ready to be weighed. To get all the snow from the cylinder into the bag, a shovel or a stiff plate was used to seal the cylinder at the bottom. Having ice at the module surface proved to be a challenge, as it made including all the material in the cylinder more difficult. Therefore, some uncertainty should be taken into account for the density values. With this method, the volume and the weight of the snow is known, enabling one to calculate the density. This is done by dividing the weight of the sample by the volume.

$$\rho = \frac{m}{V} \quad (21)$$

*$\rho$  is the density of the snow [kg/m<sup>3</sup>]*

*$m$  is the measured weight [kg]*

*$V$  is volume of the snow filled part of the cylinder [m<sup>3</sup>]*

When measuring depth at the modules, all 4 corners and the middle of the module were measured. In general, the corner depth was measured at a distance of 15 cm from the module edge. This was to ensure that the area measured was well within the effective area of the module.

### 3.4.3 Cases

#### Case 1 – ASKO equivalent power

The intent of the first case was to do a test with a similar electric effect as to the maximum possible power at ASKO. The rectifiers were set to a voltage of 50 V, and the current to 10 A, which is the upper power limit of the system at the ASKO roof.

For all the cases, outside air temperature and humidity were logged. In case 1, loggers were additionally placed at the top and bottom of the snowpack at module 1 and 3.



*Figure 35. The setup before the start of case 1.*

## Case 2 – Sublimation

The intent of the second case was to further investigate the potential of sublimating snow from PV-modules. The case was conducted over 3 days. For sublimation to occur, the temperature of the modules should remain just below 0°C. A digital thermometer was placed at the surface of module 1 and provided live information of the surface temperature to an external screen. The current was adjusted according to the module surface and air temperature. The current was always between 0,3-2,0 A or off. The voltage was set to 50 V, but auto-adjusted when turning on the rectifiers and remained between 36 and 39 V.

A fresh snowfall fell on top of the modules during the night before the experiment providing a completely natural layer of snow. The modules were cleared from any snow and ice before the snowfall occurred. The layer of snow also covered the side of the modules, preventing wind from blowing underneath.

The loggers were placed at the top and bottom of module 1 and 3, in addition to the air logger.

Snow samples for density estimation were taken at the beginning and at the end of the case study. The initial samples were taken from the ground, leaving the snow on the modules unspoiled. At the end of the experiment, samples were taken at the reference module, and at the heating-mode modules.

Snow depth was registered before and after the experiment.



*Figure 36. The setup before the start of case 2*

### **Case 3 – Maximum effect**

This case was performed with intent to document the effect of maximum power applied to the modules. The voltage was set to 50 V, and the current to 30 A. The current dropped to 26 A and the voltage to 48V when the rectifiers were turned on.

Snow was shoveled onto module 2 and 3. The approximate depth was 19 cm.

The Temp/RH loggers were placed at the bottom of module 2 and 3.

No density samples were taken.



*Figure 37. The setup before the start of case 3*



### 3.5 Estimating sublimation using the Bulk Aerodynamic Flux method

A calculation was made estimating sublimation rates with the data logged from the Nordmarka sublimation case. The input data needed for the BF method, includes the humidity of the snow and air, wind speed and air pressure. The estimated rates are later compared with actual measured rates from the Nordmarka study. As explained 2.5.5, the BF method assumes large, flat surfaces with uniform heat flux. The estimation of sublimation rates from this case study is not inside the methods intended use. The results aim to provide insight into the validity of estimating sublimation in an area of non-uniform heat flux with the BF-method. Also, the estimated sublimation rates can provide insight to the impact of changing weather conditions. The measured sublimation rates are only telling of the total sublimated amount, from start to end. Estimating sublimation over different time periods allow for gaining perspective of when the highest sublimation rates occur. Three cases are made, estimating sublimation over different time periods during the case study.

To perform the calculation, some simplifications were made:

The transfer coefficient for latent heat ( $C_E$ ) is not calculated, due to the complicated process of doing so. As mentioned in 2.5.5,  $C_E$  is always between  $1,0 \cdot 10^{-3}$  and  $1,5 \cdot 10^{-3}$ . The two extremes values of  $C_E$  are used, representing the outer borders of the estimated sublimation. The actual sublimation occurring should be between the two extreme values.

The latent heat of sublimation ( $L_s$ ) is set to 2830 kJ (Oke 1987)

The air density ( $\rho$ ) is set at  $1,2 \text{ kg/m}^3$  and assumed constant.

The changing parameters in the calculation is the wind speed ( $u_r$ ), the specific humidity of the snow ( $q_s$ ) and the specific humidity of the air ( $q_r$ ). The input data of specific humidity is derived from the temperature and humidity loggers used in the case study. The specific humidity is calculated from the values of temperature and RH using the psychrometric chart (figure 5). The sublimation estimated is based on the values of the specific humidity of the air and of the bottom of the snowpack.

The effect of wind in the bulk aerodynamic flux method is highly determinative for the outcome of the result. However, the effect of wind might not be as significant for a non-uniform induced flux as to a uniform flux working over a large area. Therefore, the values used for the wind factor is not the data collected from the weather station in Nordmarka in this estimation. The wind factor  $U_r$  is set to 4 m/s and is further discussed in 5.1.2.

Sublimation rates are estimated for three different periods of time during the sublimation case at Nordmarka. The estimated sublimation rate in period 1 is for the complete duration of the sublimation case. The intent is to produce a result to compare with the measured results. In addition to estimating the sublimation rate for the whole experiment, additional estimations are made – period 2 and period 3, highlighting the effect of episodic events. Both periods isolate the effect of two overnight sublimation events. The time period used in period 2 and 3 are chosen due to the climatic impact of cold nights. The specific humidity (SH) of the snow at the module surface remains approximately constant throughout the case study, but the SH of the air varies more. The SH in the period 2 and 3, dropped towards nightfall, resulting in a large humidity gradient between the air and the snow pack, highly conducive for sublimation. Period 1 and 2 aims to investigate the impact of cold nights and to quantify the influence.

Period	Time interval	Duration
1	22.02, 22:43 – 25.02 08:35.	57 hours 52 minutes
2	23.02, 21:00 – 24.02, 08:00	11 hours
3	24.02, 18:00 – 25.02, 07:00	13 hours

Table 12. Time table of the period of estimated sublimation rates.

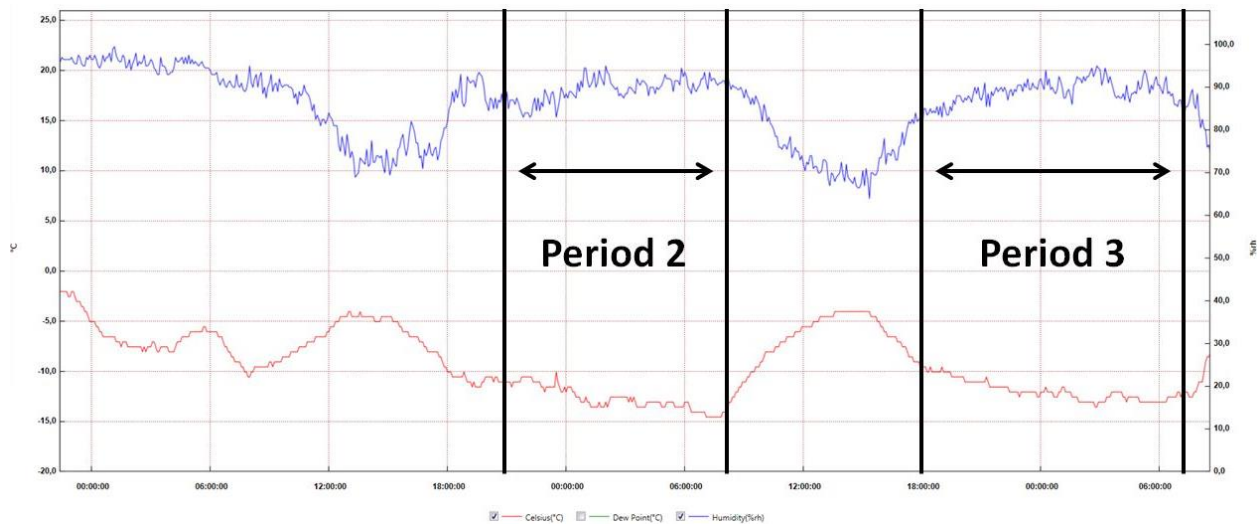


Figure 38. Air temperature and relative humidity of the outside air during the sublimation experiment. Period 2 and 3 are isolated on the basis of lower specific humidity in the periods. Period 1 uses the time period of the whole graph.

The existing humidity gradients are illustrated to gain perspective of the magnitude and relative difference in humidity.

Period	Bottom	Top	Air
1	3,7	1,8	1,6
2	3,7	1,1	1,2
3	3,7	1,8	1,3

Table 13. The average specific humidity [g/kg] for the different periods.

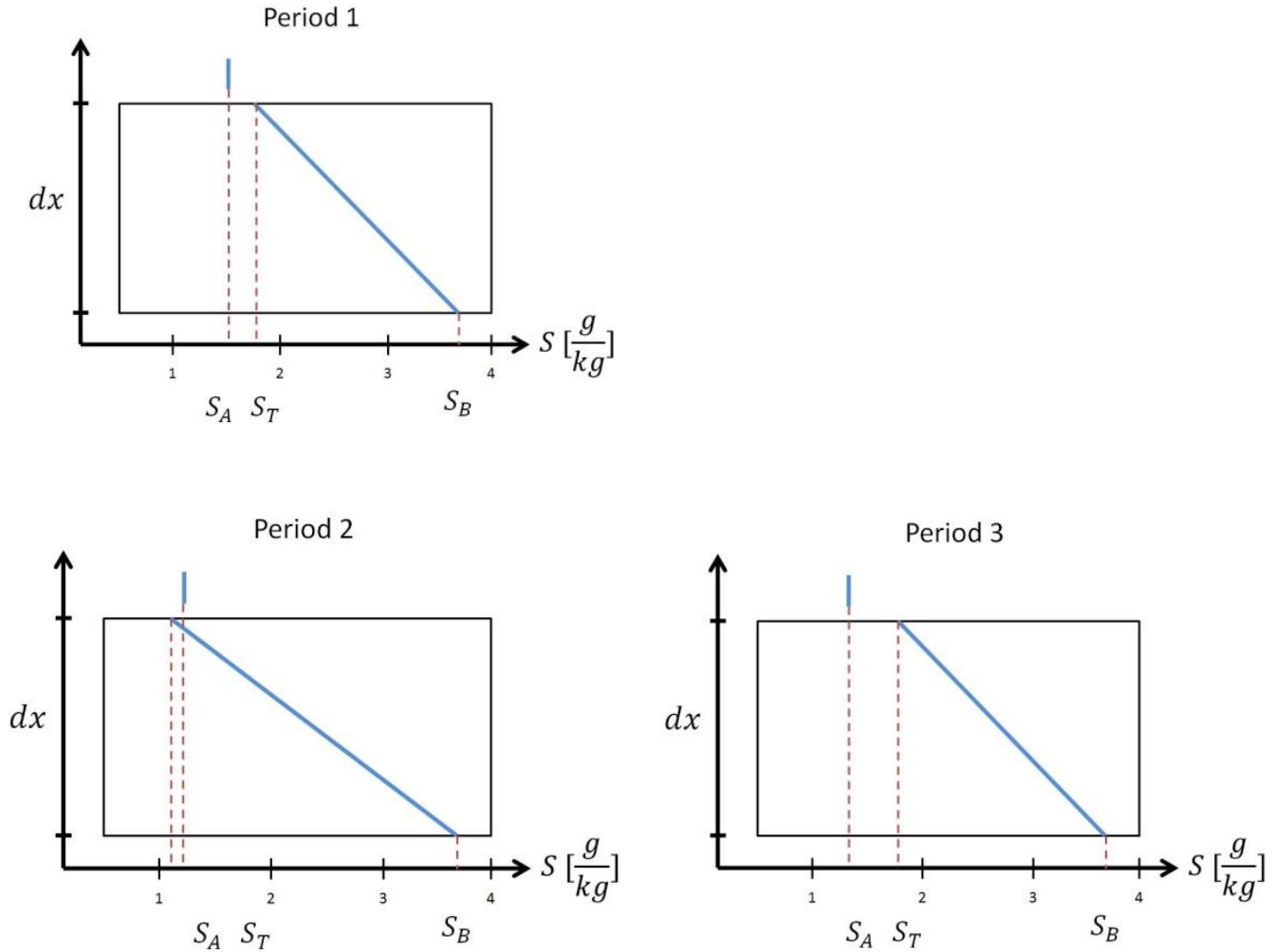


Figure 39. A graphic illustration of the temperature gradients occurring during the sublimation case. These values are used to estimate episodic sublimation events to gain understanding of the impact of cold nights.

Period 2 have to lowest air humidity, although the humidity of the snow top layer was even lower at the time. Period 3 show the greatest humidity difference between the air and the top layer of snow.

## 4 Results

The results presented consist of all the measurements performed previously presented in the method chapter. This includes the aerial thermography of a PV-system, the snow load reduction test at the ASKO facility and the Nordmarka case study. In addition to the measurements, several analytical calculations are made, using theory from chapter 2. The calculations use data collected from the measurements. The calculations provide additional information of the systems performance and seek to quantify values relevant for snow load reduction. All the calculations are presented in the analysis chapter 4.4.

### 4.1 Aerial thermography of a PV system

Two infrared maps and three single pictures were produced from the aerial thermography session at ASKO. The maps give an overlooking view of the system, providing documentation for the quality of the modules and for the efficiency of the system. The infrared maps are corrected for atmospheric transmission and emissivity, and are supported by a scale giving values to the temperatures. The single pictures provide the greatest detail on cell level, but only cover smaller areas and are not supported by a temperature scale.

The radiated effect from the PV-modules is calculated based on the temperatures measured from the infrared pictures. The calculated effect is then used to calculate the thermal coefficient  $C_t$  for the roof.

Full size versions of the pictures are attached in Appendix A.

### 4.1.1 Overview map

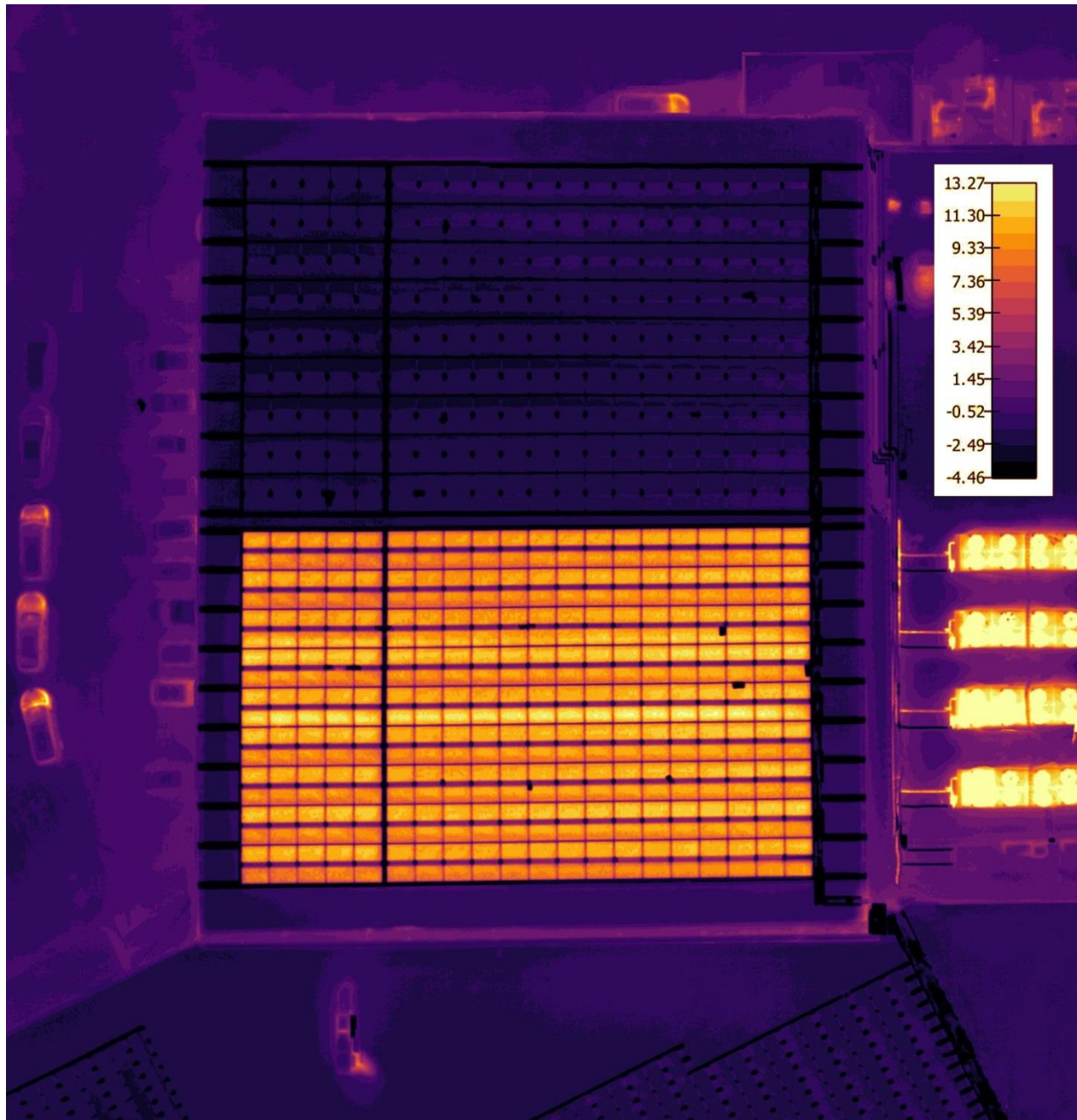


Figure 40. Overview infrared map of PV-system in heating mode.

The map gives an overviewing look of the roof with the PV-heating system. The scale is set to the wide range of -4.46 to 13.27 °C and the map includes a larger area than the roof itself. The cell temperatures are not in focus, but rather the roof as a whole with the surrounding objects. The infrared map is made of 79 single images taken from a height of 50 m. Areas at the edge of the map was originally not covered

by the photos, but was later edited to be included in the photo. Therefore, some of the temperatures in the outer edges are not correct. Temperatures of the modules are unedited and correct.

The map include surrounding objects such as cars recently used, smaller buildings at ground level, and the cooling system clearly running at the left end of the map. Even the cables running from the cooling system to the main building are visible.

The black grid lines surrounding the modules are the frame of the PV-panels and the gutters of the drainage system. Both are made from aluminum. Between the modules are black dots, most clearly visible in the upper part of the PV-system not subjected to current. These dots are a part of the load carrying frame, stretching from array to array. The frame is only visible between the modules, appearing as dots rather than as a continuous component.

#### 4.1.2 Module detail map

A map was produced focusing on the details of PV-modules. The scale is optimized for viewing temperature distribution of the semystem and single cell temperature. The narrow scale between 10.00 -15.85°C excludes the surroundings, but amplifies the distribution of heat over the modules. The infrared map is made of 68 single images taken from a height of 30 m above the roof. This is the most accurate representation of the temperatures actually occurring made in this thesis.

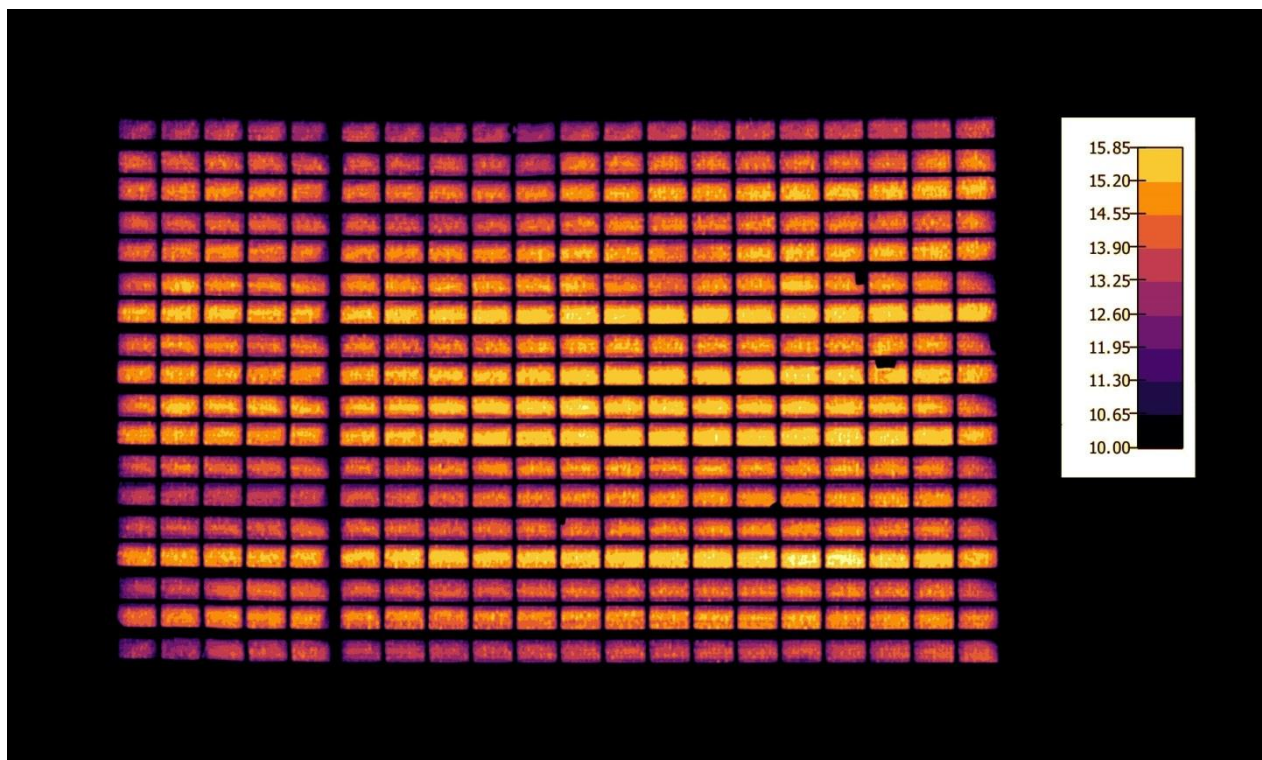


Figure 41. Detailed infrared map of the PV-system in heating mode

The highest temperature of a cell in a PV-module is 15.85°C in this infrared map. The color representing this temperature is beyond the scale, but can be seen as the white pixels on the map. No temperature higher than 15.85°C is registered. The temperature difference across a single module is usually between 1-3 °C.

The temperature difference across a single module is usually between 1-3 °C.

It appears to be a pattern of equal temperatures across the different strings of modules. Modules at the same string have similar temperatures, from one end to the other. It is also evident that the rows facing south-west have a higher average temperature than the rows facing north-east.

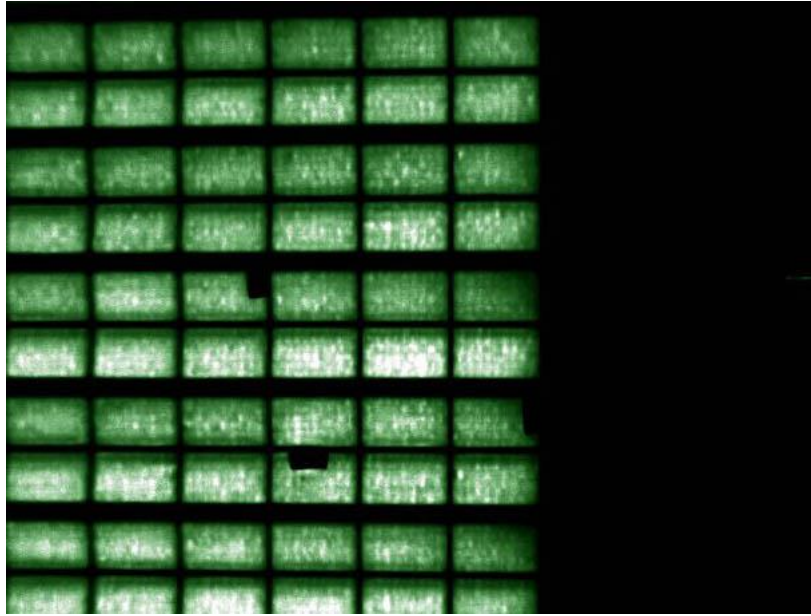
Modules placed at the ends of the roofs appear to have a lower temperature compared to the modules placed further towards the center.

#### 4.1.3 Single infrared photos

Three single infrared pictures were produced with intent to highlight the details of temperature distribution across the module surface. The pictures shown are all in a narrow temperature scale, highlighting detail, but excluding the surroundings. All the pictures shown are taken from a height of 30 m. The brighter the pixel, the higher the temperature.



*Figure 42. Infrared photograph of the PV-system. The single cells in a module are clearly distinguishable from one another. Each module contains 6 x 10 cells.*



*Figure 43. Infrared photograph taken at the edge of the roof. The black squares appearing at the module surface are aluminum foil, reflecting the temperature of the sky.*



*Figure 44. The trend of similar temperatures for modules in the same string are evident.*

The relative temperature difference between modules and strings uncovered via the infrared pictures are low in magnitude. Although temperature differences between string and modules do occur, the relative temperature difference does not indicate any deficiencies of the system. The defects described by IEC and Testo in 2.6.4 cannot be recognized in the pictures. The results indicate that the PV-system is in a healthy state.



#### 4.1.4 Calculation of radiated effect from PV-modules

A calculation is performed with intent to estimate the radiated effect from the PV-modules at the ASKO-facility. The calculation is based on values from the aerial thermography maps. Effects of atmospheric transmission and emissivity of the modules is compensated for when processing the pictures, as explained in chapter 3.2. The calculation only estimates radiated effect, - convection and conduction is not a part of this calculation.

The highest temperature registered at the module detail map (figure 41) is 15.85 °C.

Stefan-Boltzmann's law (equation 15) is used to calculate the radiated or absorbed energy between to objects. The area factor is not used, changing the output result to  $W/m^2$  rather than W.

Factor	Value	Unit	Comment
$T$	15.85 / 28.85	°C / K	Measured temperature of the PV module
$T_0$	-5.0 / 268.0	°C / K	Temperature of the outside air/snow
$\sigma$	$5.6703 \cdot 10^{-8}$	$W/m^2K^4$	Stefan Boltzmann constant
$e$	1	-	Compensated for in the infrared pictures(chapter 3.2)
$Q$	102.2	$W/m^2$	Radiated transfer between the module and air/snow

*Table 14. Table of the results showing the radiated effect from the PV-modules in heating mode*

The result show a radiated effect of  $102.2 W/m^2$ . This is lower than the modules electrical effect of  $252.1W/m^2$ . The difference between measured radiated effect and electrical effect indicate significant convection and conduction losses.

#### 4.1.5 Calculation of thermal coefficient $C_t$ , using heat flow from PV-modules

A calculation is made with the intent of determining the thermal coefficient from a roof with PV-modules running in heating mode. The framework used for the calculation is presented in 2.1.2. The calculations takes basis in one single module, but is later applied to a roof by converting the number through the weighing of effective area of snow load reduction. The validity of the calculation is discussed in 5.2.3.

The formula assumes a characteristic snow load higher or equal to  $1,5 \text{ kN/m}^2$ . A value of  $1,5 \text{ kN/m}^2$  is the lowest possible characteristic snow load a municipality can have in Norway, making the calculation of the thermal coefficient valid for the whole country. This specific calculation is done for a characteristic snow load corresponding to the amount for Oslo.

##### Results:

Factor	Value	Unit	Comment
U	< 4,5	W/m <sup>2</sup> K	* See discussion
$\beta$	0	Deg, °	* See discussion
$S_0$	3,5	kN/m <sup>2</sup>	Characteristic snow load Oslo (0-150 moh)
$\theta$	18	°C	* See discussion
$f(U_0, \theta)$	13	-	
$C_t$	0.298	-	Thermal coefficient for the module surface

Table 15. Table of the input values used.

The  $C_t$  value calculated only applies for the module surface. A calculation is made estimating an area-weighted value  $C_t$  for the roof as a whole in relation to the PV-module covered area. The  $C_t$  factor is divided by the module-to-roof area ratio, reducing the  $C_t$  value. The area numbers applied are taken from the ASKO roof.

Component	Area [m <sup>2</sup> ]	$C_t$	S [kN/m <sup>2</sup> ]
Module	1210,6	0,298	1,04
Roof	1920	0,473	1,65

Table 16. Area weighted values of snow load reduction

S is the characteristic snow load of  $3.5 \text{ kN/m}^2$  multiplied with  $C_t$ . The exposure coefficient and the shape coefficient are not taken into account.

The results show a design load reduction from  $3.5 \text{ kN/m}^2$  to  $1.65 \text{ kN/m}^2$  for the whole roof surface at ASKO.

The thermal coefficient of 0,298 and respective load reduction is calculated as an estimate applicable for the ASKO roof. Both the thermal coefficient and the resulting load reduction is accurate for this exact roof and climate. However, the effect of the characteristic snow load strongly influences the coefficient value. An additional calculation is performed, exhibiting values suitable for other locations in Norway and the following characteristic snow load. The calculation is made for the complete range of characteristic snow load values, from 1.5 kN/m<sup>2</sup> to 9.0 kN/m<sup>2</sup>. This calculation is performed in the same manner as the previous. The calculation is valid for the module surface; no weighing of module/roof area has been made. The reduction column multiplies the thermal coefficient with the characteristic snow load.

$S_k$ [kN/m <sup>2</sup> ]	$U$	$\theta$	$\vartheta$	$f(U_0, \theta)$	$C_t$	$S$ [kN/m <sup>2</sup> ]	Reduction [kN/m <sup>2</sup> ]
1.5	< 4,5	0	18	13	0.43	0.65	0.85
3.0	-	-	-	-	0.32	0.97	2.03
4.5	-	-	-	-	0.25	1.13	3.37
6.0	-	-	-	-	0.20	1.18	4.82
7.5	-	-	-	-	0.15	1.13	6.37
9.0	-	-	-	-	0.11	1.00	8.00

*Table 17. Thermal coefficients and the respective load reduction for different characteristic snow loads.*

The results show that although the thermal coefficient varies between 0.43-0.11, the design load only differentiate by relatively small amounts. The most significant reduction is for areas with a characteristic snow load of 9 kN/m<sup>2</sup>, which is reduced by 8 kN/m<sup>2</sup>.

## 4.2 Test of a full scale PV-heating system

A total of 3 cases were performed simultaneously at the ASKO facility. The current was on for a total of 2 hours for all the cases. The data presented consist of snow depth measurements, temperature and humidity of the snow and air, snow density measurements and visual observations.

Measurement	Value	Unit
Outside temperature avg	-6.8	°C
Outside relative humidity avg.	69.8	%
Snow density avg.	101,1	Kg/m <sup>3</sup>
Snow depth at module avg.	4,83	Cm

Table 18. Table of the initial conditions.

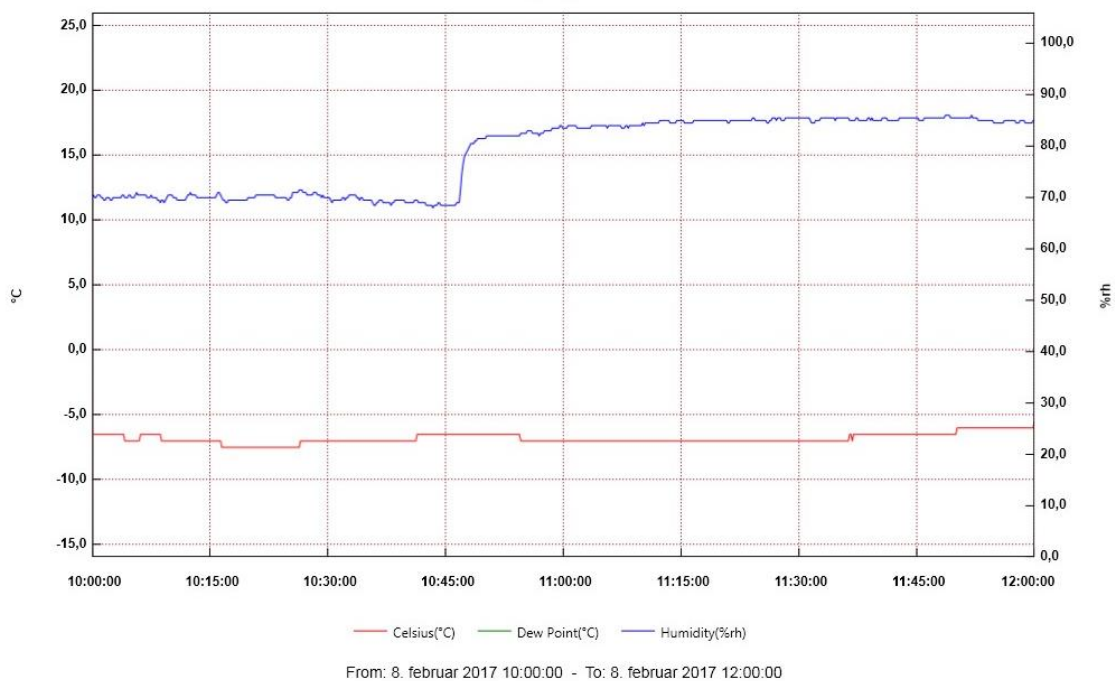


Figure 45. The outside air temperature and RH during the experiment. The logger was blown in the snow after 45 minutes of testing, affecting the values measured.

### 4.2.1 Case 1

For case 1, maximum effect of 50 Volts and 10 Ampere were applied to 2 strings of modules with natural snow depth. The results showed 2 different scenarios for the two different strings applied power. For both strings, melting snow at the module surface proved to be effective. But for the string facing the wind, the melt-water froze when approaching the rim of the modules. A 0,5 - 2 cm ice cap at the lower edge of the modules formed, acting as a dam for the melted water below. The melting-water was unable to run off the modules, leaving the weight approximately the same as before. For the modules being sheltered from the wind, there were no signs of ice forming at the surface.

#### Measured data:

Avg.Snow depth before[cm]	Avg.Snow depth after[cm]	Snow depth reduction[cm]	Snow depth reduction [%]
4,83	1,83	3,0	62

Table 19. Snow depth data for case 1. The data presents depth reduction; although the depth decreased, the load was not necessarily reduced.

A temperature and RH logger were placed in the snowpack. The temperature gradually increased, barely rising above zero. The humidity increased at first, but then dropped when approaching 0°C. This is a repetitive pattern for the loggers, seemingly occurring when the logger gets wet.

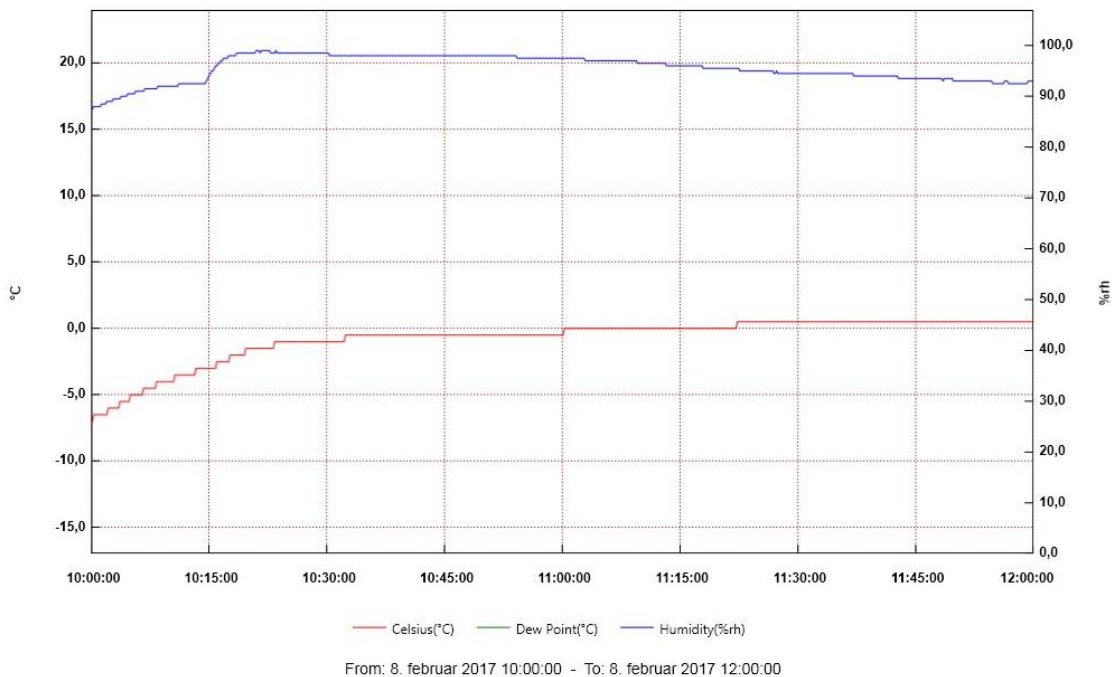
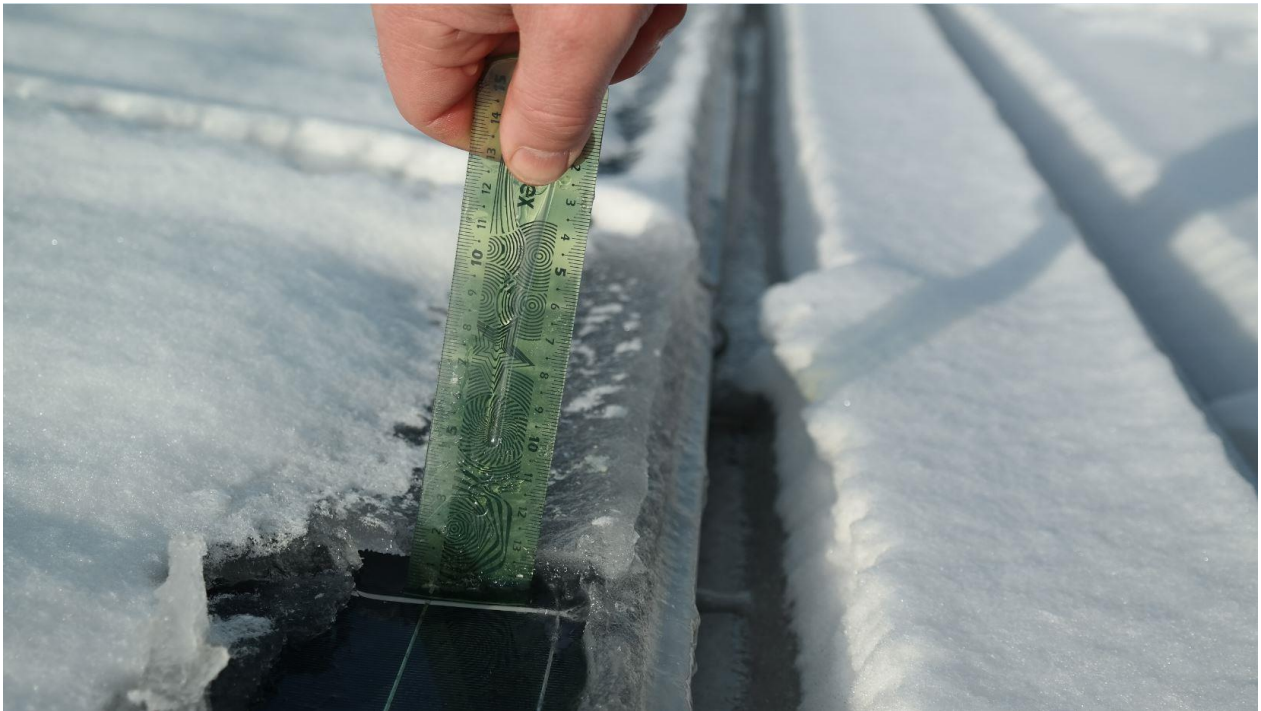


Figure 46. Temperature and RH of the snow for case 1.

Visual observations:



*Figure 47. An ice cap forming at the lower edge of the modules facing the wind*



*Figure 48. Scale of the ice cap. The heated drainage duct is located directly beneath the modules edge. The exposed gap between prevented the water from coming that far.*



*Figure 49. The photo shows the 2 strings subjected to current, with the untouched strings next to it on the right. The modules facing the wind(left) formed an ice cap, while the modules sheltered from the wind(right) did not.*



*Figure 50. The modules thermal footprint became visible through the snow. The ice cap is seen at the bottom of the photograph.*

### 4.2.2 Case 2

For case 2, the maximum effect of 50 Volts and 10 A were also applied, but additional snow was shoveled onto one module. The module did not experience the same ice cap as in case 1 due to the increase in snow depth. However, the snow at the bottom of the module became saturated with water. Water was absorbed by the dry snow, creating a saturated layer of 1-3 cm in the bottom layer of the snowpack. The snow depth was reduced, but no water could be seen running from the module.

#### Measured data:

Avg. depth before[cm]	Avg. depth after[cm]	Reduction[cm]	Reduction[%]
11,1	9,5	1,6	14,3%

Table 20. Snow depth data for case 2. Although the depth decreased, the weight remained approximately the same due to insufficient water drainage.

Temperature and RH were logged at the top and bottom of the snowpack of the module. The logger at the bottom showed similar results as in case 1, a gradual increase in temperature rising slightly above 0°C. The logger at the top of the snowpack showed an increase in both temperature and RH, increasing with up to 3°C in temperature.

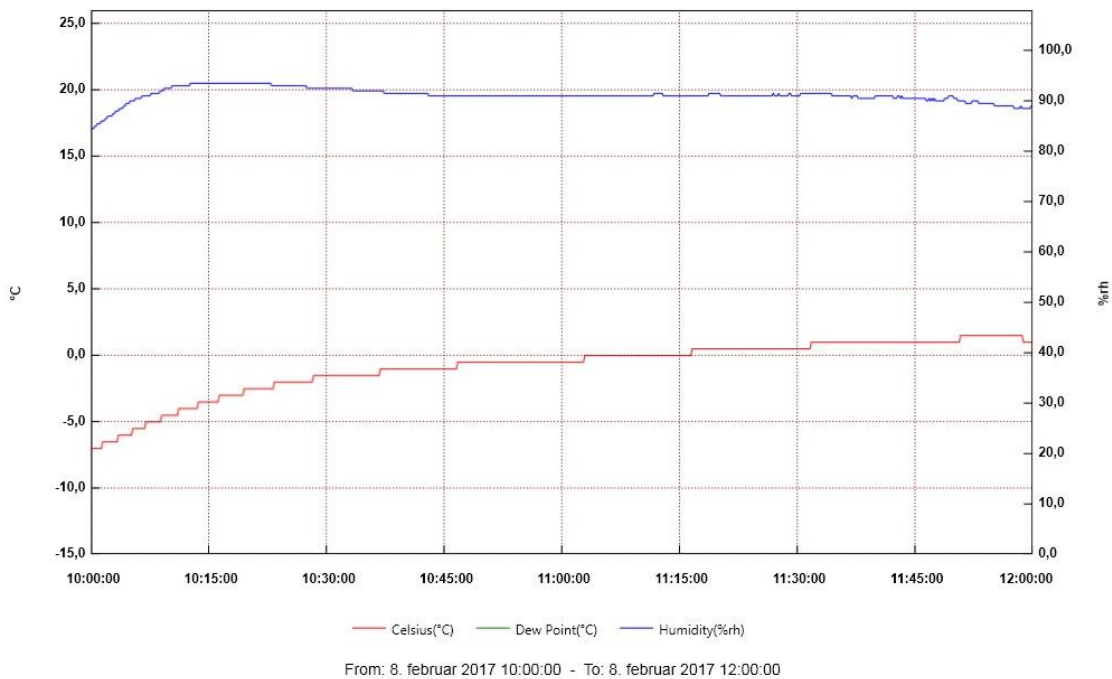


Figure 51. Logger placed at the bottom of the snowpack.



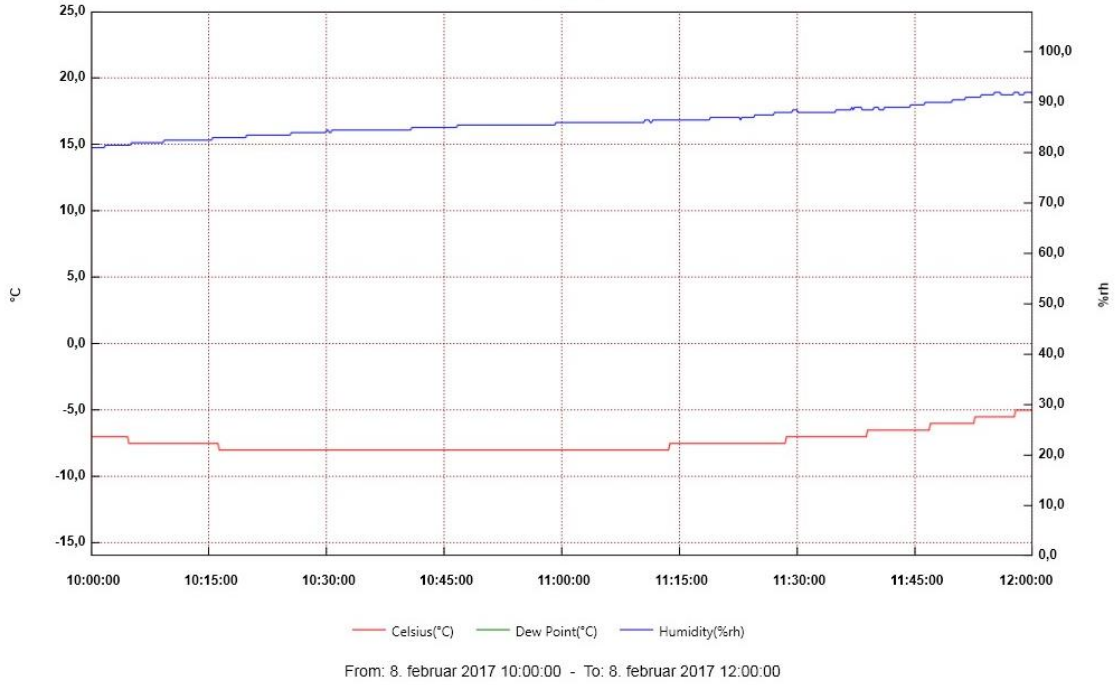


Figure 52. Logger placed at the top of the snowpack.

**Visual observations:**



Figure 53. Photograph of the module taken halfway through the test.



*Figure 54. Photograph from a cross section of the snowpack after the experiment. The thickness of the saturated snow-layer is gradually increasing towards the bottom of the module, indicating that water is transported towards the lower edge of the module.*



*Figure 55. A close up of the cross section.*

### 4.2.3 Case 3

One string of modules was applied 50 Volts and 5 A with the intent to sublimate the snow. Not much data was collected in this case. A two hour window is not sufficient for sublimating snow of a considerable amount. However, temperature and RH were logged in the snowpack, providing insight into the behavior of an induced moisture and temperature gradient.

#### Measured data:

The logger showed a gradual increase in temperature, though not rising above zero. The maximum temperature at the module is  $-0,5^{\circ}\text{C}$ . The relative humidity increased gradually from 86% up to 99%. The non-existent drop in RH indicate that the snow was not melted to a considerable extent.

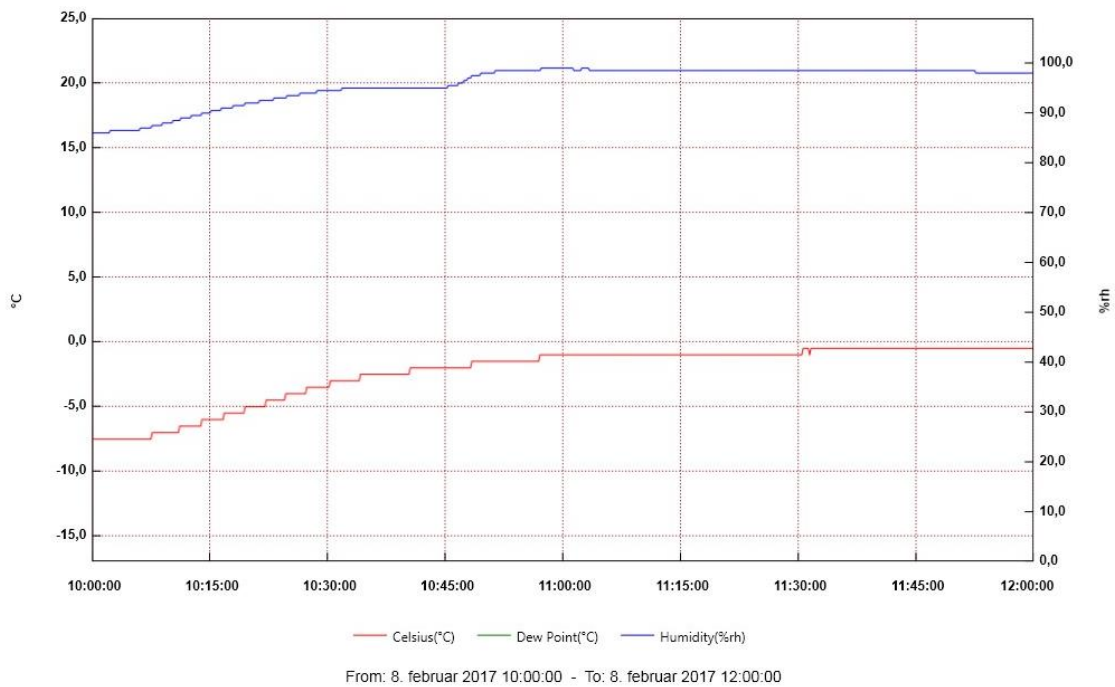


Figure 56. Temperature and RH of the snow in case 3.

### 4.3 Case study in Nordmarka

A total of 3 cases were performed at the Nordmarka study. The cases were performed in chronological order. The data presented consists of snow depth measurements, temperature and humidity logging of the snow and air, snow density measurements and visual observations.

Due to the large amount of data collected, especially in the sublimation case, a large portion of the data is presented in Appendix B. This includes all the temperature and humidity graphs, depth and density measurements, electricity log, wind data and average/max/min values for temperature, RH and SH. The data presented here is concentrated and selected information from the appendix.

#### 4.3.1 Case 1 – ASKO Setup

For case 1, an effect of 50V and 10A equivalent to the upper limit at ASKO, was applied. The initial depth was 21,5 cm and the measurements show a depth reduction of 2,4 cm after 3,5 hours with power. No density measures were taken, leaving the total weight reduction unknown. The initial density was 140 kg/m<sup>3</sup>. The surface temperature increased to 6°C for module 3. A layer of slush of little magnitude was observed at the module surface.



Figure 57. Photograph of the setup for case 1 subjected to power.

## Temperature and RH

Humidity and temperature were logged at the top and bottom of module 1 and 3 in addition to logging the outside air.

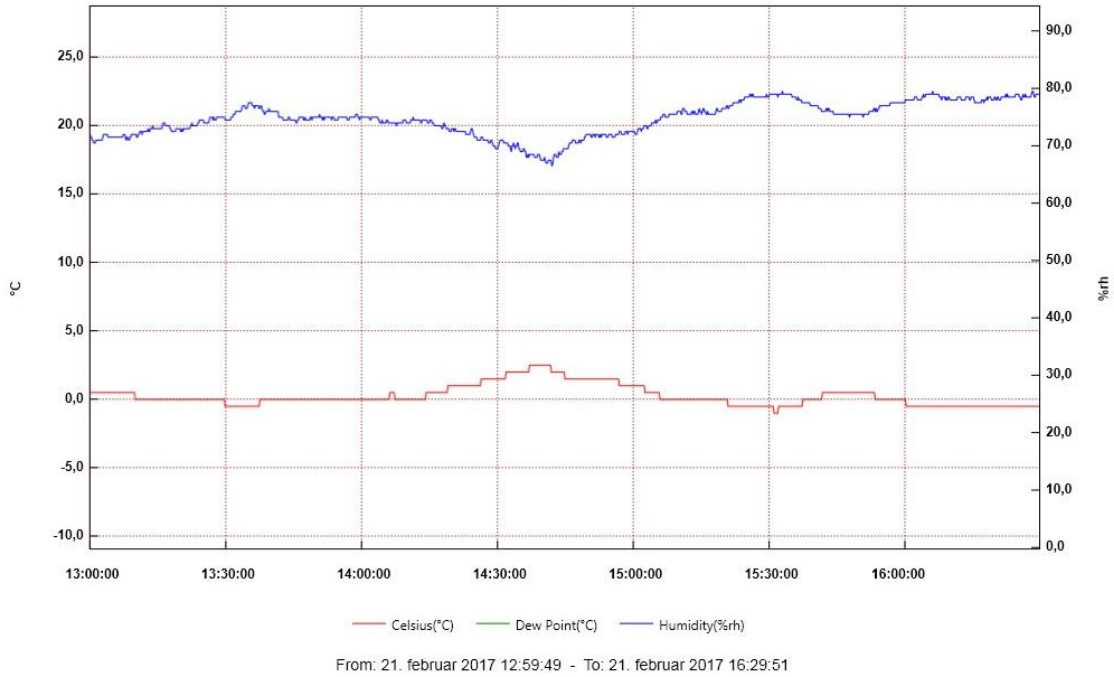


Figure 58. The outside air temperature and RH during the experiment.

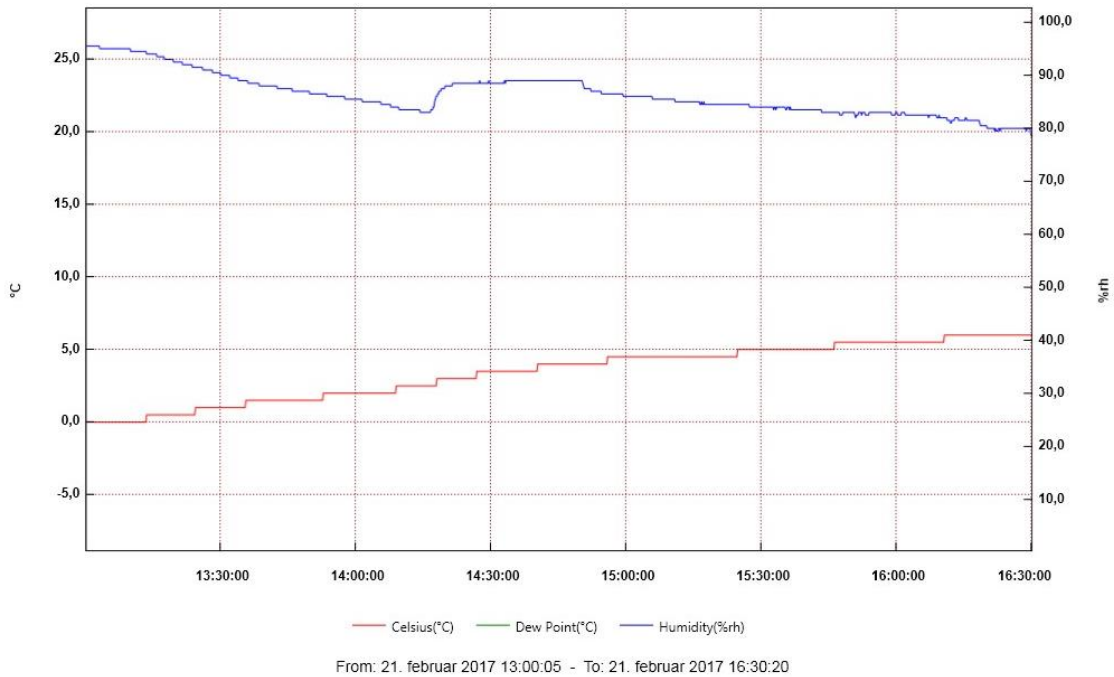


Figure 59. Module 3, bottom snowpack

**Visual observations:**



*Figure 60. The snow at the bottom of the modules was slushy after the test.*

### 4.3.2 Case 2 – Sublimation

For case 2, a low effect of 50 V and 0.3 – 2.0 A was occasionally applied during a time span of 58 hours. The results show the specific humidity at the surface of module 3 was raised close to the maximum value of what can occur in snow under normal conditions. The loggers indicate an induced humidity gradient between the modules subjected to current and the air. A humidity gradient was also present for the reference module, although of less magnitude. The snow depth for module 2 and 3 was reduced by a total of 7 cm since the start of the experiment. However, the density did increase by 71.7%. This resulted in the weight being reduced by a total of 2,18 kg/m<sup>2</sup> during the course of the experiment. The reference module experienced a depth reduction due to settling of the snow, but no weight reduction when taking the increase in density into account. At the end of the experiment an ice sheet was uncovered at the surface of module 2 and 3, although temperatures did not exceed zero. The ice sheet was thin and porous and covered the complete module surface, indicating some sort of snow metamorphism. Depth hoar crystals were looked after, but not found.

#### General data

As mentioned, most of the data is presented in Appendix B. The data presented here is concentrated to the most relevant information.

Module	Reference	Power
Depth before [cm]	14.05	14.05
Depth after [cm]	10.6	7.05
Density before [kg/m <sup>3</sup> ]	106.9	106.9
Density after [kg/m <sup>3</sup> ]	142.7	183.6
Weight reduction[kg/m <sup>2</sup> day]	-0.046	0.863
Energy used [kJ/kg]	-	2299.3

*Table 21. Data of snow depth, density, weight reduction and energy used. The average weight reduction for the modules applied power is 0.86 kg/m<sup>2</sup>day, while the reference module actually gained a small amount of weight during the experiment.*

## Temperature and RH

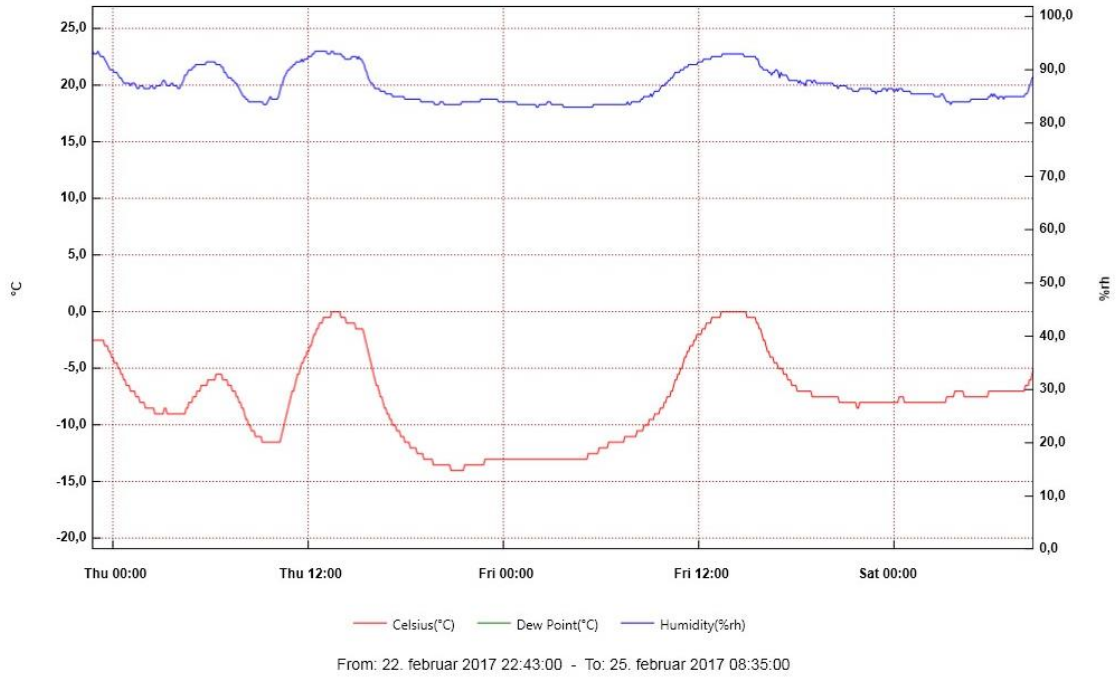


Figure 61. Module 3, top snowpack

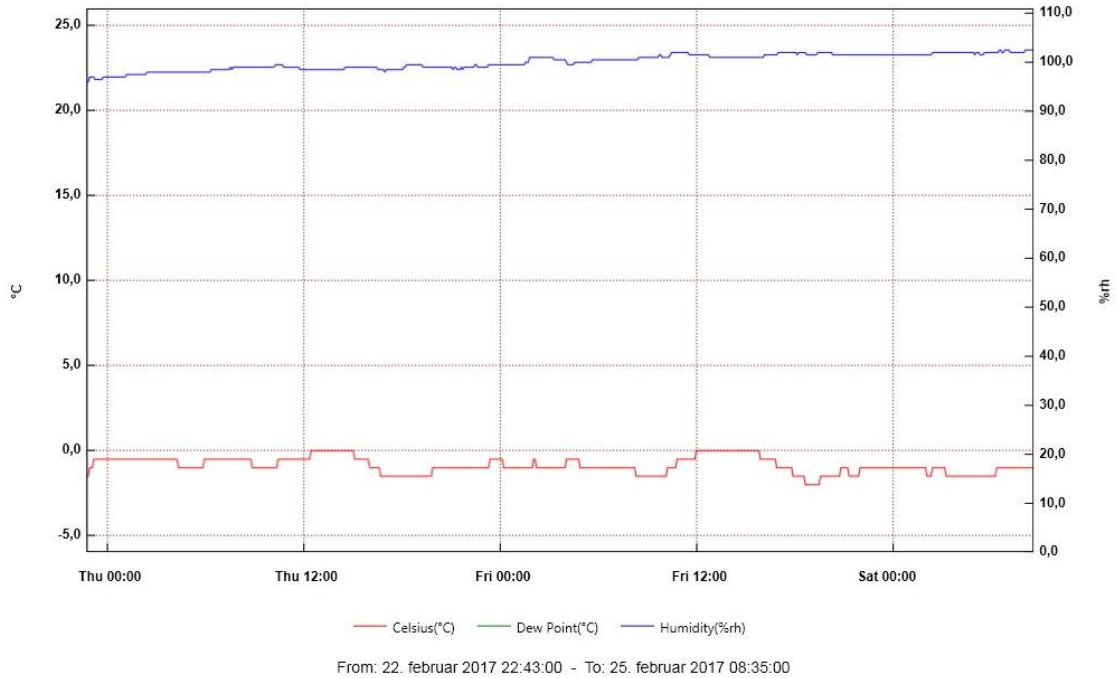


Figure 62. Module 3, bottom snowpack



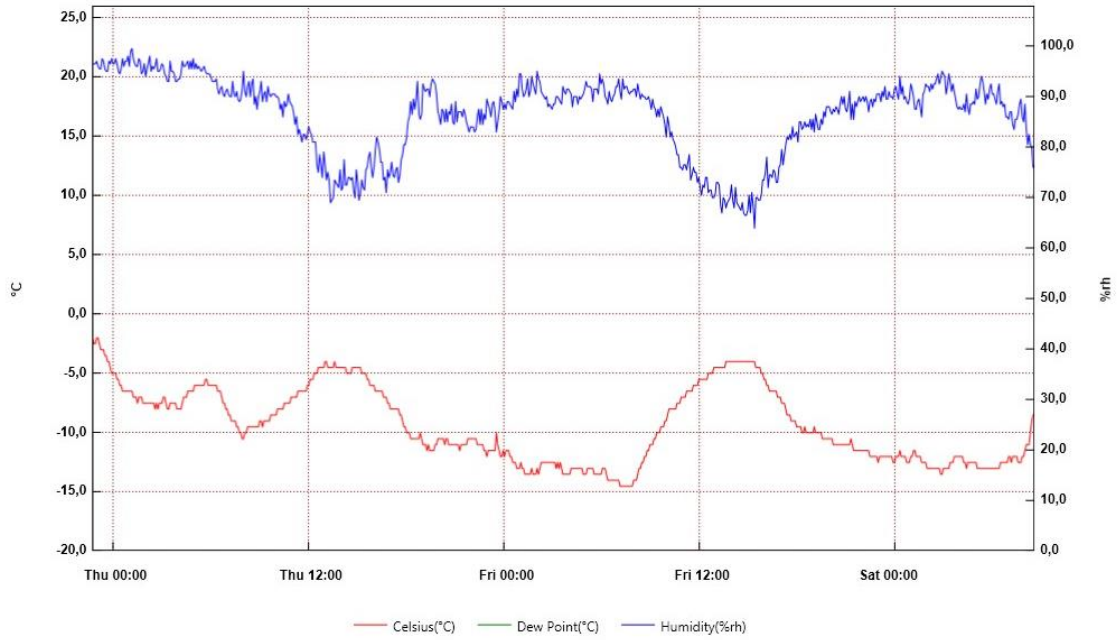


Figure 63. Outside air logger.

The table below shows the average values of temperature and humidity logged during the experiment. The specific humidity is estimated with the psychrometric chart. The logged specific humidity is used to illustrate the temperature gradients occurring in the snowpack.

Module	1	1	3	3	
Placement	Top	Bottom	Top	Bottom	Air
Temperature [°C]	-11,3	-3,6	-7,8	-0,9	-9,3
Relative hum. [%]	85,6	94,4	87	100,1	86,3
Specific hum. [g/kg]	1,294	2,796	1,794	3,723	1,559

Table 22. Table of logged temperature, relative humidity and specific humidity.

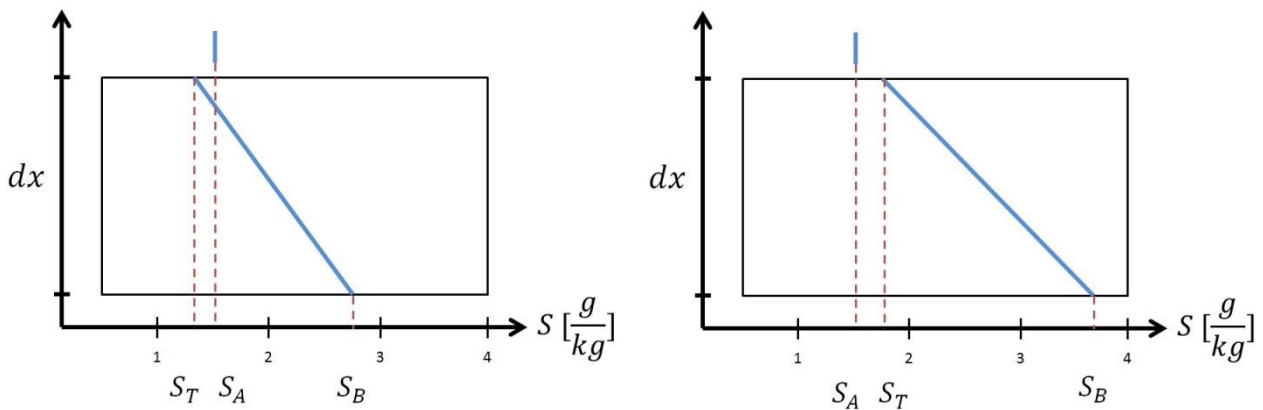


Figure 64. Illustration of the humidity gradients occurring for module 1 (left) and module 3 (right).  $S_T$  is the moisture logged at the top of the module,  $S_B$  is for the bottom, while  $S_A$  is for the air.

For module 3, there is a positive difference between the moisture of the air and top layer of the snow, indicating sublimation. For module 1, the difference is negative, indicating condensation. The numbers match with the calculated weight change, module 1 gained weight, while module 3 significantly lost weight.

## Visual Observations



*Figure 65. Photograph before the start of the case. Fresh snow fell on top of the exposed modules during the night leading up to the start of the sublimation case.*



*Figure 66. Photograph of the modules after the first night of sublimation. A relative reduction of snow depth on modules 2 and 3 can be observed.*



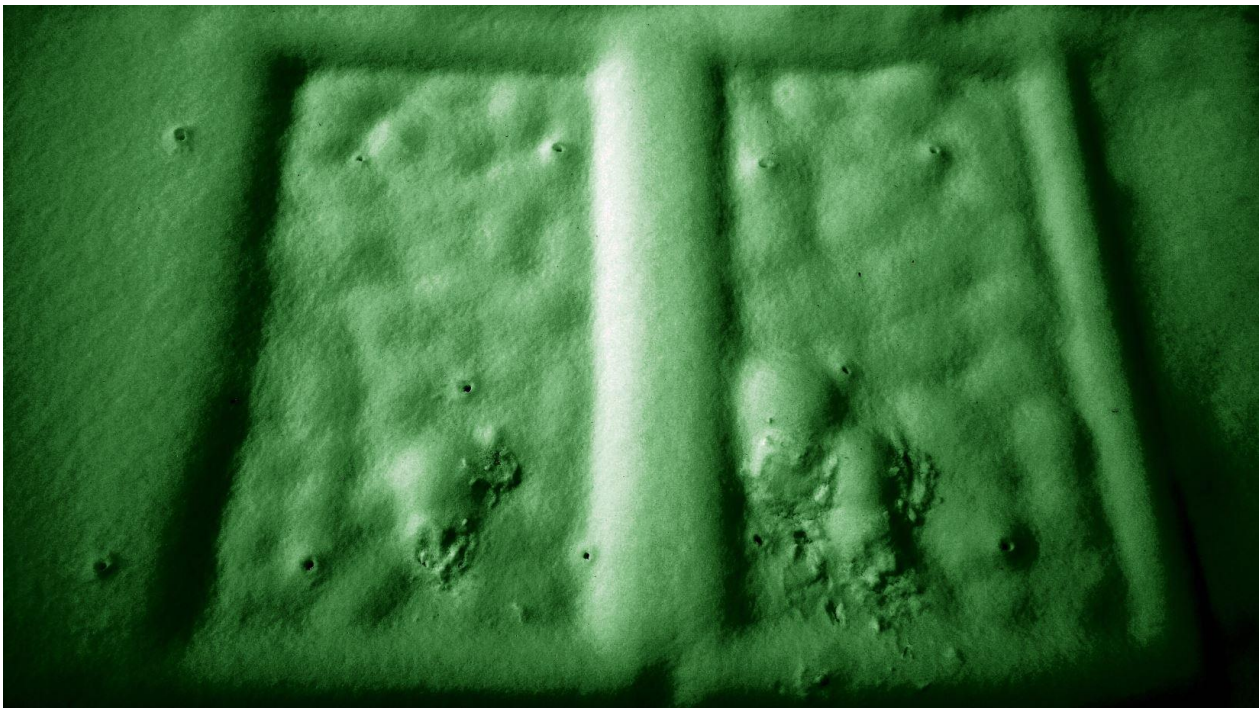
*Figure 67. Photograph after the second night of sublimation. A clear dent in the snow can be seen at module 2 and 3. Module 1 is buried beneath the snow next to module 2, appearing as a flat surface.*



*Figure 68. At the end of the experiment it became apparent that an ice sheet had formed at the bottom of the module. The sheet was thin and porous with a surface of something that resembled ice pellets. The ice covered the complete module.*



*Figure 69. A bump between the modules indicate the relative change of depth.*



*Figure 70. An edited photo taken with a normal camera highlights small differences in depth reduction at the modules. The differences are caused by the thermal photoprint of the modules, as showed through infrared pictures in figure 25. The larger bumps at the modules are where the digital temperature sensor and the loggers were placed. The small, black holes show where the depth measurements are taken.*

### 4.3.3 Case 3 – Maximum effect

For case 3, the maximum power was applied for 3,5 hours. The voltage was set to 50 V and current to 30 A, but showed an operating effect of 48 V and 26 A. This results in a total power of 762,5 W/m<sup>2</sup>. Loggers were placed at the bottom of module 2 and 3 to record the increase in temperature.

The results show a high increase in temperature for module 2 and 3. The highest temperature registered at module 2 was 11.0°C, while module 3 showed temperatures up to 19.5°C. A dent in the snowpack became apparent halfway through the experiment. Snow fell during the experiment, making depth measurements invalid. At the end of the experiment, a large layer of water-saturated snow was discovered at the module surface. The capillary suction of the dry snow created a slush-like layer up to 5 cm thick.

### Temperature and RH

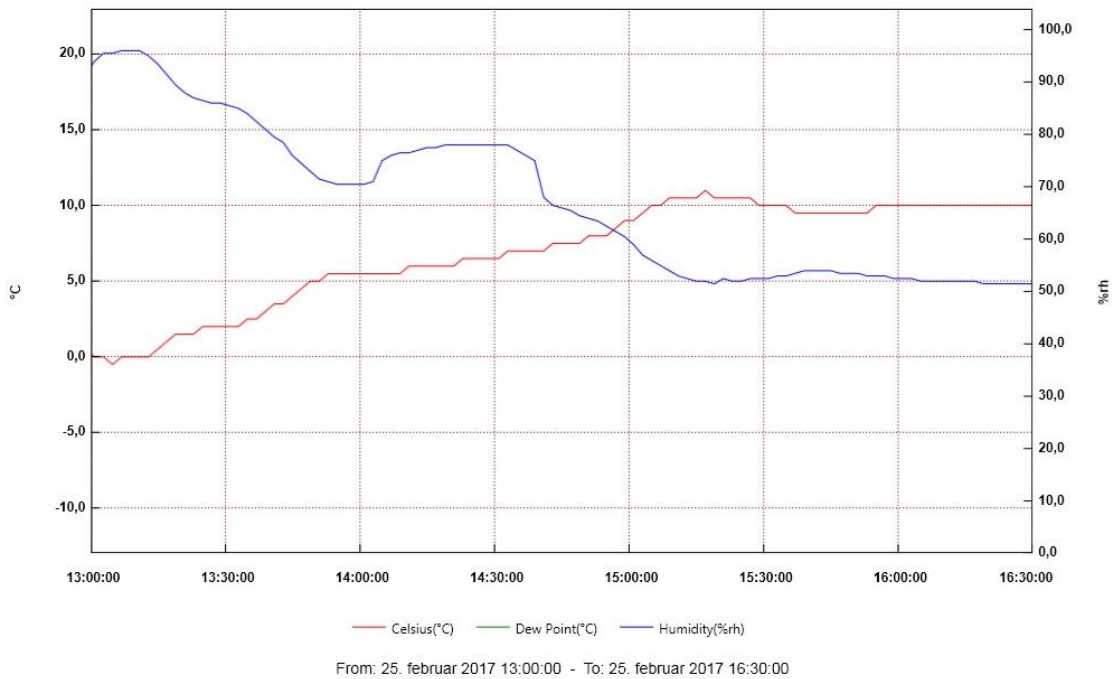


Figure 78. Module 3, bottom snowpack

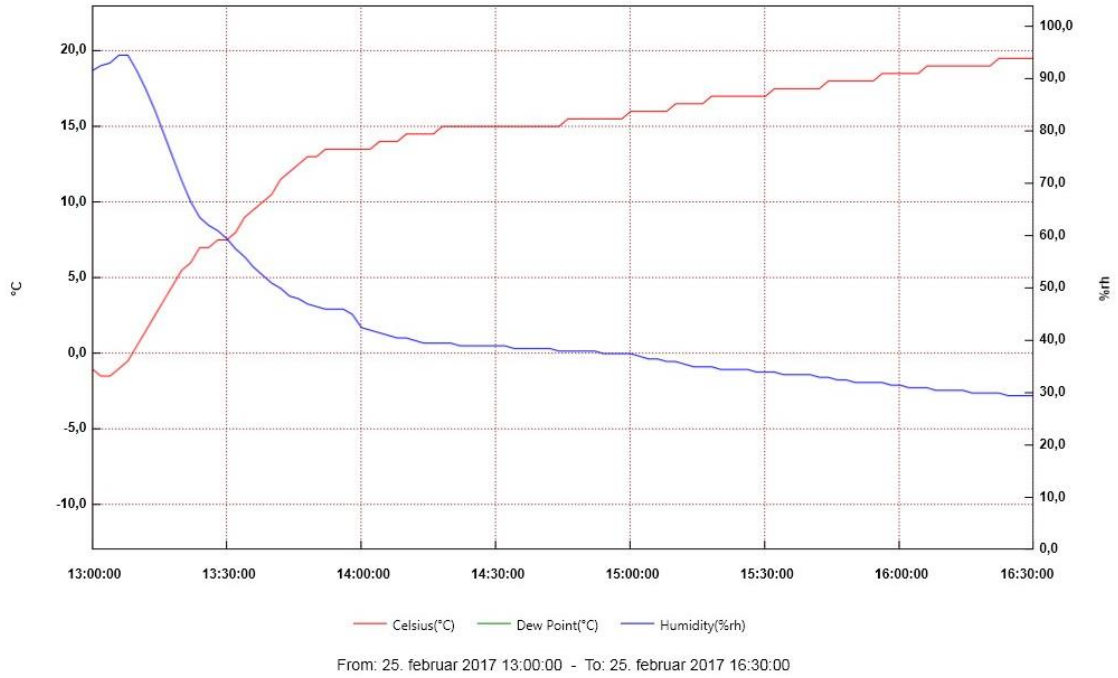


Figure 79. Module 2, bottom snowpack

**Visual observations**



Figure 80. Snow fell during the experiment making snow depth measurements invalid.



*Figure 81. A cavity formed at the center of each module. Flat light and snow made difficult conditions for photography making editing necessary.*



*Figure 82. A slush layer formed at the modules surface. The capillary suction of the dry snow created a layer of water-saturated snow.*





Figure 83. Scale of the saturated layer. The highest point is 5 cm above the module surface.

## 4.4 Analysis

The analysis chapter includes 5 calculations in addition to a diagram illustration based on measurements and knowledge acquired through the conduction of experiments during this thesis.

### 4.4.1 Equivalent heat emission through a roof

A calculation was made to estimate how much heat is transferred through a roof during the course of a winter, and how much time it would take for a PV-module to produce the equivalent heat emission. The calculation is based on simple heat transfer mechanics using the temperature difference between the two sides of the roofs and the corresponding U-value of the roof (equation 5).

Several simplifications/assumptions were made for the calculation:

- Mean month values for outside temperature was used from December to March.
- The inside temperature was set to 21 °C.
- The U-value of the roof is set to 0,34 W/m<sup>2</sup>K
- The effect of the module was set to the maximum power possible power generation at ASKO, equal to 252.1 W/m<sup>2</sup>.

Month	Mean temperature[°C]
December	-2,0
January	-4,7
February	-4,0
March	-0,5

Table 23. Mean month temperature values for Oslo. (Wolleng 1979)

## Results

Factor	Value	Unit	Comment
Q <sub>roof</sub>	8,02	W/m <sup>2</sup>	Average heat emission through the roof
Q <sub>pv</sub>	252,1	W/m <sup>2</sup>	Maximum heat emission through a module
E <sub>tot</sub>	23,67	kWh/m <sup>2</sup>	Total heat emitted through the roof during winter
T <sub>eq</sub>	3,91	Days	Number of days for the PV module to match the heat loss from the roof
Relative Time	3,18	%	Percentage of the time needed for the modules to produce the equivalent heat

Table 24. Results comparing the heat emission of a roof to PV-modules in heating mode. It takes 4 days or 3.18% of the time for the modules to produce the heat emitted through the roof during winter.

#### 4.4.2 Energy and time required for melting snow into water

A calculation was made estimating how much energy it takes to melt snow into water, providing insight to the energy used to reduce snow load for a PV-heating system. The results presented are mere energy calculations, using simple thermodynamic theory presented in 2.4.6 (equation 6). The calculation is based on the required energy to induce the phase change from snow to water. The snow and water temperature is assumed to be zero.

Two scenario based calculations are performed. Both scenarios are based on an imaginary situation at the PV-heating system at ASKO, using values from the power output from PV-modules and module/roof area ratio.

The first case is based on a load of  $1.5 \text{ kN/m}^2$  that is to be reduced to  $1.0 \text{ kN/m}^2$ . This equals a load reduction of  $0.5 \text{ kN/m}^2$  or  $50 \text{ kg/m}^2$ . The load reduction is calculated for the module surface and for whole roof. Only 63% of the roof is covered with modules, making it necessary to calculate how much snow needs to be reduced at the module surface for the load to be reduced from  $1.5 \text{ kN/m}^2$  to  $1.0 \text{ kN/m}^2$  for the whole roof.

The second case calculates the time and energy needed to melt the maximum possible amount of snow occurring within a day in Oslo calculated with a return period of 50 years. 34 mm SWE (snow-water equivalent) precipitation is the highest precipitation intensity that can occur within 24 hours in the months from December to March. The data used is provided by [eklima.met.no](http://eklima.met.no) through special access.

The time needed for the snow to melt is calculated assuming the maximum power of  $252.1 \text{ W/m}^2$ . The Total Energy column in the tables multiplies the energy per square meter with the PV covered area of the ASKO-roof ( $1210,6 \text{ m}^2$ ).

#### Results

Area	Load reduction [kN/m <sup>2</sup> ]	Mass reduction [kg]	Energy [kWh/m <sup>2</sup> ]	Total Energy [kWh]	Time [h]
Module	0.5	50.0	4.63	5608.6	18.37
Roof	0.5	79.3	6.34	7677.7	25.16

Table 25. Scenario of a  $50 \text{ kg/m}^2$  load reduction

Area	Precipitation [mm]	Energy [kWh/m <sup>2</sup> ]	Total Energy [kWh]	Time [h]
Module	34,0	3.15	3813.1	12.5
Roof	53,9	4.99	6044.8	19.8

Table 26. Scenario of a 34 mm SWE load reduction occurring at one day

The results show that load reduction is relatively fast. The load can be reduced faster than it occurs.

#### 4.4.3 Equivalent solar gain – for which snow depth is melting expedient?

A calculation was made balancing snow melting losses and solar gains. The calculation was based on the premise that if the weather forecast predicts clear skies for a given period, how much snow is it expedient to melt with intent to clear the modules for the coming solar gains, totaling a net zero when adding melting losses to solar gains. The calculation is done by comparing energy produced by a PV-system with energy required to melt snow determined by the latent heat of fusion (equation 11).

Several simplifications are made for the calculation:

- No power production when a snow cover is present.
- Evenly distributed snow at the module surface and even melting of the snowpack.
- Only the energy required for the phase change from snow to water is used. Temperature of water and snow equal to zero.
- The input data of produced energy are arranged in whole weeks, ranging from Monday to Sunday.

The input data is actual logged data from power production during the winter of 2016-2017 at the 1210,6 m<sup>2</sup> PV-heating system at ASKO. The numbers are provided by the system designer.

4 cases are made, each case in a different month in winter ranging from December to March. Each case estimates how much snow one can melt with the energy produced from the respective month. The highest day and week of energy production in the respective month is chosen to represent the “clear skies” scenario occurring that month. The weeks range from Monday to Sunday.

Time to melt describes how long it would take to melt the specified amount of snow assuming an effect of 252.1 W/m<sup>2</sup>, equal to the maximum effect at ASKO.

Month	Date	Energy produced [kWh]	Energy produced [kWh/m <sup>2</sup> ]	Equivalent weight [kg/m <sup>2</sup> ]	Time to melt
December	22-29	217	0,179	1,93	43 min
January	15-22	291	0,240	2,59	57 min
February	15-22	416	0,344	3,71	1h 22min
March	22-29	4254	3,514	37,93	13h 56min

Table 27. Energy equivalent snow melting amount for 1 week of solar gains

Month	Date	Energy produced [kWh]	Energy produced [kWh/m <sup>2</sup> ]	Equivalent weight [kg/m <sup>2</sup> ]	Time to melt
December	28	40	0,033	0,36	8 min
January	21	76	0,063	0,68	15min
February	22	110	0,091	0,98	22min
March	26	734	0,606	6,54	2h 24min

Table 28. Energy equivalent snow melting amount for 1 day of solar gains

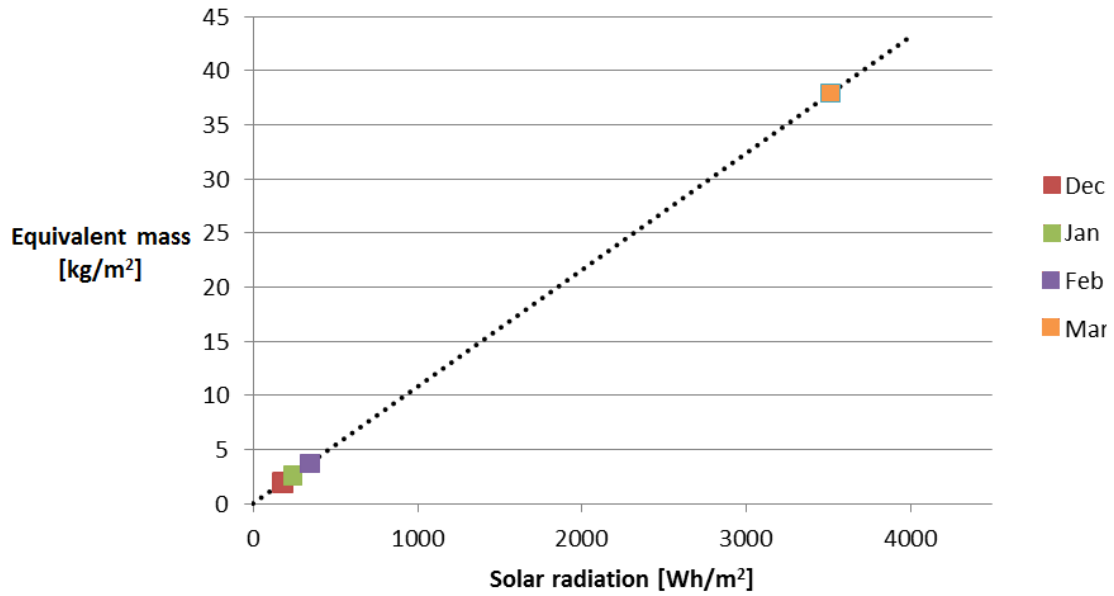


Figure 84. Graph of the weekly solar radiation measured and the energy equivalent mass

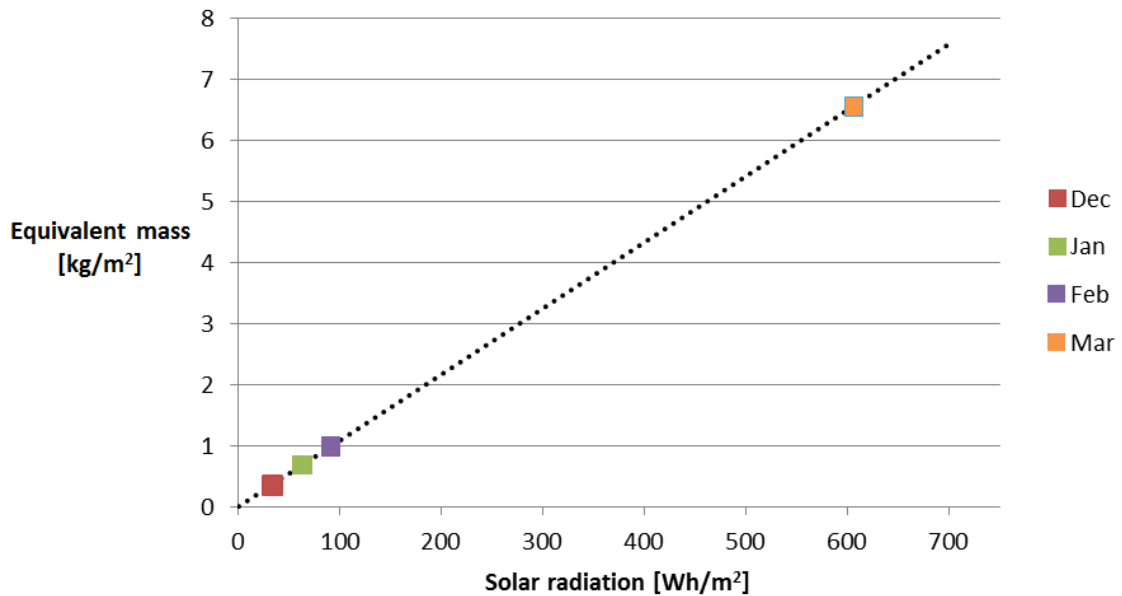


Figure 85. Graph of daily solar radiation measured and the energy equivalent mass

The results show that the power produced at ASKO is significantly larger in March than the previous months. The weekly solar radiation produced at ASKO in March is more than 10 times higher than for the second best month. The results are indicative of how melting snow is more advantageous towards spring than in the winter months of low solar irradiance.

#### 4.4.4 Roof surface temperatures under a snowpack

The roof surface temperatures present under a snowpack is interesting when evaluating the drainage capabilities of a roof with the PV-heating system. This calculation aims to uncover which temperatures that can occur under a thick snowpack of an unventilated hoot roof. The insulating effect of the snow combined with the heat transfer through the roof will cause a temperature gradient from the inside of the roof to the upper boundary of the snow. Ventilated flat roofs are not evaluated. Ventilated roofs will experience roof surface temperatures similar to that of the outside air.

Equation 6 and 7 presented in 2.1.2 are used to determine the roof surface temperature.

The thermal resistance of snow varies between 0.025 W/mK to 0.56 W/mK for densities between 10 to 550 kg(Cote et al.(2012) cited by Nuijten et al. 2016 p.263). The thermal resistance is dependent on density and microstructure of the snow(Nuijten et al. 2016). An average snow density of 200 kg/m<sup>3</sup> and a conductivity of 0.2 W/mK is used in this calculation. The snow depth is set be 0.6 m.

The U-value of the roof is set to be 0.13 – 0.34 W/m<sup>2</sup>K representing a high and low heat emission coming from the roof. The boundary conditions in all cases are a constant inside temperature of 21°C and a varying outside temperature between 0°C and -20°C.

<b>T<sub>Outside</sub> [°C]</b>	<b>U<sub>roof</sub> = 0,13</b>	<b>U<sub>roof</sub> = 0,34</b>
0	5,9	10,7
-5	2,4	8,2
-10	-1,2	5,8
-15	-4,8	3,3
-20	-8,4	0,2

Table 29. The surface temperature of the roof determined by outside air temperature and U-value of the roof.

The results show that temperatures below zero do occur for a well-insulated roof experiencing temperatures below -10°C. For a poorly insulated roof, the temperatures at the surface are likely to be above zero under a snowpack of substantial thickness.

#### 4.4.5 Estimated sublimation rates

The cases and method used for calculating the sublimation rates is presented in 3.5.

The table below shows the estimated weight reduction based on specific humidity of the air and snow in addition to wind speed. The transfer coefficient  $C_e$  varies between and  $1,0 \cdot 10^{-3}$  and  $1,5 \cdot 10^{-3}$ , both extremes are calculated.

Period	1		2		3	
Module	Pow	Ref	Pow	Ref	Pow	Ref
Input						
$q_s$	0,0037	0,0028	0,0037	0,0024	0,0037	0,0025
$q_r$	0,0016	0,0016	0,0012	0,0012	0,0013	0,0013
$U_r$	4	4	4	4	4	4
$C_e = 1,0 \cdot 10^{-3}$						
$Q_{bf}$	29,4	16,8	34,2	16,8	32,3	17,0
$m$	0,90	0,51	1,05	0,51	0,99	0,52
$C_e = 1,5 \cdot 10^{-3}$						
$Q_{bf}$	44,1	25,2	51,3	25,3	48,5	25,5
$m$	1,35	0,77	1,57	0,77	1,48	0,78

Table 30. Table of the estimated sublimated snow in the 3 different period.

$q_s$  is the specific humidity of the snow [kg/kg]

$q_r$  is the specific humidity of the air [kg/kg]

$U_r$  is the wind speed [m/s]

$Q_{bf}$  is the calculated latent heat flux [ $W/m^2$ ]

$m$  is weight reduction per day [ $kg/m^2$  per day]

The average sublimation occurring for the modules with current in period 1, is estimated to be between 0.90 and 1.35  $kg/m^2$  per day. However, sublimation is also estimated to occur for the reference module, averaging out at 0.51-0.77  $kg/m^2$  per day. The estimated sublimation is approximately twice as much for the modules subjected to current compared to the reference module.

In period 2 and 3, higher values of sublimation are estimated. The specific humidity occurring at the module surface is approximately the same for all the periods, but the impact of the reduced specific humidity in the air at night creates a larger humidity gradient and increases the sublimation rates. Period 2 gives the highest results with an estimated sublimation of 1.05-1.57  $kg/m^2$  per day. Sublimation rates at night are higher than the average rate sublimation rate for the documented at the study.

#### 4.4.6 Activity diagram for the automation of a PV-heating system

Three activity diagrams are made, illustrating how the automation a PV-heating system can be designed based on live data. The activity diagrams are mere suggestions of how the automation of the system can be designed based on knowledge of the system acquired in this thesis. It is the process of automation that is in focus, no specific numbers for limits triggering the system are suggested.

An activity diagram show the activities involved in a process or in data processing (Sommerville 2010). Every geometric shape in the diagram has a certain purpose:

- Blue circle indicates the start
- Blue dot inside a white circle indicates the end
- An oval square represent an action being made
- A regular square represent the source of data
- The rhombus represents a decision being made posed with 2 or more options

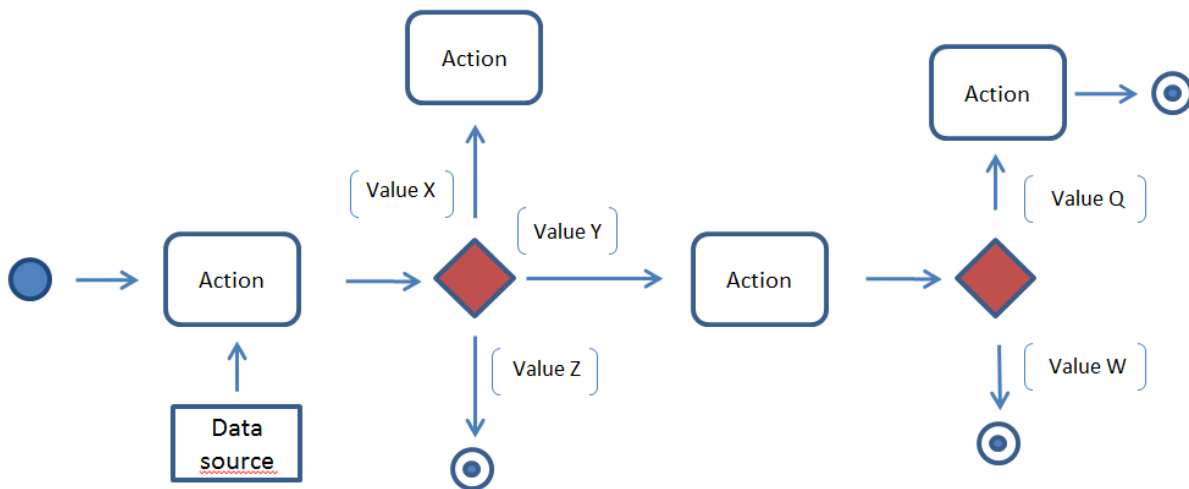


Figure 86. An example of an activity diagram.

All the diagrams are created in accordance with the method presented in the book Software Engineering(Sommerville 2010).

The diagrams made basically suggest how the automation of the PV-system can be designed. Live data measured on site or provided by a weather forecast triggers a decision of how the system should operate. Three diagrams are made, presenting 3 different automation situations:

- The first illustrates when snow load reduction should be initiated
- The second illustrates how the clearing of snow from modules can be performed with intent to enhance solar gains
- The third illustrates how to go about the ablation,- whether to sublimate or to melt



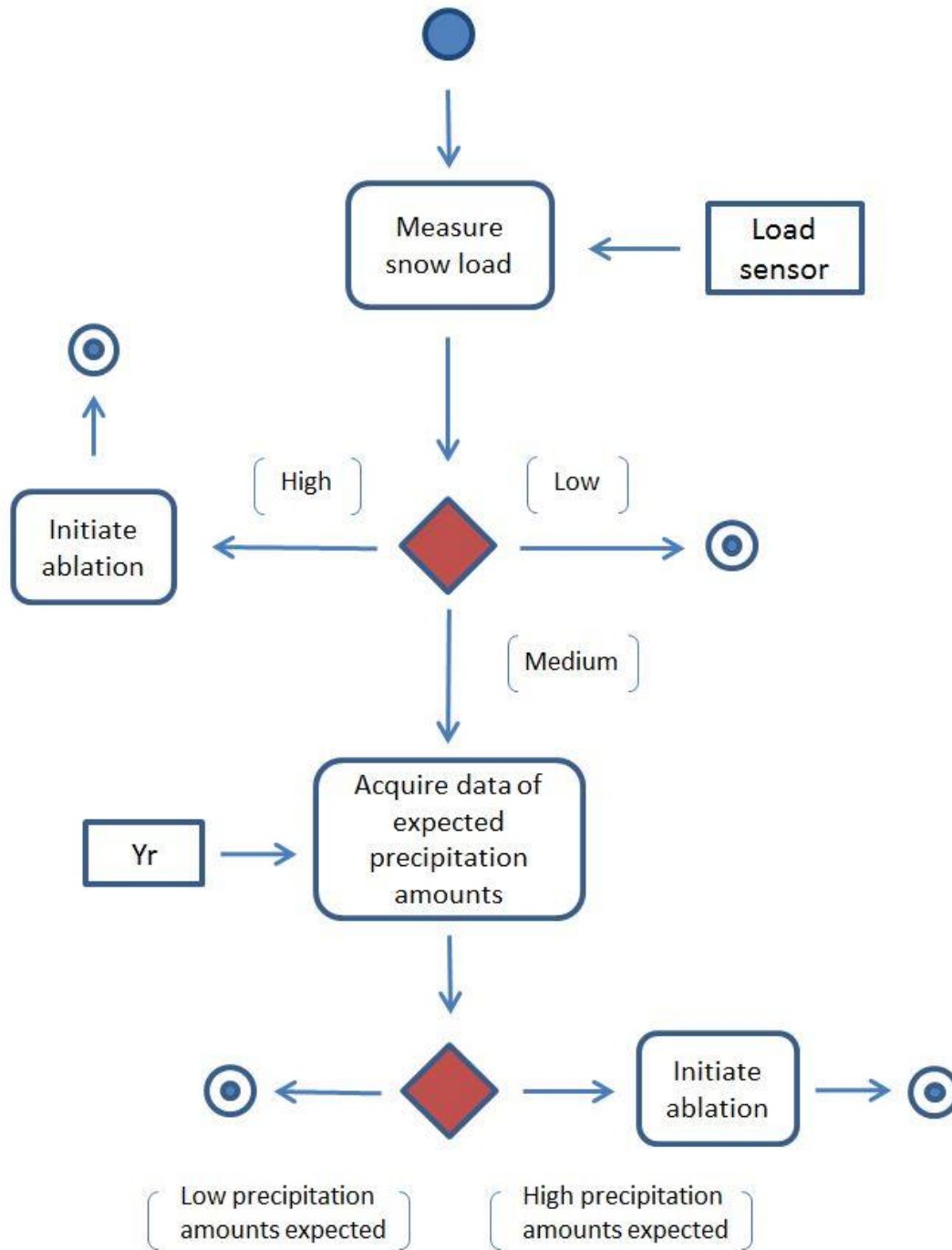


Figure 87. Diagram 1 – The automation of snow load reduction.

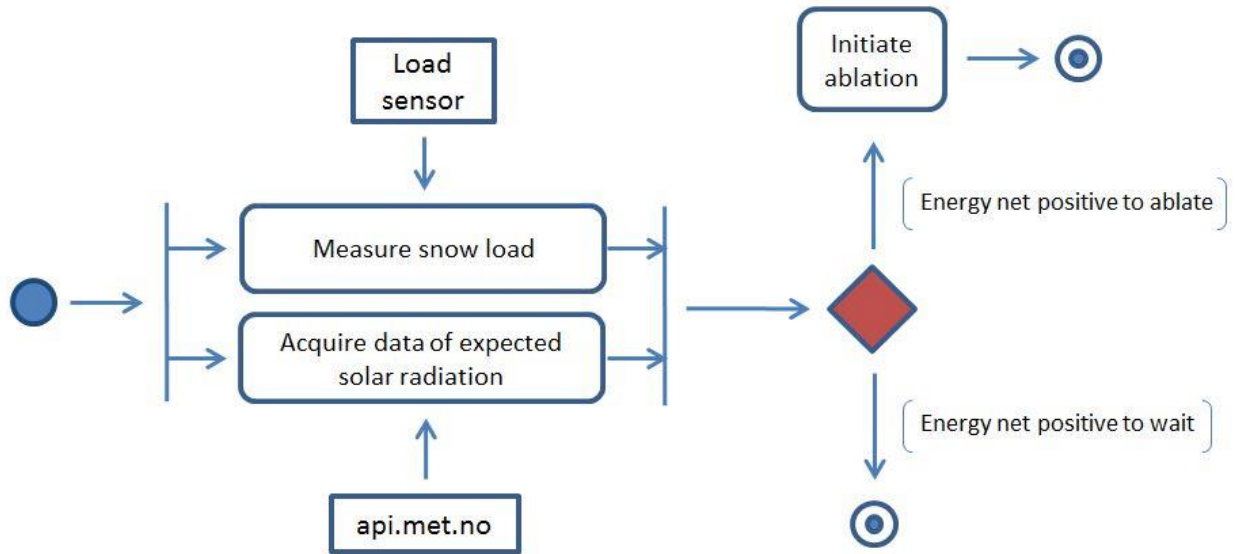


Figure 88. Diagram 2 - The automation of enhanced solar gains.

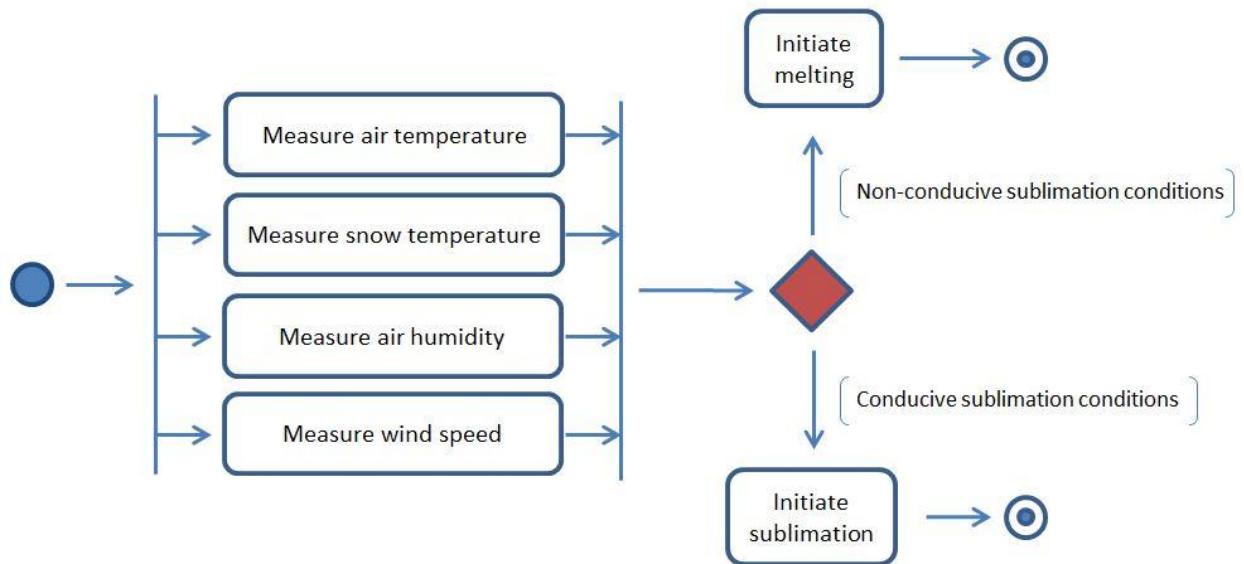


Figure 89. Diagram 3 – The automation of snow ablation.

All the diagrams are discussed in 5.1.3.

## 5 Discussion

The discussion chapter is organized according to the research questions stated in the beginning of the thesis. Each chapter uses the relevant theory and results from measurements and analysis to address the research question. Each chapter ends with a summary, directly addressing the research question.

### 5.1 Optimal strategy for snow load reduction under varying climatic conditions

This part of the discussion aims to answer the research question stated in the beginning of the thesis:

- *What is the optimal strategy for reducing snow load under varying climatic conditions?*

The measurements conducted, including the snow load reduction test of the full scale PV-heating system and the case study in Nordmarka, were performed with the specific intent of documenting the optimal strategy for snow load reduction. Investigating how melting and sublimation is best performed is an obvious way of optimizing the snow load reduction, but how the system is to be controlled can also have a significant impact on the load-reduction efficiency and energy consumption of the system.

Although snow load reduction with PV-modules in heating mode was thoroughly measured during this thesis, the optimal strategy is not only dependent on weather, but also on snow depth. It is with a large snowpack that snow load reduction is most relevant, and the depth of the snow is strongly determinative for the microclimatic conditions beneath the snow. The winter of 2016-2017 was lacking of snow in the eastern parts of Norway. The test of the full scale facility at ASKO roof would have been performed under a large snow pack, providing for a more realistic snow load reduction scenario. Unfortunately, the conditions did not allow for it. The results collected are therefore limited to the specific climatic conditions and snow depth at the time of the conducted experiment. Although the system was not tested in a heavy snowfall scenario, the results are indicative of phenomena that might occur under such conditions.

#### 5.1.1 Melting

The most obvious way to reduce the snow load with a PV-heating system is to melt it. Melting is easily performed with a PV-heating system, and requiring little finesse with the power adjustments. Measurements were performed testing how melting occurs on PV-modules in heating mode, both at the test of the full scale PV-heating system and during the Nordmarka case study. In addition, several calculations presented in the analysis chapter provide information indicating the sufficiency of melting snow with a PV-heating system.

Although melting snow is pretty straight forward, sufficient drainage of water is needed to ensure the reduction of load. Water unable to be transported off the roof can aggravate the situation. The snow might melt, only to be redistributed at the roof in unwanted places. Water at the roof surface can freeze,

creating further problems. Water dams at roof surfaces is a normal cause for moisture related problems for buildings. Freezing water might also serve as an obstruction for the water to come, retarding the possibilities for future load reduction. Either way, if the water is not properly drained, the load on the roof will not be reduced. Proper drainage is therefore highly important when melting the snow with a PV-heating system.

If a specialized drainage system with heated gutters is needed for a PV-heating system has not been thoroughly researched, but the experiments conducted indicate some possible consequences of not having it. At case 2 at the snow load reduction test at ASKO, a thick layer of snow was shoveled on to one module. The snow did melt at the module surface, but it was absorbed by the dryer snow above. The snow appeared to be increasingly more saturated towards the lower part of the module. A temperature of 1,5°C was registered at the module surface, however little water seemed to reach the end of the module even with a strong tilt of 10°. In case 3 at the Nordmarka-study, similar results were observed. Two modules with snow depth of approximately 20 cm were applied maximum power for 3.5 hours. Here, the modules laid approximately flat, providing little natural drainage of water. Visual observations revealed a slush layer up to 5 cm thick. The loggers placed at the module surface registered temperatures of 19.5°C for one module and 11°C for the other. The results indicate that even if temperatures are high at the module surface, or that the pitch of the module is strong, the water does not necessarily flow due to the snow's capacity for water saturation. The water saturation capacity of the snow depends on the snow density and microstructure.

Case 1 in the Nordmarka-study was similar to case 3 in terms of depth, effect and module tilt, but the quality of the snow was different. The snow was old, moist and grainy compared to the fresher snow in case 3. The weather that day was characterized by temperatures above zero and clear skies with solar radiation. Here, the snow did not seem to get saturated to the same degree, and the slush layer was of significantly lower magnitude than in case 3. The results indicate the importance of snow structure and density regarding the snow's capacity to suck up water.



*Figure 90. Different cases showing some degree of water saturated snow. Case 2 at ASKO, Case 3 at Nordmarka, and Case 1 at Nordmarka, ranging left to right.*

Although these results were observed at a module surface, it is still applicable to a hot-roof surface. Heat emitted through a roof combined with the isolating effect of snow is likely to produce temperatures

above zero between the snowpack and the roof surface. The calculations from 4.4.4 show that temperatures above zero are likely to occur for both a well- and poorly-insulated roof under a thick snowpack. However, with the results from the performed measurements in mind, water does not necessarily flow although temperatures are high and the pitch is strong. Also, changing conditions can result in lower temperatures at the roof surface, freezing the meltwater. For this reason, it is recommended to have a drainage system with heated gutters installed for a PV-heating system intended to reduce load. The consequence of not having it is not thoroughly researched yet, but can be severe.

For a ventilated flat roof, the surface temperatures will be approximately the same as the outside air temperature. For such roofs, heated gutters are a must-have when installing a PV-heating system intended to reduce load.

A redistribution of load due to unsuccessful transport of meltwater can be extremely unfavorable for an under-designed roof. The pitches of flat roofs lead the water to drainage points. If the water freezes along the way, the load can be concentrated at the lower parts of the roof. Such a redistribution of load could be highly problematic and dangerous.

Transporting the water away from the module surface can also prove challenging. The test at the full scale facility at ASKO showed that reducing the load of a thin, non-coherent snowpack in cold and windy conditions can be difficult. In case 1, two strings of modules were applied full power, one row facing East-North-East located at the outer edge of the roof, the other facing West-South-West placed one row in from the edge. The weather conditions that day was characterized by temperatures averaging out at  $-6,8^{\circ}\text{C}$  and wind speeds of 6 m/s. The wind was blowing perpendicular to the rows of modules (from East-North-East), affecting every other row of modules significantly, while sheltering the next. For the ENE-row the water was melted at the module surface, only to be frozen at the rim of the frame. The space between the modules in the outer row and the drainage duct was too large and exposed for the weather conditions to provide a safe path for free flowing water. The same result was not observed for WSW-row, sheltered from the wind. Here, no observations were made of ice forming at the module surface. Figure 49 show how ice formed at the row facing the wind, while the sheltered row was left intact. The rows not located at the edge adjoin closely, minimizing the exposure for wind and allowing for a continuous snowpack across the rows. The snow depth reduction at the sheltered row and the non-existent ice layer at module indicate a load reduction on the module surface. If the water was successfully transported off the roof is unknown. If the wind direction had been different, the outcome might not have been the same. The observations highlight the effect of microclimate on the roof.

If a larger snowpack was present, able to cover the frame of the modules, the effect of the low temperatures and wind would not have been as significant. A full covering snow layer would insulate the modules from the wind exposure and provide higher temperatures under the snow cover. If the conditions created by such a snow cover would enable the water to successfully flow into the drainage gutter is still unknown. The test at the ASKO facility clearly showed the problems of melting snow of an

incoherent snowpack under cold, wind-exposed conditions. Melting snow with a PV-heating system is not recommended to attempt under such conditions. Luckily, it is not in such a situation that snow load reduction is relevant. A larger snow depth will likely produce more favorable load reduction conditions.

Melting snow in conditions characterized by temperatures above zero and high solar radiation is less problematic. Warm temperatures and high solar radiation provide conducive conditions for melting. The transportation of water underneath the snow should also be less problematic due to the snow's decreased capacity for water saturation. The effect of warm air at the top of the snowpack combined with an induced heat at the module surface, has the potential of eliminating the temperature gradient, creating similar boundary conditions at both sides of the snowpack. The snowpack becomes like waffle batter in the waffle iron. The second law of thermodynamics state that the materials in a closed system will move towards the state of equilibrium due to inevitable heat transfer. The phase diagram also indicates how the snow is not in an equilibrium state when subjected to temperatures above zero under normal atmospheric pressure. The increase in temperature at both boundaries of the snowpack is highly conducive for the ablation of snow, effectively transforming snow into water. The results from case 1 at the Nordmarka study indicated a lower degree of water saturation allowing for proper drainage of the water as previously explained. The experiments performed and general thermodynamic theory indicates that load reduction by melting is effective under conditions characterized by high air temperatures and solar radiation.

The next paragraphs will focus on the time needed to melt snow into water. Time is of essence for a PV-heating system. It is important for the system to be able to reduce to load faster than it can occur. If the system is able to reduce the load relatively fast, and a medium heavy snow load is present at the roof, load reduction can be put off until further precipitation occurs, allowing for saving energy in the long run.

In 4.4.2, the time and energy required for melting snow is calculated in two different cases. Case 1 illustrates a scenario of reducing a snow load from  $1.5 \text{ kN/m}^2$  to  $1.0 \text{ kN/m}^2$ . The case evaluates time and energy for a load reduction at the module surface and for the roof as a whole. The results show that the time needed to perform such a reduction can be done within a day. The last row in table 25 provide the worst case scenario, reducing a snow amount of  $79.3 \text{ kg/m}^2$ . This scenario provide largest amount of snow being melting, and the calculations show that the load reduction of  $0.5 \text{ kN/m}^2$  can be done within 25.2 hours. This is a relatively fast load reduction, if comparing with maximum precipitation intensity rates in an Oslo climate. Case 2 illustrates exactly this scenario, looking at maximum precipitation rates ranging from December to March in an Oslo climate. With a maximum precipitation of 34 mm SWE occurring within the meteorological rain day from 07:00 to 07:00 (nedbørsdøgnet), the equivalent time for melting needed is 12.5 hours. This is a module surface scenario, but even with accounting for the share of modules covering the roof at 63%, the time needed is still only 19.8 hours. Such intense precipitation rates rarely continue for more than a day.

It should be mentioned that the precipitation amounts from case 2 does not include the maximum precipitation intensity for November and April. This is due to that the data used does not separate between snow and rain. To be more sure of that the precipitation actually occurring is snow, or to increase the chance that a snow layer is present, the typical winter months with the lowest mean monthly temperatures values was used. Although the precipitation is rain, a snow layer on the roof is likely to absorb water and increase the load accordingly. For this reason, the form of the precipitation is not necessarily determinative for load increase of the roof, although it will affect the thermal capabilities of the snow, and affect the load reduction rate. This is a complex and dynamic situation, requiring further analysis to be thoroughly investigated.

Although the calculations are simplified by only estimating the energy required to induce the phase change of the snow (the latent heat of fusion), the margins are solid. The implementation of sensible heat in the calculation has a minimal impact on the outcome, with a mass reduction of 3% less for the same energy input if the snow temperature is  $-5^{\circ}\text{C}$  instead of  $0^{\circ}\text{C}$ .

With the simplifications in mind, the results show that the snow load can be reduced faster than it is likely to occur in an Oslo-climate. The results indicate that the system is theoretically able to melt the snow faster than it occurs, preventing a buildup of snow at the roof.

The promising results of a fast snow load reduction allows for waiting longer before melting in a heavy snow load scenario. If a heavy snow load of  $1.0\text{ kN/m}^3$  is present at a roof designed for  $1.5\text{ kN/m}^3$ , and the weather forecast does not predict more precipitation, melting can be postponed. In this sense, fast melting allows for avoiding false alarms. A fast snow load reduction can therefore save energy in the long run if properly controlled.

The calculation in 4.4.2 showed that the energy required to reduce the load from  $1.5\text{ kN/m}^2$  to  $1.0\text{ kN/m}^2$  for the complete roof surface is equal to 7677.7 kWh. This is a substantial amount of energy making up 71.8% of what the PV-heating system at ASKO produced in March 2017 (Innos 2017). However, snow loads heavy enough to require snow load reduction action does not occur every year. To gain a true perspective of the energy budget of snow load reduction, a long term perspective should be applied. The frequency of heavy snow loads and the capacity of the under-designed roofs should be taken into account to calculate the long term energy consequences of such a load reduction system.

### 5.1.2 Sublimation

In this thesis, sublimation of snow as a mean to reduce snow load using PV-modules in heating mode is investigated. The advantage of sublimating snow is that the mass is directly transferred to the atmosphere, eliminating the need for a proper drainage system. As discussed in the previous chapter, the effectivity of melting snow is highly depend on the weather conditions, snow depth and snow structure. If the conditions does not allow for sufficient melting, sublimation can serve as an alternative. Sublimating snow on PV-modules also differs from melting in terms of the required performance of the modules. Instead of creating a high temperature on the module surface, sublimation occurs when the module surface temperature is below zero degrees. A module surface temperature just below zero induces a humidity gradient between the snowpack and the air, resulting in moisture flux through the snowpack. The required applied power is significantly less, opening up for new possible scenarios where sublimation might be a more appropriate option than melting. Two measurements were performed with intent to uncover the potential of sublimation using PV-modules in heating mode. Theory, measurements and analysis presented in this thesis provide insight into sublimation and its feasibility and is further discussed in this chapter.

In case 3 at the ASKO facility, sublimating snow was attempted. Although the short time interval of 2 hours was not enough to sublimate a considerable amount, the temp/RH logger in the snowpack showed an increase in humidity when power was applied. The humidity and temperature increased to the ideal level of 99% and -0.5°C within the first hour of applying power. However, this relatively fast increase in temperature and RH up to ideal sublimation levels can correlate with the typical symptoms of melting snow. As shown in figure 4, a solid material will have relatively constant temperature during the transition to the liquid phase. Surely, it is conducive for sublimation whenever the humidity levels increase relative to the air, but the risk of melting snow at the surface might be preventive for long term sublimation.

At the sublimation case in the Nordmarka study, ice was found at module surface at the end of the experiment. According to the loggers, the only time surface temperature of the modules rised above zero was during daytime after 12 o'clock when the power was off or very close to zero. The increase in temperature on the module surface was likely caused by increasing outside air temperature and solar radiation. If the ice layer was created by the rising temperatures during daytime or due to the long term effect of module surface temperatures close to zero is unknown. Significant snow metamorphism can occur under zero degrees celsius, but due to the fact that the modules were only checked at the end of the study, it is difficult to conclude what happened. It is sure that some sort of metamorphism did occur, but for what reason is unknown.

The density of the snow increased by at module 2 and 3 increased by 71,7% from beginning to the end of the experiment and by 28,6% compared to module 1. It is possible that the increase in density was affected by the deposition of vapor from sublimated snow. Ideally, the moisture flux caused by



sublimation at the bottom of the snow pack is depositing vapor directly into the air. However, it is a possible scenario that vapor from snow sublimated can be deposited further up in the snow pack due to decreased moisture levels throughout the snowpack as illustrated in figure 64. This can be one factor influencing the increased density levels at module 2 and 3 in addition the formation of ice on the module surface.

The possibility that the presence of an ice layer prevents sublimation of snow, raises the question if the impact of changing weather conditions and the consequences of a possible failure due to a too high surface temperature of the module can be preventive of sublimation. Is correct that if the temperature increase episodically, and the snow structure changes thereafter, that the possibility of sublimation has decreased? As explained in 2.5.4, the microstructure of the snow is an ever-changing property which is determinative for the potential of sublimation. This phenomenon is not thoroughly documented in this thesis and is recommended to be researched further.

Weather conditions are strongly determinative for the possibility of sublimating snow. As explained in chapter 2.5.1, sublimation occurs when there exists a humidity gradient between the snow and the air. Wind is an accelerator of the process, preventing the stagnation of air layers above the snow surface and water-saturation of the air. The previous research done on sublimation of snow focuses on large areas with homogenous snowpack, with more or less uniform moisture flux. Here, wind is essential to transport gradually saturating air, but for sublimation occurring over a smaller area, the influence of wind might not be as significant. Locally induced sublimation is less dependent on wind due to the surrounding air not being as saturated with moisture. Small wind speeds is likely to be sufficient for the transportation of moisture away from the snowpack of local induced sublimation. This is of course dependent on the size of the area experiencing sublimation. With this in mind, the validity of the Bulk Aero Dynamic Flux method for a locally induced sublimation can be discussed. When estimating sublimation using data from the Nordmarka study with the BF method, sublimation rates are significantly lower than the measured values when applying the wind data registered at the site. The estimated values indicate an underestimation of sublimation rates when using the real wind data. The average wind speeds registered are between 0.2-0.5 m/s. The estimated sublimated amounts are most similar to the measured amounts when applying a wind speed factor of 3.5 m/s. If the numbers measured are correct, and the BF-method's validity holds up for this application, the wind speed factor is significantly underestimated when applying the BF-method to an area of locally induced sublimation.

If this is true, sublimating snow on a local scale should be easier than for large areas with uniform moisture flux. The sublimation rates documented in previous studies presented in 2.5.3 are all done for large areas with quite uniform moisture flux. Perhaps sublimation on a local scale can exceed the amounts previously documented due to the decreased reliability of high wind speeds. Further research should be performed to uncover the potential of local sublimation.

Since sublimation occurs when there is a large humidity gradient between the snowpack and the air, sublimating at nighttime might be strongly favorable. Specific humidity usually drops towards nightfall, creating the potential of a larger humidity gradient. Here, induced sublimation differs from natural sublimation. Natural sublimation is reported to have a diurnal periodicity in some studies, due to an increasing snow temperature caused by rising air temperatures or solar radiation. However, it is at daytime that the specific humidity is at its highest, lowering the potential. The drop of specific humidity at night enhances the potential of high sublimation rates. The estimated sublimation rates presented in 4.4.5 indicate that the drop of specific humidity at night should theoretically increase sublimation rates. The estimated sublimation rates for nightly events is 16.3% (period 2) and 9.6% (period 3) higher than the average rate (period 1), indicating a larger potential of induced sublimation at night.

At the Nordmarka study, sublimation rates equal to  $0.86 \text{ kg/m}^2$  per day was documented. This number is calculated by multiplying the snow depth reduction with the increased density. This is the first induced sublimation of snow using PV-modules documented to this day, and the potential of induced sublimation rates is not investigated thoroughly enough. A better control of the system based on live data and different weather conditions provide the potential of surpassing the rates documented in this thesis. However, rates of  $0.86 \text{ kg/m}^2$  per day are significant. The conditions conducive for sublimation are opposite of the conditions conducive for melting in regards to temperature. Sublimation might be an appropriate option to melting, when temperatures are low and wind speeds are high. It is exactly these conditions that were observed at full scale PV-heating system when load reduction by melting was problematic.

Both measurements of inducing sublimation in this thesis were performed with a thin snowpack theoretically conducive for sublimation. The effect of inducing sublimation at a significant snow depth, when snow load reduction is of highest relevance, is not investigated yet. It is therefore somewhat difficult to conclude if sublimation can serve as a realistic option for snow load reduction using a PV-system in heating mode. A large snowpack also brings higher temperatures at the module surface due to heat flow through the roof as shown in 4.4.4. The calculation of surface temperature at a roof under a thick snowpack show that negative temperatures only occur when for well-insulated roofs on very cold days. The metamorphism of snow caused by plus degrees might be destructive for the possibility of sublimation. If sublimation of snow can be induced with PV-modules under a snowpack of substantial thickness is not uncovered through the measurements performed in this thesis. Further research is recommended.

Sublimation requires far more energy than melting. The latent heat of sublimation is 8.5 times higher than the latent heat of fusion. This means that 8.5 times as much snow can be melted compared to sublimated for the same energy input. However, sublimation is a natural process occurring to some extent regardless of whether power is applied to the modules or not. Applying a small current to the modules would simply amplify the process. A large portion of the energy used to sublimate snow is naturally provided by the climatic conditions. The energy relation of sublimation and melting at 8.5 is to

some extent provided by natural forces when working with the conditions. The study at Nordmarka showed an energy consumption of 2299.2 kJ/kg. This amount was calculated by dividing the total power applied to the modules during the experiment with the estimated weight reduction. This is much lower than the latent heat of sublimation at 2830 kJ/kg for snow at 0°C. The results show that less energy than the theoretical limit was needed to sublimate, indicating some contribution from natural forces. A further collection of empirical data is recommended to uncover the energy required to sublimate compared to melting.

Sublimating snow does not require a proper drainage system with heated gutters. If a PV-heating system needs heated gutters to ensure free flowing water off the roof surface, additional energy is needed for keeping the gutters warm. Sublimation is independent of the drainage system, avoiding the need for heating the gutters, saving energy.

### 5.1.3 The Automation of the PV-heating system

The CAN bus device installed in the PV-heating system allows for decision-taking of when and how to apply power to the modules for best possible snow ablation, based on live data. If the PV-heating system is to become a more widespread solution for under-designed roofs as a mean to reduce snow load or enhance higher solar gains, the system should be controlled in a more complex manner than manually turning the power switch. This chapter aims to provide a base for which data that can be used, and how to use these parameters to control the power output to the modules. This chapter discusses the implementation of live data in regards to three different scenarios

- How to determine if snow load reduction is necessary
- How to go about the ablation - whether to melt or to sublimate
- How to determine if clearing the module surface from snow is favorable for enhancing the solar gains

The three activity diagrams are presented in 4.4.6, one for each scenario. The diagram intends to illustrate how the automation of the system can be designed.

The data relevant for when and how to optimize snow ablation can be separated into data being measured on site or data of conditions to come provided by a forecast. A combination of these main sources is considered optimal as decisive parameters for when and how to initiate snow ablation. The live data measured on site would provide information for the conditions as they are. The forecast would provide data of the weather to come, for a long and short term time interval. As previously explained, the process of melting or sublimating snow is highly dependent on the climatic conditions and how they change. The implementation of live data in a PV-heating system can optimize reduction, save energy and possibly enhance the solar gains.

Live data measured on site will provide accurate information on the real-time climatic conditions on the roof. The data of interest is all the measurable factors influential for the ablation of snow. A table is made classifying the data of interest and how it can be measured.

Data	Sensor
Air/snow temperature	Digital thermometer
Air/snow humidity	Hygrometer
Wind	Anemometer
Solar radiation	Pyranometer
Precipitation	Rain gauge
Weight	Load sensors
Snow depth	-

Table 30. Table of data relevant for snow ablation.

Regarding weather forecast data, there is free forecast data available online. Several different sources publish forecast data in programming-compatible formats. Yr.no provides general forecast data of temperature, cloud coverage, wind etc., while api.met.no provides more specific weather data such as a prognosis of UV-radiation. Both websites offers the data in an XML-format, allowing for a user-friendly programming.

```

▼<time from="2017-04-28T14:00:00" to="2017-04-28T18:00:00" period="2">
  ▼<!--
    Valid from 2017-04-28T14:00:00 to 2017-04-28T18:00:00
  -->
  <symbol number="9" numberEx="9" name="Regn" var="09"/>
  <precipitation value="2.5" minvalue="1.6" maxvalue="4.0"/>
  <!-- Valid at 2017-04-28T14:00:00 -->
  <windDirection deg="26.0" code="NNE" name="Nord-nordøst"/>
  <windSpeed mps="4.7" name="Lett bris"/>
  <temperature unit="celsius" value="3"/>
  <pressure unit="hPa" value="1014.1"/>
</time>

```

Figure 90. An example of the weather data provided by Yr in a XML-format.

The weather forecast for the relative long time interval of a week can be decisive for whether or not to initiate the ablation of snow. In this situation it is particularly precipitation that is of interest for a snow load reduction scenario, or incoming solar radiation in the enhanced solar gain scenario. In 4.4.2, an example was made of a roof designed for 1.5 kN/m<sup>2</sup>, experiencing a load of 1,0 kN/m<sup>2</sup>. If no precipitation is expected within a week, and the system is capable of reducing snow loads of 0.5 kN/m<sup>2</sup> in less than a day, the need to reduce the load is not pressing. Having an estimate of expected precipitation rates can help putting of snow load reduction until it is eminent. This will save energy in the long run without posing a larger risk for the roof. The uncertainty of the forecast should weigh how much the parameter should count when the decision is made.

Diagram 1 (figure 87) illustrates how the process of snow load reduction can be designed based on information of measured snow load on the modules and long term weather forecast. If a high load is measured at the module, snow load reduction is eminent and will immediately be initiated. If a medium snow load is measured and no significant precipitation is expected in the near future, snow load reduction can be postponed. If significant levels of precipitation is expected, ablation should be initiated. No specific values are suggested for which limits of load or precipitation that should decide if ablation should be initiated or not. The values triggering the system should be decided individually for the specific roof, depending on load capacity, climate and the load reduction speed of the PV-heating system.

In the case of the enhanced solar gain scenario, illustrated by diagram 2 (figure 88), the balance between expected solar radiation and the existing snow amount is of essence. If clear skies is expected for 5 days, a decision can be made if to initiate snow ablation or not, depending on the time of year and amount of snow. No values are suggested for this case either, but the diagram illustrates how the automation can

be designed. The values triggering the clearing of the modules surface should be determined by the possible power production of the system with its seasonal variations. Empirical documentation of how much energy is needed to clear the module surface from snow should also be collected to assist the calculated snow amount values. The case of enhanced solar gains versus snow depth is further discussed in 5.3.

For both scenarios of snow load reduction and enhanced solar gains, a long term forecast will provide useful information of how to control the system, allowing for the saving or even gaining of energy.

Diagram 3 suggests how to go about snow ablation. For the two other diagrams, the term initiate ablation is used as the cue for reducing the snow load. How to go about the ablation depends on the real-time climatic conditions on site. As previously explained, low temperatures with dry air and high wind speeds are conditions conducive for sublimation. The temperature of the snow at the module surface can be determinative for the snow structure and the potential of sublimation. An activity diagram is made, illustrating how the input data can decide whether to sublimate or to melt. To decide specific values of the given parameters requires more research and is to some extent dependent on the PV-system and roof in question.

Starting the process illustrated in the activity diagrams can either be done periodically or it can be triggered by a change in a specified parameter. For example, the process in diagram 1 can be done no matter what every 15 minutes, or it can be triggered by a change in measured snow load bigger than  $0.05 \text{ kN/m}^2$  for example.

How the conditions change over a short time period is important to avoid unfavorable conditions, especially in regards to temperature. Slight changes in temperature can separate phenomena such as melting and freezing or snow and rain. If snow is melted using a PV-system without a heated drainage gutters, it is crucial to avoid freezing of the meltwater. A sudden change of temperature, typically occurring towards nightfall during a high-pressure weather system, can cause water to freeze at the roof surface, creating an obstruction for the free flow of water and possibly causing moisture related problems at the roof. A short term forecast can provide significant clues of how to regulate snow ablation, preventing problems as freezing water at the roof surface. The automation of the system should take into account the combination of factors able to create such unfavorable conditions.

To this date, there is a lack of data determinative for the controlling the system. Calibrating the automation of the system should be performed based on empirical data logged from an operating PV-heating system. Empirical data of which conditions that proves to be conducive for melting and sublimation should be collected. Because the load sensors only register weight at the modules, measuring water drained from the roof might be interesting in the early stages of the systems initiation. This will provide information of the total weight reduction on the roof, not just on the module. This can help indicate the efficiency of the drainage system and the magnitude of water-saturation in the snow.

Measuring sublimation with the Eddy Covariance or Bulk Aerodynamic Flux method can also be interesting to provide empirical data of sublimation rates and conducive conditions for sublimation. Deep-learning algorithms can be implemented to provide an auto-calibrating system, perfecting itself as empirical data of the system is logged.

#### 5.1.4 Summary

The measurements and analysis conducted bring strong indications of what can be the optimal strategy for snow load reduction under varying climatic conditions.

First off, drainage of meltwater is crucial to ensure load reduction at the roof. The measurements and analysis from this thesis indicate that a PV-heating system on a flat roof should have a drainage system with heated gutters to avoid thick layers of water saturated snow and freezing of meltwater. If a PV-heating system can sufficiently reduce the load by melting under varying climatic conditions without heated gutters is likely challenging and requires further research.

Measurements of a PV-heating system in action revealed that melting can be difficult for a thin snowpack under conditions characterized by low temperatures and high wind speeds. Melting is best performed on warmer days. Higher temperatures and solar radiation accelerate the melting process. And the snow's capability for water saturation is decreased. Drainage of meltwater is less problematic, allowing for a more steady transportation of water and weight reduction at the roof. A thick snowpack is likely to bring warmer temperatures at the roof surface, which is favorable for melting. The theory indicated conditions brought by a heavy snow fall, can be favorable for load reduction by melting. This is however untested to per writing of this thesis.

Sublimation serves as an alternative to melting. Low temperatures and wind are poor conditions to performed melting, but it is exactly under such conditions that sublimation is best performed. Amounts of  $0.86 \text{ kg/m}^2$  per day was sublimated in the Nordmarka study, and it is probable that higher sublimation rates can be induced as empirical experience is collected and the control of the system improves. The results also indicate a possible higher potential of sublimating at night than during the day due to decreased specific humidity of the snow. Further research is recommended to uncover the true potential inducing sublimation in snow with a PV-heating system.

Despite all the indications from measurements and analysis conducted in this thesis, the system is untested in a heavy snow fall scenario. Both melting and sublimation is strongly influenced by the condition brought by a heavy snowpack, which makes it difficult to predict the outcome the load reduction in such a situation.

The automation of the system serves to optimize the ablation by cooperating with the conditions through the implementation of live data. It is not only how to best perform the ablation that is of interest, but when to take action and initiate the load reduction. Weather forecast combined with the measured snow amounts give significant clues of when the ablation of snow should be initiated, either in the snow load reductions or enhanced solar gains scenario.



## 5.2 The PV-heating system's relation to law and regulations

This part of the discussion aims to answer the research question stated in the beginning of the thesis:

- *How does the system relate to the law and regulations?*

The PV-heating system is most relevant for existing under-designed buildings in the need of a measure able to reduce snow load. Measures on existing buildings have to be done in accordance with the law, and it is therefore interesting to investigate how the law relates to such a measure.

The PV-heating system is a very new system and documentation of its sufficiency is lacking. To this date, no reduction in design load can be acquired with the PV-heating system. This chapter seeks to connect the system with the current design regulations and discuss how the system can reduce the design snow load, allowing for decreasing the structural capabilities of buildings.

The term “under-designed” is used in this chapter for describing buildings designed for less load than the current regulations allow for. Due to the increase of the design snow load, buildings once designed for the characteristic snow load at the time, are now regarded as under-designed.

### 5.2.1 The law regarding a PV-heating system on under-designed roofs

An under-designed roof can pose a serious danger when experiencing a heavy snow load as experienced through several severe roof collapses in Norway (Table 4). The owner is obliged to “*to keep structures and installations covered by this law in such a condition that there is no risk of damage to, or significant inconvenience to persons, property or the environment.*” (Plan og bygningsloven 2008). For most cases of under-designed roofs, owners rely on shoveling snow off the roof to keep the building safe. A structural reinforcement of the building is also possible, although this is a more comprehensive measure.

For buildings that have an under-designed roof, installing a PV-system is problematic due to the increase in payload on the roof. The system is therefore not in “*accordance with the plan*”, providing the need for an application of change of use to the municipality (Plan og bygningsloven 2008). The application must be done in accordance with SAK10.

The PV-heating system is intended to be a solution to the problem of the increased load, enabling under-designed roofs to have a PV-system. The PV-heating system serves to act as a load reducer, rather than a load imposer, increasing the snow load capacity of the building. If the system proves to be effective, safe and well documented, a *precedent* for the PV-heating system should be established by the authorities. A precedent is a principle allowing for a previous legal case to govern in which way similar cases in the future shall be decided. If a precedent is established, the process of installing a PV-heating system will be easier performed on under-designed roofs, allowing for a dispersion of the system. The PV-heating system is also a green measure, providing clean and sustainable energy. A legal precedent can be established for the PV-heating system when documentation of its sufficiency is available.

### 5.2.2 The relation to the design regulations

In this chapter, the PV-heating systems relation to current design regulations is investigated. Firstly, the validity of the thermal coefficient applied to a PV-heating system is discussed, before evaluating the effect and implications of the design value. Then, the relation between the PV-heating system and the determination of *snow load on roof with snow control* from annex F in ISO-4355 is discussed.

If the thermal coefficient  $C_t$  applies to the framework presented in ISO-4355 requires a discussion. ISO-4355 states that the thermal coefficient is valid for “*reduction of snow loads on glass roofs caused by heat flow through the roof*”. The standard further elaborates in a footnote that the value may also apply to other materials than glass. The PV-module surface is covered with glass, thus making the framework valid in terms of material.

However, a PV-module is not similar to a roof in terms of scale and composition. Normal roofs usually have a somewhat uniform pitch and coherent surface. The PV-modules pitch differs, and the surface formed is not coherent due to the array formation. The calculation can be imagined to be done for many individual roofs stacked on one larger roof. If the load is reduced for the many individual roofs and the water is properly drained, it will have the same load reducing influence on the large roof. This is provided that the snow does not slide off the individual roofs of a large thermal coefficient, onto the larger roof with a lower thermal coefficient.

Here the roof/module angle  $\beta$  is of interest. A higher value of  $\beta$  will give a lower  $C_t$  value by a factor of  $\cos(2\beta)$  for values  $0^\circ \leq \beta \leq 45^\circ$ . This factor reduces the load due to the effect of sliding snow away from the roof surface. For a surface with uniform pitch where the snow would slide off the roof, a significant angle is favorable for load reduction. For the PV-module, a large  $\beta$  would imply snow falling from the module surface onto the roof, unable to effectively reduce the load. Sliding snow off the modules is therefore unfavorable for a PV-heating system on a flat roof when the intent is to reduce load. For this reason the  $\beta$  is set to 0.

$\theta$  is the lowest expected internal temperature during the winter ( $^\circ\text{C}$ ). Here the framework does not directly fit the case, but discussing the factors intent gives insight for the estimation. A high value of  $\theta$  represents a high heat loss through the roof. The factor is set to the maximum value of 18 on the basis that a solar module is far more capable of producing heat than passive heat transfer through a roof. The calculation in 4.4.1 estimates the heat loss of a poorly insulated roof during the course of a winter, and compares the findings with the effect of the modules. The results show that it takes less than 4 days for the modules to produce the equivalent amount of heat that flows through the roof during the 4 winter months. The modules use 3,18% of the time that the roof does to produce the same amount of energy. The calculation emphasizes the power of the modules, and supports the decision of a high  $\theta$  value.

It is also necessary to discuss the validity of the thermal transmittance value  $U_0$ . For normal use, the value is determined by the U-value of the roof [ $\text{W}/\text{m}^2\text{K}$ ]. The calculation in 4.1.5 is based on the heat

flow through the PV-modules, neglecting the thermal transmittance of the roof. The framework does not differentiate between values higher than  $4.5 \text{ W/m}^2\text{K}$ . Therefore, a calculation is made proving that the heat loss through the PV-modules is higher than any roof and way beyond the heat emission of a roof with the poor U-value of  $4.5 \text{ W/m}^2\text{K}$ . A worst case scenario is made evaluating the heat loss from a roof with an U-value of  $4.5 \text{ W/m}^2\text{K}$  experiencing a temperature difference of  $43^\circ\text{C}$  ( $23^\circ\text{C}$  inside,  $-20^\circ\text{C}$  outside). This worst case scenario results in a heat flow of  $193.5 \text{ W/m}^2$  through the roof, much lower than the modules maximum effect of  $252.1 \text{ W/m}^2$ .  $U_0$  is therefor set to a number higher than  $4.5 \text{ W/m}^2\text{K}$ , illustrating a higher heat loss than the worst case roof. Since the framework does not differentiate between values higher than 4.5, a specific number is not of interest as long as a value higher than 4.5 can be argued for.

The U-value factor of the roof used in the calculation can also be based on the radiated effect calculated from the modules in 4.1.4, instead of the effect of  $252.1 \text{ W/m}^2$  stated by the manufacturer. However, the calculated effect is underestimated and does not represent an accurate value of the modules performed effect. Firstly, the calculated effect represents *radiative heat transfer*. Convection and conduction losses are not taken into account. The day of the aerial thermography was performed was characterized by temperatures at  $-5^\circ\text{C}$  and windy conditions. The convection losses were likely to be significant, reducing the temperatures of the modules and the measured radiated effect. The conduction losses were likely not as significant due to the small contact points between the modules and the frame. Secondly, the calculated effect is performed in open air, lacking the presence of a snowpack. If a snowpack would have been present, little or no convection losses would have occurred. Most of the performed effect of the modules would have been applied directly to the snow with less heat loss to the surroundings. Thirdly, the atmospheric transmission coefficient used to adjust the pixel values is likely to be underestimated. The study performed at NMBU with intent to estimate the coefficient was performed under different conditions than what was experienced at the day of the aerial thermography. At NMBU, the air temperature was approximately  $5^\circ\text{C}$  and the object of interest (the brick wall) was  $8^\circ\text{C}$ . At ASKO, the air temperature was  $-5^\circ\text{C}$  and the object of interest (the modules) was approximately  $15^\circ\text{C}$ . The temperature difference between the air and the object are far apart from the aerial thermography session and the estimation of the thermal coefficient at NMBU, resulting in an underestimation of the coefficient. The larger the temperature difference between two objects, the more radiative heat transfer occurs as stated in Stefan Boltzmann's law (equation 18). The magnitude of the atmospheric coefficient estimated at NMBU is likely underestimated due smaller temperature difference between the object and the air.

The thermal coefficient calculated for the PV-heating system is based on a periodic heat flow through the modules, applied when it is needed. This somewhat redefines the coefficient, in terms of that the coefficient is usually meant for a more consistent, passive heat flow.

In 4.1.5 a  $C_t$  coefficient of 0.298 is calculated for the module surface, and an area-weighted value of 0.47 for the whole roof, resulting in a load reduction from  $3.5$  to  $1.65 \text{ kN/m}^2$ . The value is significant, halving

the design load. The calculation does however not take into account other factors such as the exposure coefficient or shape coefficient. Applying the thermal coefficient of the modules to the whole roof surface by reducing the factor by the weighing of the area is outside of the framework's intended use of the coefficient. However, the load reduction efficiency of the calculation stands true. If the roof does experience a characteristic snow load of  $3.5 \text{ kN/m}^2$  and the modules are able to reduce their respective load in correspondence with the calculated  $C_t$  value of 0.298, the load will be reduced to an average of  $1.65 \text{ kN/m}^2$  for the whole roof. This load is reduced by more than half, significantly improving the snow load capacity of the roof.

In table 16, a thermal coefficient was calculated for climates with a different characteristic load ( $S_k$ ) than at ASKO. The calculation showed that the design load (simplified), the product of the thermal coefficient and the characteristic snow load, have little variations from location to location. For a climate with an  $S_k$  of  $1.5 \text{ kN/m}^2$  the load is reduced to 0.65, while for a climate with a  $S_k$  of  $9.0 \text{ kN/m}^2$  the load is reduced to  $1.0 \text{ kN/m}^2$ . It does not seem reasonable that climates with such big difference in characteristic snow load should have similar design values. Theoretically, this calculation is also valid for a glass roof with the extremely low U-value of  $4.5 \text{ W/m}^2\text{K}$  and the other conditions used in the calculations, although it is somewhat unrealistic. The standard shows a weakness for calculating design snow loads with a large thermal coefficient combined with various characteristic snow loads values.

In 2.1.3, a framework determining the design snow load for roofs with snow control was presented. The framework allows for a load reduction based on "*field research and experiments investigating the capacity of sliding or melting devices*" (ISO 2013a). The PV-heating system qualifies to be such load reduction systems. However, the determination controlled snow load ( $S_c$ ) can only be done through field research and experiments. To be able to calculate  $S_c$  for the PV-heating system, numerous experiments should be performed, documenting the snow load removal of the system. The system must be tested in a number of heavy snowfall scenarios to *guaranty of snow load removal* under varying climatic conditions. No such data has yet been registered due to the relatively recent installation of the system. In the winter of 2016-2017, there was a lack of heavy snowfall, disabling the  $S_c$  coefficient to be estimated. Field research and experiments should be performed to give basis for an estimation of  $S_c$ , allowing for a reduced snow load for future roofs with the PV-heating systems installed.

### 5.2.3 Summary

As stated in 2.2.2, an increase of the snow load is expected in the future, and a review of the snow load standard is recommended (Flyen et al. 2010). Instead of increasing the structural elements withstanding the snow load, the snow load itself can be reduced with a PV-heating system. If the PV-heating system proves to be efficient, safe and well documented, a decrease in the design snow load should be considered for roofs with the system installed.

The thermal coefficient has an obvious relation to the standard, but a further adaption of this factor to the system is necessary to make the coefficient valid. The current framework has to be interpreted to a too large extent for the coefficient to be calculated with heat flow from PV-modules. A further analysis of the thermal coefficient's applicability to the range of characteristic snow loads for various municipalities in Norway revealed a very large relative load reduction for the municipalities with the highest characteristic snow load and significant thermal coefficient. The standard appears not to be adapted for the combination of low thermal coefficients and high characteristic snow load.

The PV-heating system's best fit with the design regulations is in Annex F in ISO-4355: *Snow load on roof with snow control*, which allows for a reduction in the design snow load for roofs with a device or method that can guaranty snow load reduction. However, the system must be documented through field research and experiments guarantying the removal of snow load. Such documentation is lacking per writing of this thesis due to the relatively recent installation of the system. Documentation must be made in order to achieve a reduction in the design snow load.

Regarding the law, a process involving an application to the municipality is required for installing the PV-heating system on an under-designed building to this date. However, a precedent can be established, presupposed that the system is safe, effective and well documented. A precedent would allow for an easier process of acquiring the system and a possible dispersion of the system to under-designed roofs.

## 5.3 Melting snow on modules to enhance solar gains

This part of the discussion aims to answer the research question stated in the beginning of the thesis:

- *Can melting snow on modules result in higher solar gains?*

As explained in 2.6.3, snow significantly reduces energy production during winter. If snow prevent solar radiation from reaching the modules for a period with significant solar radiation, melting the snow with intent to clear the modules might be expedient. In this chapter, the energy required for melting snow is compared to the energy gained by solar radiation during winter. For this application, the seasonal variation of solar radiation in addition to the cloud cover predicted by the weather forecast is essential. For this reason, the automation of the PV-heating system is considered very relevant. For a decision to be made of whether it is expedient to melt snow or not during the winter months is strongly determined by the expected levels of solar radiation compared to the snow amount on the modules. This chapter discusses the calculations made balancing solar gains and snow amounts, and further examines how this application of the PV-heating mode can be used in different types of PV-system.

Sublimation is not evaluated as an option due to uncertainty regarding its feasibility for clearing snow off modules.

### 5.3.1 Equivalent solar gain – for which snow depth is melting expedient?

In 4.4.3 a calculation was performed, taking basis in the premise that if the forecast predicts high levels of incoming solar radiation for a specified time interval, how much snow is expedient to melt, totaling a net zero in energy use when balancing the solar gains versus melting losses. For any amount of snow lower than the calculated result, snow melting is considered expedient. Data of gained solar radiation from the PV-heating system at the ASKO facility is compared with the energy amounts required for melting snow. An equation is made with the snow amount as the unknown parameter, and solar radiation in a time interval of 1 day or 1 week as the determinative input data. Due to the strong seasonal variations of solar radiation, the calculation is done for December, January, February and March. The validity of the calculation and it's applicability to a real life scenario is discussed before evaluating the calculated snow amounts considered expedient to melt.

This paragraph discusses the input data used. The calculation uses data of power produced logged through the inverters of the ASKO facility. The data represent actual power produced at the facility, but is for this reason accurate for exactly this facility. The data is circumstantial to some extent; other PV-systems located in other places will likely have a different energy production per square meter. However, using actual logged data does provide a realistic scenario of actual energy gained, compared to using theoretical numbers of what a PV-system can produce.

Since the system was first installed November 2016, the data available was limited. In this calculation only data from the winter of 2017-2016 is used. The lack of snow cover in this winter was favorable in

this particular calculation, allowing for higher levels of solar gains compared to normal winters in Oslo. The lack of snow and high energy production allowed for a more realistic scenario of what can be produced when a snow cover is melted at the module surface.

Since the input data is actually logged data, the weather during the time of energy production is determinative for the outcome. The data chosen represents a time interval for 1 day and 1 week, and is chosen on the basis of which day or week had the highest energy production during respective the month. The time interval of weeks are whole weeks, from Monday to Sunday. The data does therefore not provide the ideal scenario of the solar gains,- the time interval of this rigid week is likely not the one of highest energy production. A more loosely based time interval will likely result in higher energy gains for the calculation.

Some assumptions were made before the calculation. The calculation assumes that no energy is gained when a snow cover is present. This is not entirely true due to the fact that the snow is not opaque. Small snow depths are likely to let radiation through, allowing the modules to produce energy. The energy production occurring under a small snow cover is not taken into account. If the radiative transmittance of the snow would have been accounted for, the result might have been different for smaller snow depths.

The calculation use simple enthalpy theory to compare the numbers of solar radiation, to the energy equivalent of completing a phase transition from snow to water. Only the latent heat required for the phase transition is used (the latent heat of fusion), neglecting the sensible heat required to increase the temperature of the snow or water. As previously explained, the implementation of sensible heat has a minimal impact on the outcome. 3% more of the total energy is used if the snow has a temperature of -5°C instead of 0 °C, justifying the neglecting of sensible heat.

It is also assumed in the calculation that the snow is evenly distributed before melting and is evenly melted when applying heat to the module surface. As experienced in through the measurements performed in this thesis, this is not entirely true. The thermal footprint of the modules is determinative for how the snow melts or sublimates. As shown in figure 50 and 70, the thermal footprint of the modules becomes evident through the snow when ablation is initiated. Small variations in snow depth occur on the modules surface, although not to a large degree.

If the snow amounts melted snow is of significant magnitude, a surrounding rim of snow might be left after melting is performed. Snow is melted at the module surface, but snow at the frame and in between modules can possibly remain. The higher snow depth melted, the higher surrounding rim will be, possibly shading the modules surface. Of course this phenomenon depends on the individual PV-system and how it is assembled, and should be tested for the individual PV-heating system to evaluate the effect on power production.

Although quite many assumptions are made for the calculation, the results bring a clear message. The results are indicative of a seasonal variation regarding the potential of enhanced solar gains. From the week interval calculation, the result show that only small amounts of snow between 2-4 kg/m<sup>2</sup> is expedient to melt for the main winter months of December, January and February. Radiation levels at low magnitude allow for only small amounts of snow to be considered melt-worthy. March provides a different outcome with high solar radiations of 4254 kWh resulting in amounts up to 37.93 kg/m<sup>2</sup> expedient to melt. This weight equals depths of approximately 10-40 cm if the density is between 400 kg/m<sup>3</sup> and 100 kg/m<sup>3</sup>. With such high levels of incoming solar radiation, melting small to medium snow covers are likely to results in an energy surplus.

The results from the daily calculation show the same seasonal trend as for the weekly. For the December, January and February it is only amounts below 1 kg/m<sup>2</sup> that are considered melt-worthy at a daily basis if high levels of solar radiation are expected. For March, amounts up to 6.5 kg/m<sup>2</sup> are considered melt-worthy at an expected high solar radiation day.

The time to melt the respective snow levels is presented (table 27 and 28) to give basis for discussing the time lag from initiating the melting process till solar radiation can be gained. For all the cases except weekly solar radiation in March, the snow amounts can be melted in less than 2,5 hours. Swift melting allows for a flexibility of the system and melting can be delayed until the forecast becomes more certain. For the snow amounts favorable to melt in the week of March, a time of almost 14 hours is needed to clear the modules from snow. The larger the snow amount, the longer the time needed to melt the snow. In such scenarios, a predictable forecast is necessary to ensure that the energy use to melt the snow is not wasted.

The climatic conditions during the melting of a snowpack requires a discussion to determine its importance. Due to fact that snow will melt by itself when temperatures are high, it is most to gain by melting snow when temperatures are low. If a cold spring with a shallow snowpack and high solar radiation occurs, melting snow on the module surface can be highly expedient. However, low temperatures allow for slower melting and slightly higher energy consumption.

### 5.3.2 Potential/applications

Due to the circumstantial data used in the previous calculation, a general discussion is made to evaluate the potential of melting snow for higher solar gains. This chapter will briefly discuss how PV-systems with a different design than the system at ASKO can be used to clear the module surface of snow.

If the modules have a significant tilt, snow is likely to slide of the modules when running in heating mode. Sliding the snow off the modules is far less energy consuming than melting a substantial snow layer from the bottom-up. For the snow to slide off, the module surface barely need to have a temperature higher than zero degrees when a significant tilt is present. The power needed to produce such a surface temperature is little dependent on snow amount. An almost fixed amount of energy is



likely to remove any amount of snow present at the module surface, presuming that the snow is able to slide completely off the module surface and that the snow does not stick to the frame. Therefore, the potential of melting snow to enhance solar gains is larger for modules with significant tilt. KEI solar and their “HAIN system” state that angles of 15° is enough to slide the snow off the module surface. Of course, this solution is not applicable to PV-heating systems designed for reducing snow load for flat roofs. If the snow is slid off the modules onto the roof surface, the possibility of further load reduction is spoiled. However, the system is likely to be highly efficient for enhancing solar gains.



*Figure 91. The HAIN system in progress. For this particular installation, the snow is only partially slid off the module, not optimal for enhanced solar gains. The installation then relies on the melting the rest of the snow to clear the module surface (KEI Solar 2017).*

The new trend of integrated PV-skins provides excellent conditions for snow to be slid completely off the roof. These new systems are usually applied for pitched roofs. Such systems have great potential of getting higher solar gains by incorporating the heating-mode into their solutions.



*Figure 92. Strand Kirke in Rogaland has a coherent, frameless, integrated PV surface, favorable for sliding snow off the roof. (Enova 2016)*

The economic effects of acquiring and installing the equipment needed to run PV-modules in heating mode is not evaluated in this thesis. The cost and efficiency of different systems should be compared with the gains of acquiring heating mode to further document the potential.

No practical testing or measurements of any kind has been performed when evaluating PV-heating systems potential of enhanced solar gains. Field research should be performed with intent to document if clearing the module surface is easily achievable and uncover the possible challenges of doing so.

### 5.3.3 Summary

The investigation and calculations presented in this thesis indicate that melting snow on PV-modules to enhance solar gains can result in a higher solar gain. However the assembly of the modules, especially the tilt, is determinative for the energy amounts required to clear the module surface.

For a PV-heating system on a flat roof originally intended to reduce the load, the system relies on melting the snow from the bottom-up. With all the simplifications made, the calculations show that melting very thin layers of snow ( $2-3 \text{ kg/m}^2$ ) during any winter month can result in a net gain if clear skies are forecasted for a week. Towards spring, melting larger amounts of snow ( $37.9 \text{ kg/m}^2$ ) can result in a net gain if clear skies are expected. Melting snow on PV-modules in spring can result in higher solar gains for system similar (in terms of assembly and climate) to the PV-heating system at ASKO.

For PV-modules with a significant tilt (more than  $15^\circ$ ), applying small amounts of power can result in the snow sliding off the module surface. A “fixed amount” of power can be used to clear the surface for snow little dependent on depth, allowing for solar production during the seasonal snow cover. This presumes that snow is slid completely off the module surface. New solutions involving integrated PV-skins covering the whole surface of a tilted roof have a higher potential of enhancing solar gains by implementing the heating mode than systems relying on melting the snow from the bottom-up.

Although the enhanced solar gain scenario seems promising, no measurements of melting snow to clear the module surface were performed in this thesis. For the time being, this remains a theoretical investigation. Further research should be performed to test the true potential of this application.

## 5.4 Further studies

The measurements performed in this thesis are limited to a certain extent, which demands for more comprehensive research to ensure that the system is a feasible load reducer in varying climatic conditions.

First off, the system is no yet tested in a heavy snowfall scenario. To be sure that the system actually performs under the conditions that a heavy snowfall brings remains to see. A thick snowpack influences the microstructure of the snow, which will to some extent influence the ablation of snow and the transportation of meltwater. Further studies are necessary to document if the system truly functions when it counts.

This thesis primarily focus on flat, hot roofs. For different types of roofs, such as ventilated flat roofs, or roofs with a significant tilt, further studies should be performed to document the how the drainage of the PV-heating system functions.

The snow amounts and precipitation occurring around the world differs a lot. Staggering precipitation rates for locations such as Japan is way beyond what is analyzed in this thesis. Extremely low temperatures in for other locations might pose new problems for load reduction with the PV-heating system not yet uncovered in this thesis. The system's feasibility is dependent on climate, making the findings in this thesis circumstantial to some extent. Further studies are required to document the system's functionality in various climates.

## 6 Conclusion

The objective of this thesis is to answer the main problem and three additional research questions:

*How feasible is a PV-system in heating mode for reducing snow load on under-designed flat roofs in a sub-arctic climate?*

- *What is the optimal strategy for reducing snow load on PV-modules in heating mode under varying climatic conditions?*
- *How does the system relate to the law and regulations?*
- *Can melting snow on modules result in higher solar gains?*

Melting is the most obvious and uncomplicated way of reducing the snow load. However, even though melting snow at the module surface is unproblematic, the transportation of water away from the roof under varying climatic conditions poses the challenge. Water saturation of the snow and possible freezing of meltwater can result in insufficient load reduction. Conditions characterized by low temperatures, wind and dry snow pose the greatest challenge for load reduction by melting. For warmer conditions, melting is considered less problematic. Calculations show that a load reduction of  $50 \text{ kg/m}^2$  can be performed in less than 19 hours for a roof surface with 63% modules. A drainage system with heated gutters is recommended for PV-heating systems on flat roofs to ensure the transportation of water off the roof. In this manner, problems associated with water-saturated snow and freezing meltwater can be avoided.

Conditions unfavorable for melting are considered conducive for sublimation, allowing for a different load reduction approach. Through experimental testing with PV-modules in heating mode, a load reduction of  $0.86 \text{ kg/m}^2$  per day was documented by sublimation. With a different control of the system and under a different climatic impact, sublimation rates can probably surpass the ones documented in this thesis. However, induced sublimation under a thick snowpack has not yet been performed. Also, the metamorphism occurring under the snowpack can pose a problem for long term sublimation. Further research is recommended to uncover the feasibility of sublimating snow with a PV-heating system.

An automation of the system implementing live data measured on site and from the weather forecast, can help determine the optimal strategy for load reduction. An automation of the system could provide for easier decision-making based on relevant data. Decisions like whether to initiate load reduction or not, and how to best perform the reduction, is highly determined by the conditions occurring on the roof and the weather to come. Such an automation allows for a dynamic cooperation with the conditions, optimizing load reduction and saving energy.

The current design regulations do not allow for a reduction of the design snow load through the implementation of a PV-heating system as per the writing of this thesis. The thermal coefficient has an obvious relation to the PV-heating system, although interpretation of the framework to a large extent is

required for the system to fit the design regulations. However, Annex F in ISO-4355 opens to the possibility of a reduction of the design snow load if field research can document the load reduction capacity of the system. Such documentation is lacking to this date.

The law requires an application to the municipality to install a PV-heating system on an under-designed roof. A precedent can be established if the system proves to be safe, efficient and well documented.

The system can be used for different purposes than to simply reduce snow load. A potential of enhancing solar gains by melting snow on the module surface is existent. If high levels of solar radiation is expected, and a snow cover is present, melting snow on the modules surface can result in a net energy gain. Calculations from this thesis, using data from an existing PV-heating system, indicate that melting snow amounts up to  $37.9 \text{ kg/m}^2$  can result in a net energy plus if clear skies are expected for a week in March. To determine whether or not it is expedient to initiate melting, an evaluation should be made for the individual system, based on solar irradiance at the location and the assembly of the system. The module angle is strongly determinative for the energy needed to clear the module surface.

The results uncovered in this thesis indicate that reducing snow loads with a PV-heating system is feasible. The most critical challenge is transporting the water away from the roof, which can be performed by incorporating a drainage system with heated gutters. The PV-heating system intends to serve as a modern solution for reducing snow load on roofs, both for existing under-designed buildings and for new buildings. However, the system is untested in a heavy snow load scenario and the climatic impact is strongly determinative for the load reduction. Further research is recommended.

## References

- Acciani, G., Simone, G. B. & Vergura, S. (2010). Thermographic Analysis of Photovoltaic Panels. *RE&PQJ*, 1 (8): 3.
- Andreas, E. (1987). A theory for the scalar roughness and the scalar transfer coefficients over snow and sea ice. *Boundary-Layer Meteorology*, 38: 159-184.
- ASKO Norge AS. (2017a). *Fokus på miljø*. Available at: <https://asko.no/om-oss/fokus-pa-miljo/> (accessed: 15.04.2017).
- ASKO Norge AS. (2017b). *Oslos største*. Oslo. Available at: <https://asko.no/nyhetsarkiv/oslos-storste/> (accessed: 30.02.2017).
- Buerhop-Lutz, C., Scheuerpflug, H. & Weißmann, R. (2011). The Role of Infrared Emissivity of Glass on IR-Imaging of PV-Plants.
- Caprona, Y. C. d. (2013). *Norsk etymologisk ordbok : tematisk ordnet*. Oslo: Kagge.
- Cumulus Weather Station Software. (2017). *Mylla weather*. Available at: <http://www.hinsch.no/mylla/Cumulus/index.htm> (accessed: 15.02.2017).
- Drews, M. (2017). *Solar Panels and What To Do About Snow*. U.S. Available at: <http://drewssolar.com/blog/2017/1/4/do-snow-and-solar-panels-get-along> (accessed: 01.04.2017).
- Dronedeploy. (2016). *Making Successful Maps*. Available at: <http://support.dronedeploy.com/v1.0/docs/making-successful-maps> (accessed: 01.10.2016).
- DRONEexpert.nl. (2017). *Official website*. Netherlands. Available at: <http://dronexpert.nl/product/phantom-4-ready-to-fly-thermal-package/> (accessed: 06.04.2017).
- Edvardsen, K. I. & Ramstad, T. (2010). *Trehus Håndbok 53*. Oslo: SINTEF Byggforsk. 331 pp.
- Elon Musk. (2016). *Twitter status*. Available at: <https://twitter.com/elonmusk/status/792218248917811204> (accessed: 10.11.2016).
- Eltek. (2017). *Official website*. Drammen. Available at: <http://www.eltek.com/> (accessed: 05.05.2017).
- Enova. (2016). *Strand Plusskirke*: Enova. Available at: <https://www.enova.no/om-enova/om-organisasjonen/teknologiportefoljen/strand-plusskirke/> (accessed: 20.04.17).
- Ferroamp. (2017). *Official website*. Available at: <http://www.ferroamp.com/home> (accessed: 05.05.2017).
- Fiji. (2007). *Official Website*. Available at: <https://fiji.sc/#> (accessed: 30.10.2016).
- FLIR. (2011). *User's Manual*: FLIR. p. 88.

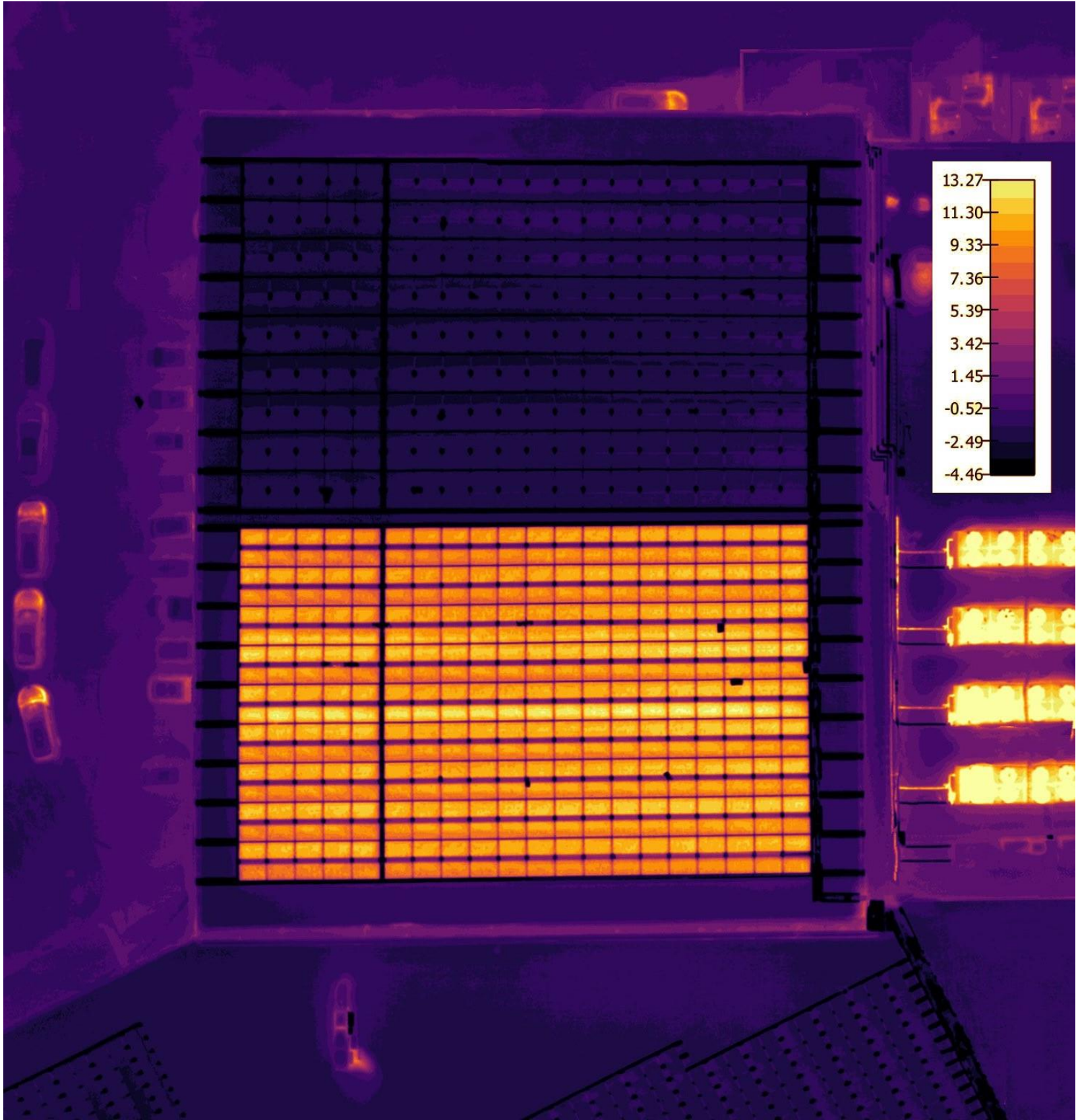
- Flyen, C., Almås, A. J., Hygen, H. O. & Sartori, I. (2010). Klima- og sårbarhetsanalyse for bygninger i Norge: Utredning som grunnlag for NOU om klimatilpassing. *Statens bygningstekniske etat: SINTEF Byggforsk*. 63 pp.
- Fuentes, M. K., Laboratory, S. & Energy, U. S. D. o. (1987). *A Simplified Thermal Model for Flat-plate Photovoltaic Arrays*: Sandia Laboratories.
- Gaitania, N., Burudb, I., Thiisb, T. & Santamourisa, M. (2017). Aerial survey and in-situ measurements of materials and vegetation in the urban fabric *International High-Performance Built Environment Conference – A Sustainable Built Environment Conference 2016 Series*: 10.
- Google. (2017). *Google Maps*. Available at: <https://www.google.no/maps/> (accessed: 10.04.2017).
- Hood, E., Williams, M., Cline, D., Hardy, J., Albert, M. & Marsh, P. (1999). Sublimation from a seasonal snowpack at a continental, mid-latitude alpine site. *Hydrological Processes*, 13 (12-13): 1781-1797.
- Hughes, N. (2013). *Orthographic projection Available at* <http://www.tech.plymouth.ac.uk/dmme/cad/design/Orthographicprojection.html>.
- IEC. (2009). *IEC 62446*. Grid connected photovoltaic systems - Minimum requirements for system documentation, commissioning tests and inspection: IEC. p. 24.
- Innos. (2017). *Intervju med Tommy Strömberg*. Oslo (08.02.2017).
- ISO. (2013a). *ISO 4355 Third edition*. Bases for design of structures - Determination of snow loads on roofs. Switzerland: ISO. p. 42.
- ISO. (2013b). *ISO 4355, Third edition*. Bases for design of structures —Determination of snow loads on roofs. Switzerland. pp. 1-42.
- Jackson, S. I., Prowse, T. D., Buttle, J. & Branfireun, B. (2009). Spatial variation of snowmelt and sublimation in a high-elevation semi-desert basin of western Canada. *Hydrological Processes*, 23 (18): 2611-2627.
- KEI Solar. (2017). *Official website*. Germany. Available at: <http://www.keisolar.com/index.html> (accessed: 20.01.2017).
- Kvande, T., Almås, A. J., McInnes, H. & Hygen, H. O. (2011). Klima- og sårbarhetsanalyse for bygninger i Norge. Videreføring av rapport 3B0325 . Versjon 01. *Statens bygningstekniske etat: SINTEF Byggforsk*. 44 pp.
- Köntges, M., Altmann, S., Heimberg, T., Jahn, U. & Berger, K. A. (2016). Mean Degradation Rates in PV Systems for Various Kinds of PV Module Failures. *32nd European Photovoltaic Solar Energy Conference and Exhibition*.
- Lascar Electronics. (2017). *EasyLog / EL-USB-2*. England. Available at: <https://www.lascarelectronics.com/easylog-data-logger-el-usb-2/> (accessed: 24.01.2017).

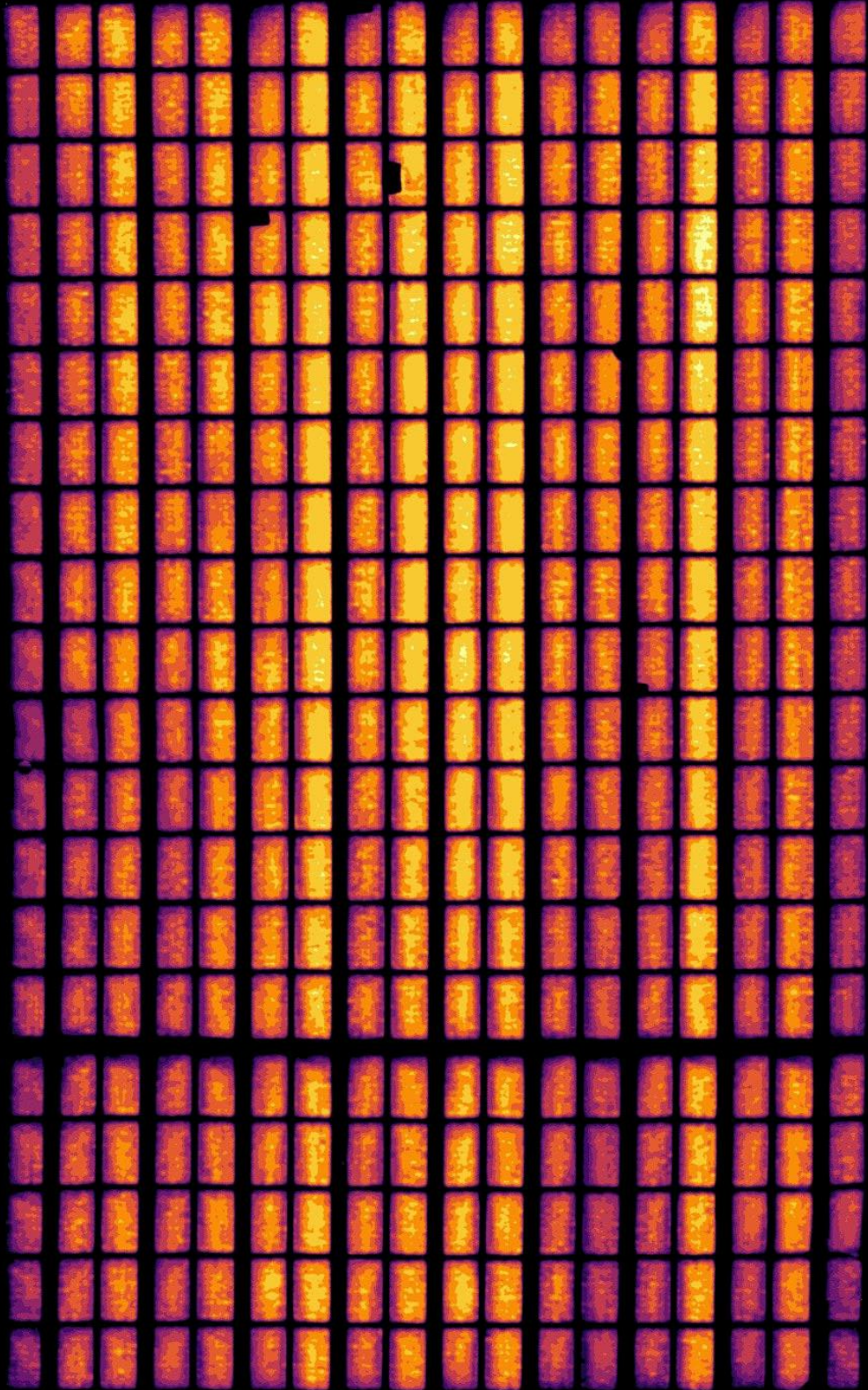
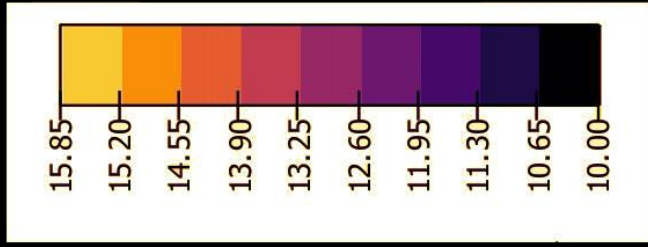
- Male, D. H. (1980). The seasonal snowcover. In Colbeck, S. C. (ed.) *Dynamics of Snow and Ice Masses*. Burlington: Elsevier Science.
- Mathiak, G., Sommer, J., Herrmann, W., Bogdanski, N., Althaus, J. & Reil, F. (2016). PV Module Damages Caused by Hail Impact and Non-Uniform Snow Load.
- Matlab. (2017). *Official Website*. Available at: <https://se.mathworks.com/products/matlab.html> (accessed: 15.10.2016).
- Meiman, J. R., Grant, L. O. & Research, U. S. O. o. W. R. (1974). *Snow-air interactions and management of mountain watershed snowpack*: Environmental Resources Center, Colorado State University.
- Meløysund, V., Karl, V. H., Bernt, L. & Lisø, K. R. (2008). Economical effects of differentiated roof snow loads. In vol. Language: eng *Proc. of the 6th International Conference on Snow Engineering*. New York, USA: Engineering Conference International.
- Meløysund, V. (2010). *Prediction of local snow loads on roofs*. Phd. Trondheim: Norges teknisk-naturvitenskapelige universitet, Fakultet for ingeniørvitenskap og teknologi, Institutt for konstruksjonsteknikk. 42 pp.
- Moore, R. D. (1983). On the Use of Bulk Aerodynamic Formulae Over Melting Snow. *Nordic Hydrology*: 193-206.
- Müller, F. (1968). *Runoff from snow and ice*: Inland Waters Branch, Dept. of Energy, Mines and Resources.
- Nuijten, A., Høyland, K. V., Kasbergen, C. & Scarpas, T. (2016). Modelling the thermal conductivity of melting snow layers on heated pavements. *8th International Conference on Snow Engineering*: 263-269.
- Oke, T. R. (1987). *Boundary layer climates*. Second edition ed. London: Routledge. 460 pp.
- Pix4D. (2017). *Official Website*. Switzerland: Pix4D. Available at: <https://pix4d.com/> (accessed: 30.10.2016).
- Pix4D & Maeder, D. (2017). Solar Photovoltaic Fault Diagnosis with Thermal Mapping. Available at: <https://pix4d.com/pix4dmapper-inspection-solar-thermal/>.
- Plan og bygningsloven. (2008). *Kapittel 31. Krav til eksisterende byggverk*.
- Planning Application Regulations. (2010a). *Part three, Approvals and Responsibilities*.
- Planning Application Regulations. (2010b). *Part two, Duty of Application, Content and Processing of Applications*.
- Schmidt, R. A. (1972). *Sublimation of wind-transported snow: a model*: Rocky Mountain Forest and Range Experiment Station, Forest Service, U.S. Dept. of Agriculture.



- Sextstone, G. A., Clow, D. W., Stannard, D. I. & Fassnacht, S. R. (2016). Comparison of methods for quantifying surface sublimation over seasonally snow-covered terrain. *Hydrological Processes*, 30 (19): 3373-3389.
- Smets, A., Jäger, K., Isabella, O., Swaij, R. V. & Zeman, M. (2016). *Solar Energy*. Cambridge: University of Cambridge.
- Sommerville, I. (2010). *Software Engineering*. Scotland: Addison-Wesley Publishing Company. 792 pp.
- Standard Norge. (2003). *NS-EN 1991-1-3:2003+NA:2008*. Eurocode 1: Actions on structures - Part 1-3: General actions - Snow loads: Standard Norge.
- Standard Norge. (2008). *Nasjonalt tillegg NA*. N.A.4.1 Karakteristiske verdier. Norway.
- Testo. (2014). *Practical Guide, Solar Panel Thermography*. Sparta, NJ: Testo. p. 19.
- Tipler, P. A. & Mosca, G. (2008). *Physics For Scientists and Engineers*. 6th ed. New York: W.H. Freeman and Company.
- Wikipedia. (2017). *Enthalpy*. Available at: <https://en.wikipedia.org/wiki/Enthalpy> (accessed: 03.03.2017).
- Wolleng, T. (1979). *VVS-tekniske klimadata for Norge*. Oslo: Norges byggforskningsinst. 111 pp.
- Yr. (2017). *Datosøk Oslo*. Oslo. Available at: <https://www.yr.no/sted/Norge/Oslo/Oslo/Oslo/almanakk.html?dato=2017-02-08> (accessed: 10.02.2017).

Appendix A





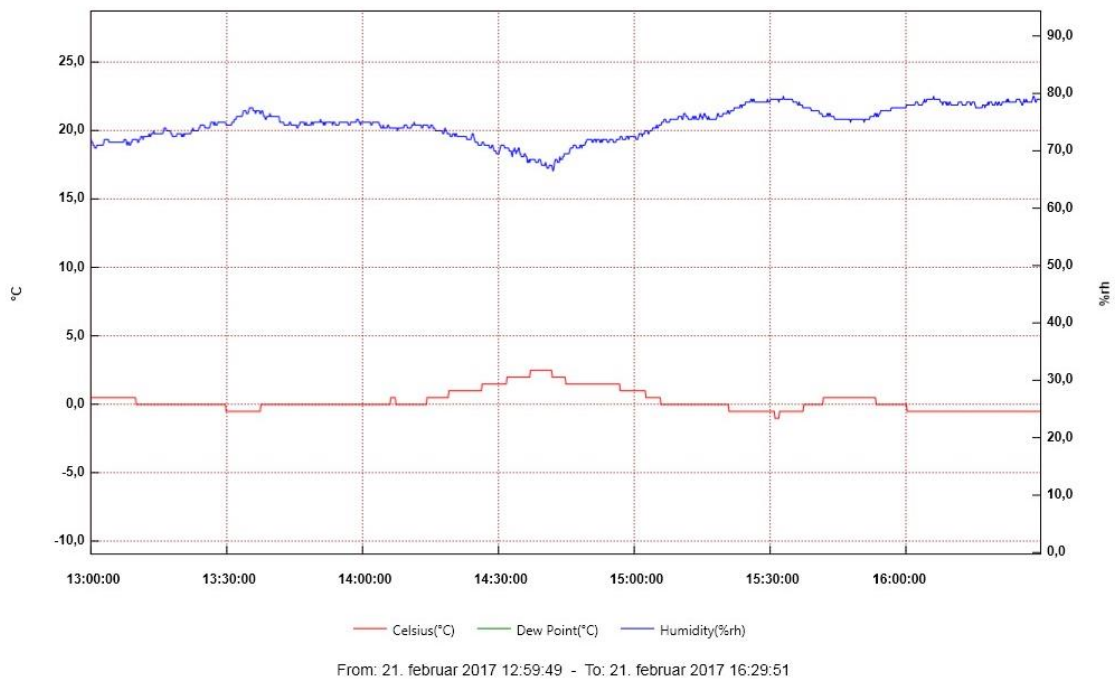
## Appendix B

Additional data for the Nordmarka case study.

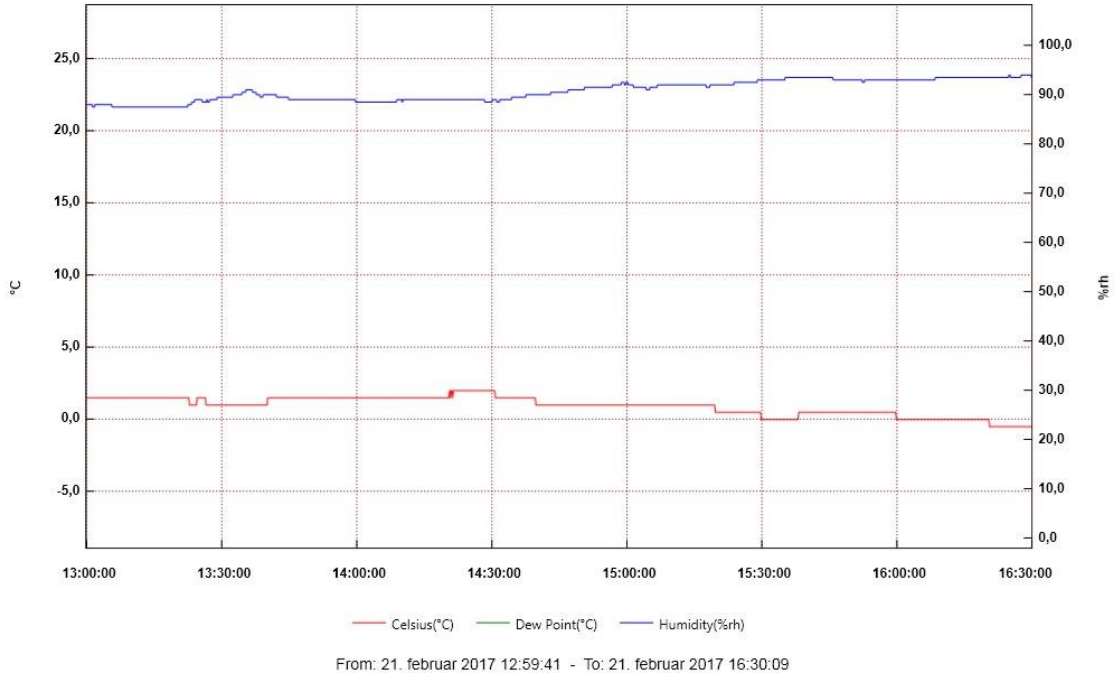
### Case 1:

Measurement	Value	Unit
Avg.Snowdepth Before	21,5	Cm
Avg.Snowdepth After	19,1	Cm
Snowdepth reduction	2,4	Cm
Time	3,5	Hours
Reduction/Time	0,7	Cm/hour
Density(before)	140	Kg/m <sup>3</sup>
Applied effect	134,4	W/m <sup>2</sup>
Energy used	1,54	kWh

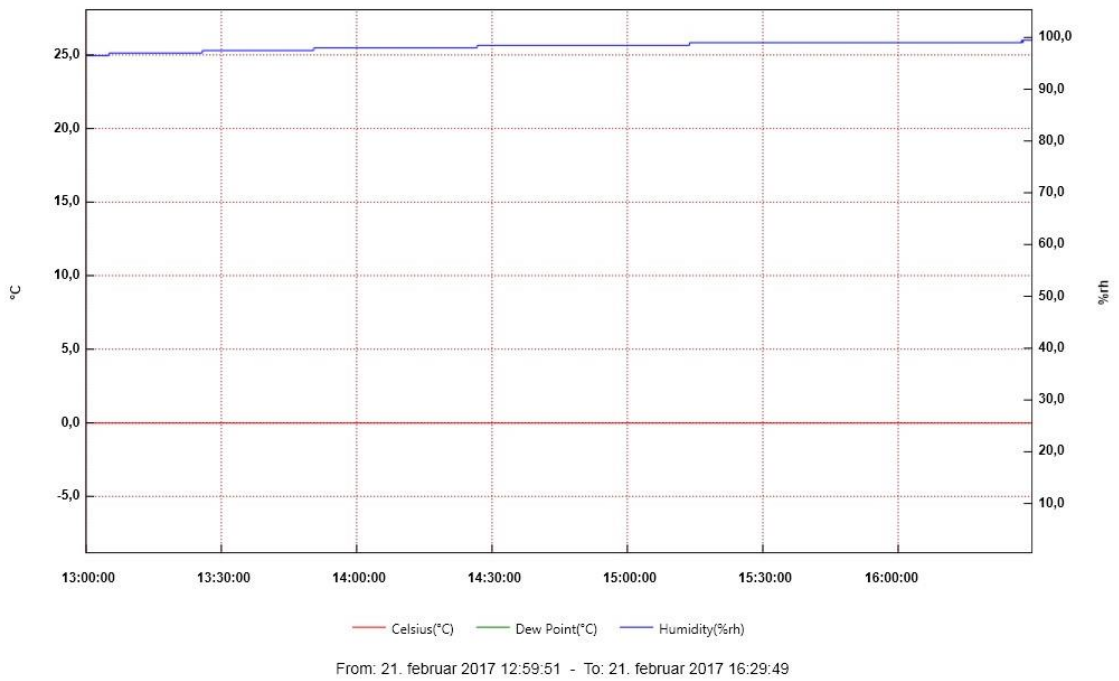
Table of general data collected.



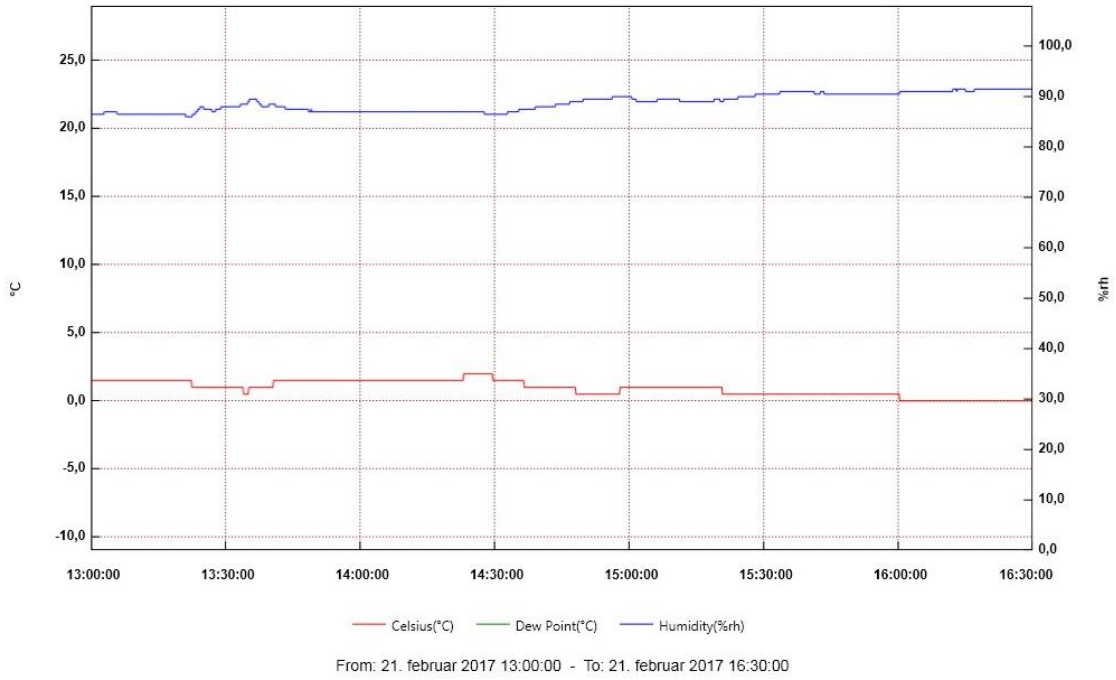
The outside air temperature and RH during the experiment.



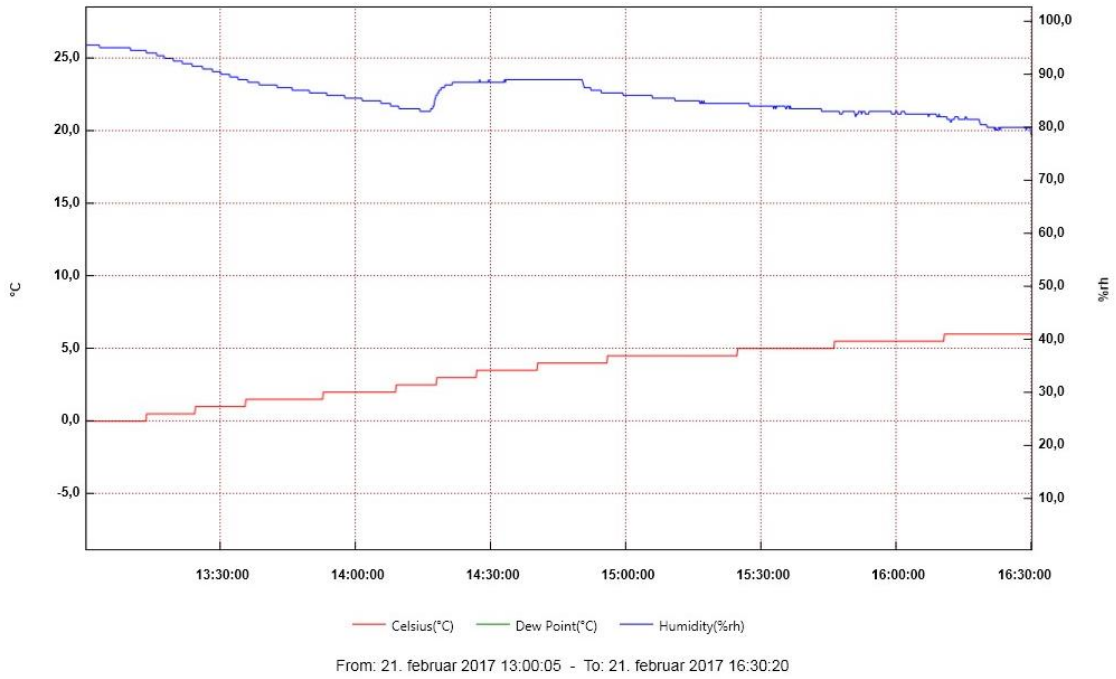
Module 1, top snowpack.



Module 1, bottom snowpack.



*Module 3, top snowpack*



*Module 3, bottom snowpack*

Case 2

	Time	Current	Electricity[A]	Voltage[V]	h	Energy[kWh]
22.feb	1715	Loggers placed	-	-		
	2243	ON	2	39	0,58	0,05
	2318	OFF				0,00
	2350	ON	0,5	36	10,5	0,19
23.feb	1020	OFF				0,00
	1648	ON	0,5	36	1,08	0,02
	1753	UP	1	38	1,22	0,05
	1905	UP	1,5	38,5	1,5	0,09
24.feb	2035	UP	2	39	11,08	0,86
	07:40	DOWN	1	38	2,92	0,11
	1035	DOWN	0,5	36	0,167	0,00
	1045	DOWN	0,3	36	2,367	0,03
	1307	OFF				0,00
	1903	ON	1,5	38,5	1,4	0,08
	2027	UP	2	39	0,367	0,03
	2049	DOWN	1,5	38,5	0,867	0,05
	2141	UP	2	39	0,533	0,04
	25.feb	2213	DOWN	1,5	38,5	10,367
08:35		OFF				
Tot:					44,95	2,19

Electricity log for the duration of the experiment. The colors signify sessions of sublimation. The current was only off during the hottest hours of the day.

Module		1	1	3	3	
Placement		Top	Bottom	Top	Bottom	Air
TEMP [C]	Max	0,5	-1	0	0	-2
	Min	-18	-6	-14	-2	-14,5
	Avg	-11,3	-3,6	-7,8	-0,9	-9,3
	Std	5,7	1,6	3,9	0,5	3,2
RH [%]	Max	92,5	96,5	93,5	102,5	99,5
	Min	81,5	93,5	83	96	64
	Avg	85,6	94,4	87	100,1	86,3
	Std	2,6	0,8	3,2	1,6	7,8
SH [g/kg]	Avg	1,294	2,796	1,794	3,723	1,559

Temperature and humidity for the whole duration of the sublimation case. Specific humidity is estimated with the psychometric chart.

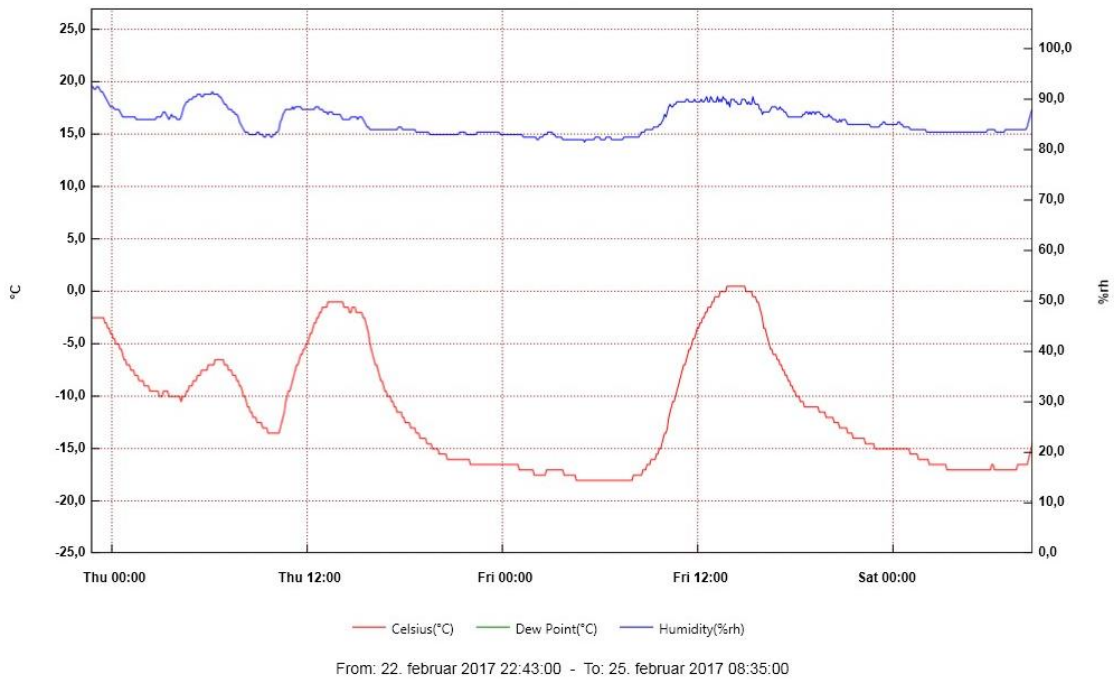
Snowdepth Before	14,05	cm
Snowdepth After Ref.	10,6	cm
Snowdepth After Pow.	7,05	cm
Snowdepth Reduction	3,55	cm
Snowdepth Reduction	33,5	%
Time, Total	57,9	h
Time, applied electricity	44,9	h
Reduction/totaltime	0,061	cm/h
Energy used, per module	2,19	kWh
Avg.Power	29,8	W/m <sup>2</sup>
Density before	106,9	kg/m <sup>3</sup>
Density after Pow.	183,6	kg/m <sup>3</sup>
Density after Ref.	142,7	kg/m <sup>3</sup>
Density increase Pow.	71,7	%
Density increase, relative (Pow/Ref)	28,6	%
Weight Reduction	2,08	kg/m <sup>2</sup>
Weight Reduction per Day	0,863	kg/m <sup>2</sup> dag
Total sublimated mass	6,81	kg
Energy used to sublimate	2299,2	kJ/kg

Data of snow depth, density, weight reduction and power applied during the sublimation case.

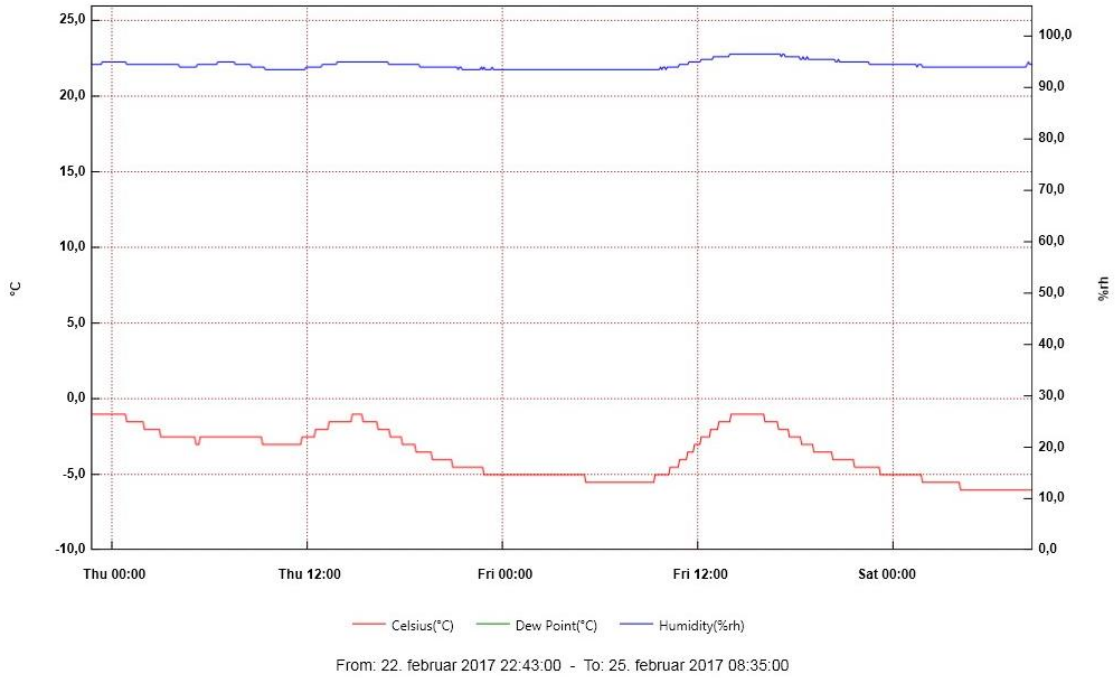


Measurement	23.feb	24.feb	25.feb	Unit
WindRun	17,9	46,6	41,6	km
Avg.Speed	0,207	0,54	0,48	m/s
Gust	6,5	5,4	4,8	m/s
10MinAvg	3,4	4,1	3,4	m/s
DominantDir	211(SSW)	185(S)	153(SSE)	°

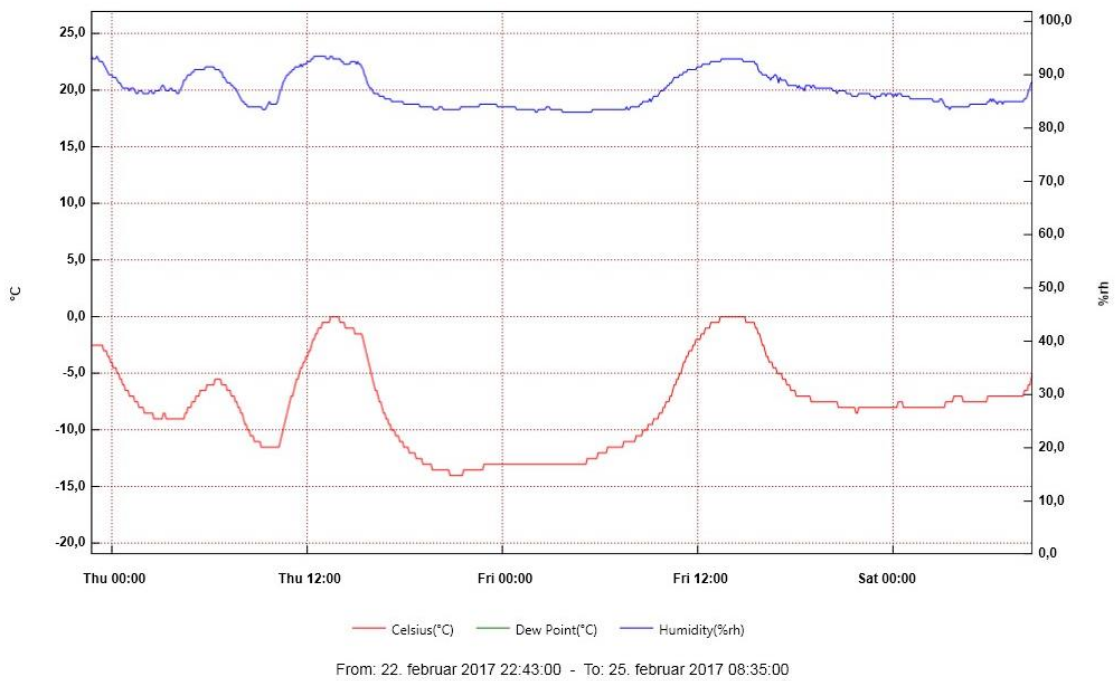
Wind data collected from the nearby weather station.



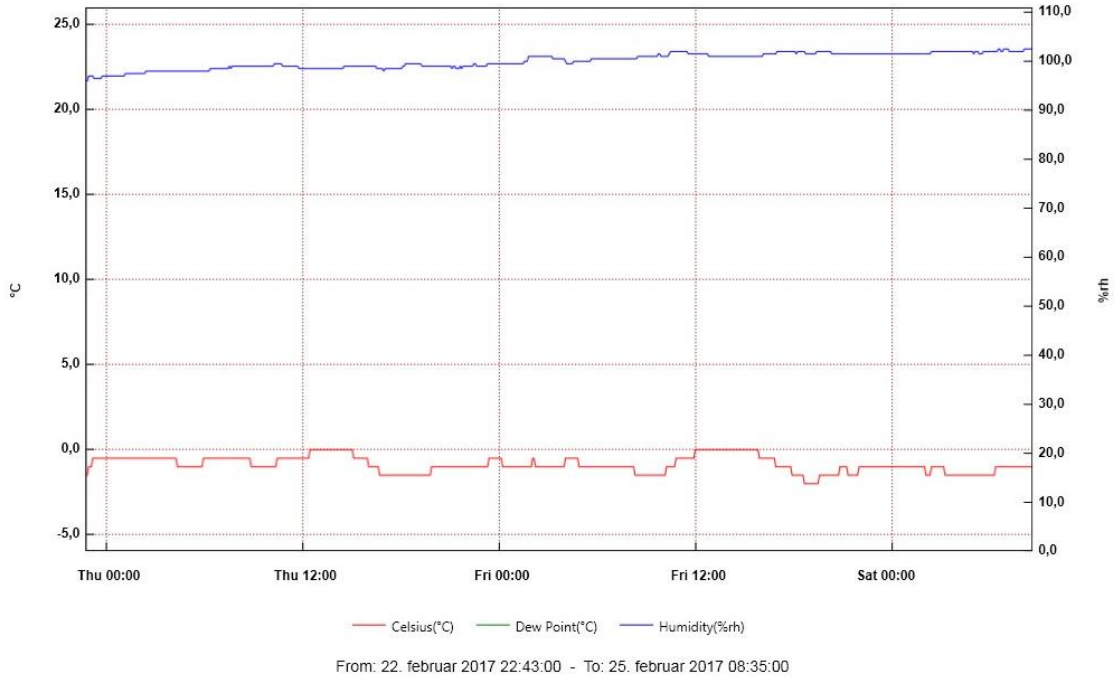
Module 1, top snowpack



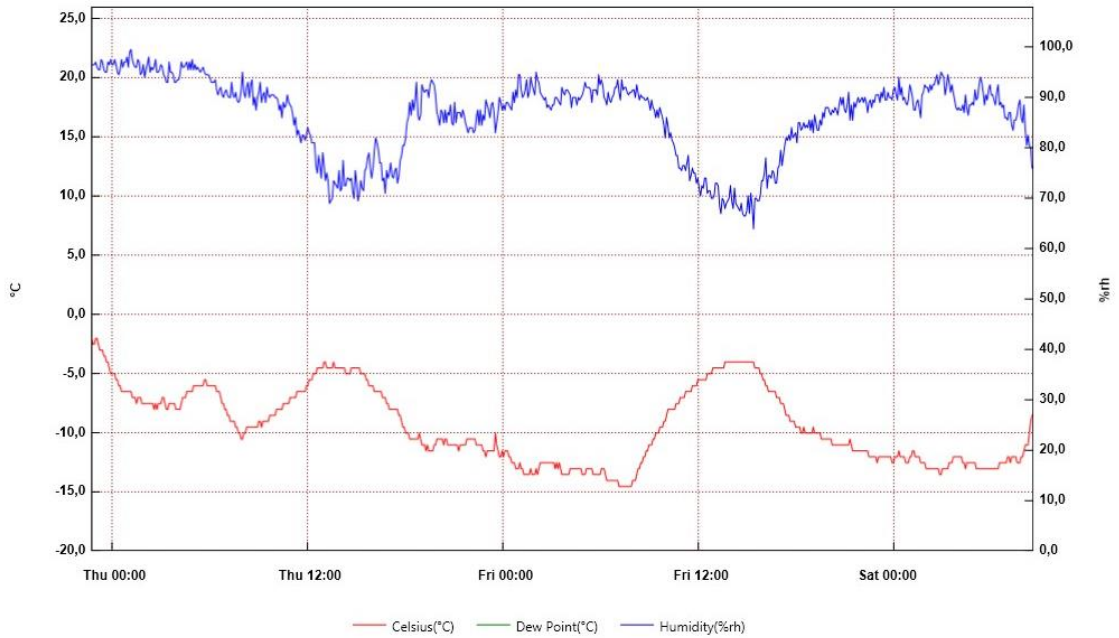
*Module 1, bottom snowpack*



*Module 3, top snowpack*

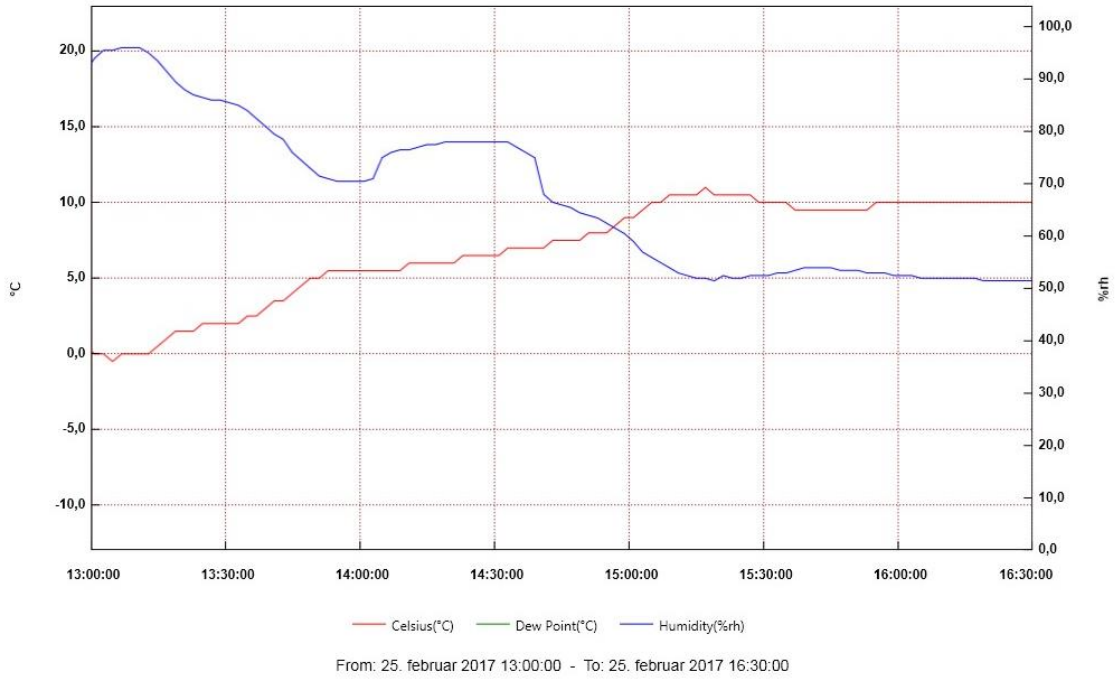


*Module 3, bottom snowpack*

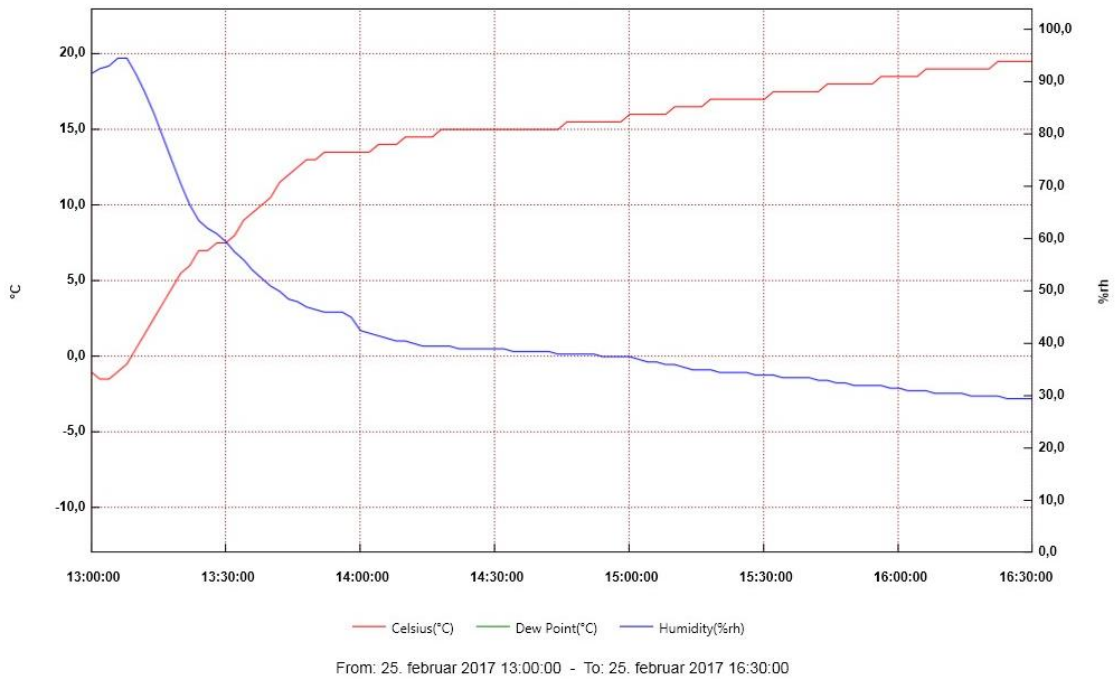


*Outside air logger*

**Case 3:**



*Module 3, bottom snowpack*



*Module 2, bottom snowpack*



Norges miljø- og biovitenskapelig universitet  
Noregs miljø- og biovitenskapelige universitet  
Norwegian University of Life Sciences

Postboks 5003  
NO-1432 Ås  
Norway